TECHNICAL OPERATING REPORT [redacted]

C72 12554

REFERENCE NO. 64 831

COPIES

(UNCLASSIFIED TITLE)

APOLLO HEAT SHIELD MONTHLY PROGRESS REPORT (AUG - SEPT 1964)

Prepared by

RESEARCH AND ADVANCED DEVELOPMENT DIVISION
AVCO CORPORATION
Wilmington, Massachusetts

RAD-SR-64-249
Contract M3J3XA-406012
Avco Report Series 201

THIS REPORT WAS PREPARED IN ACCORDANCE WITH NAA/S&ID CONTRACT M3J3XA-406012. IT IS SUBMITTED IN PARTIAL FULFILLMENT OF THE CONTRACT AND IN ACCORDANCE WITH NAA/S&ID PROCUREMENT SPECIFICATION MC999-0025.

9 October 1964

SCD No. ME364-0001, Ablative Panel Shield

[redacted]

Prepared for

NORTH AMERICAN AVIATION, INC.
SPACE AND INFORMATION SYSTEMS DIVISION
Downey, California

TECHNICAL OPERATING REPORT [redacted]

This document consists of 126 pages, 90 copies, Series A

(UNCLASSIFIED TITLE) C72 72554

APOLLO HEAT SHIELD MONTHLY PROGRESS REPORT (AUG - SEPT 1964)

Prepared by

RESEARCH AND ADVANCED DEVELOPMENT DIVISION
AVCO CORPORATION
Wilmington, Massachusetts

RAD-SR-64-249
Contract M3J3XA-406012
Avco Report Series 201

[redacted]

9 October 1964

SCD No. ME364-0001, Ablative Panel Shield

APPROVED

W. Zeh
Project Manager
Apollo Vehicle Design

C. L. Huffine
Project Manager
Materials Development and Fabrication

E. Offenhartz
Project Director
Manned Space Systems

Prepared for

NORTH AMERICAN AVIATION, INC.
SPACE AND INFORMATION SYSTEMS DIVISION
Downey, California

[redacted]

(NOT USED)

[redacted]

CONTENTS

[redacted]

(NOT USED)

[redacted]

ILLUSTRATIONS

[redacted]

ILLUSTRATIONS (Cont'd)

ILLUSTRATIONS (Cont'd)

[redacted]

TABLES

[redacted]

(NOT USED)

I. VEHICLE DESIGN

A. AEROTHERMODYNAMICS

1.0 Thermal Design

1.1 Main Ablator

1.1.1 Main Ablator Thickness Definition

Subsequent to the freeze date for airframe 006 ablator thickness definition, additional thermal analyses indicated the desirability for minor thickness refinements at certain locations over the Command Module. It was also discovered that the thickness at Station 250 was erroneously reported. A revised thickness table has been compiled for the entire Command Module and will be incorporated into the design for airframe 009. Table I lists the thicknesses; formal notification of this revision has been transmitted to NAA/S&ID in letter, R&DJAC/126.

1.1.2 Shear Pad Thickness Perturbations

Ablator thicknesses for the areas affected by the shear/compression pad perturbations were updated for airframe 009 assuming a radial orientation. Two principle reasons were considered as the basis for this updating. First, the reference design for airframe 006 does not consider the variation of radiant heating over the relatively large area affected by the pads. This variation of heating is quite significant particularly for radially oriented perturbations which reach the crew compartment. The revised perturbations reflect the appropriate variation of radiant heating. Second, the locus of the heating value, q_{local}/q_o = 1.0, was originally interpreted as being the locus of local nominal convective heating. The revised thicknesses consider a literal interpretation of this value; thus the line becomes the locus of points experiencing heating equal to the reference shear pad heating. Figure 1 shows schematically the points considered for this analysis while table II lists the associated total ablator thicknesses for each shear pad area.

1.1.3 RTV-560 Void Analysis

It was reported previously that analyses were performed at two RTV-560 gasket installations to evaluate the effects of a 0.075-inch void.

Results of an analysis of voids in RTV-560 gaskets indicate that a 0.075-inch void will not adversely backface temperature unless located within the outer 15 to 40 percent of the gasket, depending upon vehicle location. Further analyses were performed in this region of adverse

temperature effects to evaluate the effects of smaller voids. The results, along with those shown previously, are presented in figures 2 and 3 for an aft compartment and a crew compartment location, respectively. It is evident that basing criteria upon smaller void sizes near the surface of the RTV-560 depresses these upper bound responses significantly. Based upon these results, the following thermal acceptance criteria were established for RTV-560:

a. Aft compartment -- void size shall not exceed 0.03 inch in the outer 40 percent of the gasket and 0.075 inch in the remainder of the material.

b. Crew and forward compartments -- void size shall not exceed 0.03 inch in the outer 15 percent of the gasket and 0.075 inch in the remainder of the material.

These criteria are considered realistic due to the one-dimensional nature of the analysis, thus establishing upper bound effects.

1.1.4 Bond Line Temperatures at Forward Pitch Engine Loose Ablator Panel

A one-dimensional thermal analysis was performed to determine maximum bond line temperatures along the forward pitch engine loose ablator panel for trajectory HSE-3A. The wedge configuration of this panel, shown in figure 4, is imposed by NAA/S&ID position of the engine and the forward compartment separation plane. The back side of the RTV-560 was considered as adiabatic since definition of the possible heat transfer effects from the liner to the gasket has not been provided by NAA/S&ID. Figure 5 summarizes the maximum bond-line temperatures experienced at the reentry times at which these values occur. It is seen that extremely high bond-line temperatures occur near the apex of the wedge and that all maximum values occur prior to the end of reentry heating.

The results of this analysis have been given to structures for examination.

1.1.5 Abort Tower Well Ablator Thicknesses

A detailed review of the radiation view factors used as a basis for sizing the abort tower well ablator has been conducted. Results indicate that in general the view factors are higher; consequently, the ablator thickness requirement mass is reduced somewhat. The new requirements and the corresponding locations are shown in Table III and on figures 6 and 7.

TABLE I

MAIN ABLATOR THICKNESSES

Heating Location No.	Theta (degrees) 0^{o}=Windward	X_c (inches)	Reentry Thickness (inches)	Boost Thickness (inches)	Launch Thickness (inches)
100	Origin of C/M	0	1.82		1.82
101	0	4.59	2.16		2.16
102	11.25	↑			
103	22.5		2.11		2.11
104	33.75				
105	45.0		1.94		1.94
106	67.5				
107	90.0		1.71		1.71
108	112.5				
109	135.0		1.62		1.62
110	157.5	↓			
111	180.0	4.59	1.54		1.54
112	0	9.947			
113	11.25	↑			
114	22.5				
115	33.75				
116	45.0				
117	67.5				
118	90.0				
119	112.5				
120	135.0				
121	157.5	↓			
122	180.0	9.947			
200	0	15.495	2.46		2.46
201	11.25	↑			
202	22.5		2.43		2.43
203	33.75				
204	45.0		2.15		2.15
205	67.5				
206	90.0		1.82		1.82
207	112.5				
208	135.0		1.55		1.55
209	157.5	↓			
210	180.0	15.495	1.41		1.41
211	0	17.0			
212	11.25	↑			
213	22.5	↓			

TABLE I (Cont'd)

Heating Location No.	Theta (degrees) 0^{o}=Windward	X_c (inches)	Reentry Thickness (inches)	Boost Thickness (inches)	Launch Thickness (inches)
214	33.75				
215	45.0				
216	67.5				
217	90.0				
218	112.5				
219	135.0				
220	157.5				
221	180.0	17.0			
222	0	18.0	2.67	0.07	2.74
223	11.25				
224	22.5		2.53	0.07	2.60
225	33.75				
226	45.0		2.27	0.07	2.34
227	67.5				
228	90.0		1.90	0.07	1.97
229	112.5				
230	135.0		1.67	0.07	1.74
231	157.5				
232	180.0	18.0	1.07	0.07	1.14
233	0	19.0			
234	11.25				
235	22.5				
236	33.75				
237	45.0				
238	67.5				
239	90.0				
240	112.5				
241	135.0				
242	157.5				
243	186.0	19.0			
244	0	20.0	1.97	0.08	2.05
245	11.25				
246	22.5		1.90	0.08	1.98
247	33.75				
248	45.0		1.77	0.08	1.85
249	67.5				
250	90.0		1.23	0.08	1.31
251	112.5				
252	135.0		0.83	0.08	0.91

TABLE I (Cont'd)

Heating Location No.	Theta (degrees) 0°=Windward	X_C (inches)	Reentry Thickness (inches)	Boost Thickness (inches)	Launch Thickness (inches)
253	157.5				
254	180.0	20.0	0.76	0.08	0.84
255	0	21.0			
256	11.25				
257	22.5				
258	33.75				
259	45.0				
260	67.5				
261	90.0				
262	112.5				
263	135.0				
264	157.5				
265	180.0	21.0			
266	0	22.0			
267	11.25				
268	22.5				
269	33.75				
270	45.0				
271	67.5				
272	90.0				
273	112.5				
274	135.0				
275	157.5				
276	180.0	22.0			
277	0	23.2			
278	11.25				
279	22.5				
280	33.75				
281	45.0				
282	67.5				
283	90.0				
284	112.5				
285	135.0				
286	157.5				
287	180.0	23.2			
300	0	23.875	1.76	0.09	1.85
301	11.25				
302	22.5		1.64	0.09	1.73
303	33.75				

TABLE I (Cont'd)

Heating Location No.	Theta (degrees) 0° = Windward	X_c (inches)	Reentry Thickness (inches)	Boost Thickness (inches)	Launch Thickness (inches)
304	45.0	23.875	1.49	0.09	1.58
305	67.5	↑			
306	90.0	↕	1.01	0.09	1.10
307	112.5	↕			
308	135.0	↕	0.71	0.09	0.80
309	137.5	↕			
310	180.0	23.875	0.60	0.09	0.69
311	0	30.	1.45	0.10	1.55
312	22.5	↑	1.36	0.10	1.46
313	45.0	↕	1.20	0.10	1.30
314	67.5	↕	1.00	0.10	1.10
315	90.0	↕	0.80	0.10	0.90
316	112.5	↕	0.42	0.10	0.52
317	135.0	↕	0.37	0.10	0.47
318	157.5	↕	0.11	0.10	0,21
319	180.0	30.	0.05	0.10	0.15
320	0	35.	1.42	0.10	1.52
321	22.5	↑	1.30	0.10	1.40
322	45.0	↕	1.18	0.10	1.28
323	67.5	↕	1.03	0.10	1.13
324	90.0	↕	0.78	0.10	0.88
325	112.5	↕	0.51	0.10	0.61
326	135.0	↕	0.38	0.10	0.48
327	157.5	↕	0.19	0.10	0.29
328	180.0	35.	0.19	0.10	0.29
329	0	43.425	1.36	0.10	1.46
330	22.5	↑	1.32	0.10	1.42
331	45.0	↕	1.13	0.10	1.23
332	67.5	↕	0.97	0.10	1.07
333	90.0	↕	0.79	0.10	0.89
334	112.5	↕	0.58	0.10	0.68
335	135.0	↕	0.39	0.10	0.49
336	157.5	↕	0.28	0.10	0.38
337	180.0	43.425	0.39	0.10	0.49
338	0	48.	1.35	0.10	1.45
339	22.5	48.	1.30	0.10	1.40
340	45.0	48.	1.12	0.10	1.22
		↕			

TABLE I (Cont'd)

Heating Location No.	Theta) (degrees) 0^{O}=Windward	(inches)	Reentry Thickness (inches)	Boost Thickness (inches)	Launch Thickness (inches)
341	67.5	48.	0.97	0.10	1.07
342	90.0	↑	0.78	0.10	0.88
343	112.5	↕	0.61	0.10	0.71
344	135.0	↕	0.40	0.10	0.50
345	157.5	↓	0.35	0.10	0.45
346	180.0	48.	0.48	0.10	0.58
347	0	58.	1.31	0.10	1.41
348	22.5	↑	1.28	0.10	1.38
349	45.0	↕	1.09	0.10	1.19
350	67.5	↕	0.95	0.10	1.05
351	90.0	↕	0.78	0.10	0.88
352	112.5	↕	0.58	0.10	0.68
353	135.0	↕	0.42	0.10	0.52
354	157.5	↕	0.45	0.10	0.55
355	180.0	58.	0.61	0.10	0.71
356	0	68.	1.28	0.10	1.38
357	22.5	↑	1.24	0.10	1.34
358	45.0	↕	1.03	0.10	1.13
359	67.5	↕	0.91	0.10	1.01
360	90.0	↕	0.78	0.10	0.88
361	11.25	↕	0.58	0.10	0.68
362	135.0	↕	0.45	0.10	0.55
363	157.5	↕	0.52	0.10	0.62
364	180.0	68.	0.70	0.10	0.80
365	0	81.13	1.21	0.10	1.31
366	22.5	↑	1.19	0.10	1.29
367	45.0	↕	1.00	0.10	1.10
368	67.5	↕	0.89	0.10	0.99
369	90.0	↕	0.74	0.10	0.84
370	112.5	↕	0.57	0.10	0.67
371	135.0	↕	0.49	0.10	0.59
372	157.5	↕	0.58	0.10	0.68
373	180.0	81.13	0.73	0.10	0.83
400	0	88.	1.09	0.09	1.18
401	22.5	↑	1.08	0.09	1.17
402	45.0	↕	0.97	0.09	1.06
403	67.5	↕	0.88	0.09	0.97
404	90.0	↕	0.74	0.09	0.83
405	112.5	↕	0.56	0.09	0.65
406	135.0	↕	0.50	0.09	0.59
407	157.5	↓	0.59	0.09	0.68

TABLE I (Cont'd)

Heating Location No.	Theta (degrees) 0^{o}=Windward	X_c (inches)	Reentry Thickness (inches)	Boost Thickness (inches)	Launch Thickness (inches)
408	180.0	88.0	0.70	0.09	0.79
409	0	98.0	1.05	0.08	1.13
410	22.5	↑	1.04	0.08	1.12
411	45.0		0.95	0.08	1.03
412	67.5		0.87	0.08	0.95
413	90.0		0.74	0.08	0.82
414	112.5		0.66	0.08	0.74
415	135.0		0.60	0.08	0.68
416	157.5	↓	0.62	0.08	0.70
417	180.0	98.0	0.65	0.08	0.73
418	0	107.0	1.01	0.07	1.08
419	22.5	↑	1.00	0.07	1.07
420	45.0		0.94	0.07	1.01
421	67.5		0.87	0.07	0.94
422	90.0		0.74	0.07	0.81
423	112.5		0.63	0.07	0.70
424	135.0		0.74	0.07	0.81
425	157.5	↓	0.66	0.07	0.73
426	180.0	107.0	0.56	0.07	0.63
427	0	112.25	0.98	0.05	1.03
428	22.5	↑	0.96	0.05	1.01
429	45.0		0.93	0.05	0.98
430	67.5		0.86	0.05	0.91
431	90.0		0.74	0.05	0.79
432	112.5		0.54	0.05	0.59
433	135.0		0.72	0.05	0.77
434	157.5	↓	0.69	0.05	0.74
435	180.0	112.25	0.69	0.05	0.74
500	0	115.347	0.98	0.05	1.03
501	22.5	↑	0.95	0.05	1.00
502	45.0		0.86	0.05	0.91
503	67.5		0.76	0.05	0.81
504	90.0		0.75	0.05	0.80
505	112.5		0.57	0.05	0.62
506	135.0		0.70	0.05	0.75
507	157.5	↓	0.75	0.05	0.80
508	180.0	115.347	0.80	0.05	0.85
509	0	122.5	0.94	0.02	0.96
510	22.5	↕	0.92	0.02	0.94

TABLE I (Concl'd)

Heating Location No.	Theta (degrees) 0^{o}=Windward	X_c (inches)	Reentry Thickness (inches)	Boost Thickness (inches)	Launch Thickness (inches)
511	45.0		0.84	0.02	0.86
512	67.5		0.72	0.02	0.74
513	90.0		0.77	0.02	0.79
514	112.5		0.61	0.02	0.63
515	135.0		0.75	0.02	0.77
516	157.5		0.78	0.02	0.80
517	180.0	122.5	0.84	0.02	0.86
518	0	128.0	0.88	0.01	0.89
519	22.5		0.87	0.01	0.88
520	45.0		0.80	0.01	0.81
521	67.5		0.74	0.01	0.75
522	90.0		0.78	0.01	0.79
523	112.5		0.65	0.01	0.66
524	135.0		0.75	0.01	0.76
525	157.5		0.78	0.01	0.79
526	180.0	128.0	0.82	0.01	0.83
527	0	131.0	0.59	0.0	0.59
528	22.5		0.57	0.0	0.57
529	45.0		0.50	0.0	0.50
530	67.5		0.46	0.0	0.46
531	90.0		0.54	0.0	0.54
532	112.5		0.38	0.0	0.38
533	135.0		0.49	0.0	0.49
534	157.5		0.52	0.0	0.52
535	180.0	131.0	0.54	0.0	0.54
536	Appex	133.5	0.53	0.0	0.53

TABLE II

SHEAR COMPRESSION PAD ABLATOR THICKNESSES
AVCOAT 5026 - 39/HC-G
RADIAL ORIENTATION

Location	Pad 1 (inches)	Pad 3 (inches)	Pad 5 (inches)
A	2.02	1.91	1.52
B	2.11	1.97	1.58
C	2.19	2.03	1.63
D	2.41	2.17	1.70
E	2.41	2.17	1.70
F	2.12	1.97	1.59
G	2.09	1.97	1.62
H	1.97	1.89	1.55
I	1.89	1.98	1.47
J	2.00	2.03	1.54
K	2.11	2.07	1.60
L	2.41	2.17	1.70
M	2.41	2.17	1.70
N	2.26	1.95	1.61
O	2.19	1.87	1.55
P	2.12	1.78	1.48

Pad 1 θ_c = 42° 45'
Pad 3 θ_c = 152° 45'
Pad 5 θ_c = 282° 45'

TABLE III

ABORT TOWER WELLS - ABLATOR THICKNESS
AVCOAT 5026-39/M

Windward				Leeward			
Location	Reentry	Ascent	Total	Location	Reentry	Ascent	Total
1	0.91	0.08	0.99	1	0.54	0.09	0.63
2	0.85	0.06	0.91	2	0.52	0.09	0.61
3	0.84	0.06	0.90	3	0.51	0.08	0.59
4	0.90	0.06	0.96	4	0.67	0.04	0.71
5	0.98	0.08	1.06	5	0.67	0.08	0.75
6	0.89	0.08	0.97	6	0.57	0.04	0.61
7	0.82	0.04	0.86	7	0.43	0.04	0.47
8	0.84	0.04	0.88	8	0.24	0.04	0.28
9	0.87	0.04	0.91	9	0.35	0.08	0.43
10	0.96	0.08	1.04	10	0.56	0.08	0.64
11	0.84	0.08	0.92	11	0.64	0.08	0.72
12	0.77	0.04	0.81	12	0.68	0.08	0.76
13	0.84	0.04	0.88	13	0.59	0.04	0.63
14	0.86	0.04	0.90	14	0.41	0.04	0.45
15	0.96	0.08	1.04	15	0.40	0.04	0.44
16	0.79	0.09	0.88	16	0.47	0.08	0.55
17	0.76	0.04	0.80	17	0.55	0.08	0.63
18	0.82	0.04	0.86	18	0.61	0.08	0.69
19	0.86	0.04	0.90	19	0.66	0.08	0.74
20	0.94	0.08	1.02	20	0.59	0.06	0.65
21	0.81	0.09	0.90	21	0.38	0.06	0.44
22	0.87	0.04	0.91	22	0.48	0.06	0.54
23	0.87	0.04	0.91	23	0.45	0.08	0.53
24	0.91	0.09	1.00	24	0.57	0.08	0.65
25	0.84	0.09	0.93	25	0.56	0.08	0.64
26	0.90	0.09	0.99	26	0.64	0.08	0.72
27	0.94	0.11	1.05	27	0.58	0.06	0.64
28	0.89	0.06	0.95	28	0.53	0.06	0.59
29	0.91	0.06	0.97	29	0.54	0.08	0.62
30	0.93	0.06	0.99	30	0.53	0.06	0.59
31	0.99	0.11	1.10	31	0.60	0.11	0.71
				32	0.64	0.08	0.72
				33	0.59	0.11	0.70
				34	0.66	0.08	0.74
				35	0.61	0.06	0.67
				36	0.60	0.06	0.66

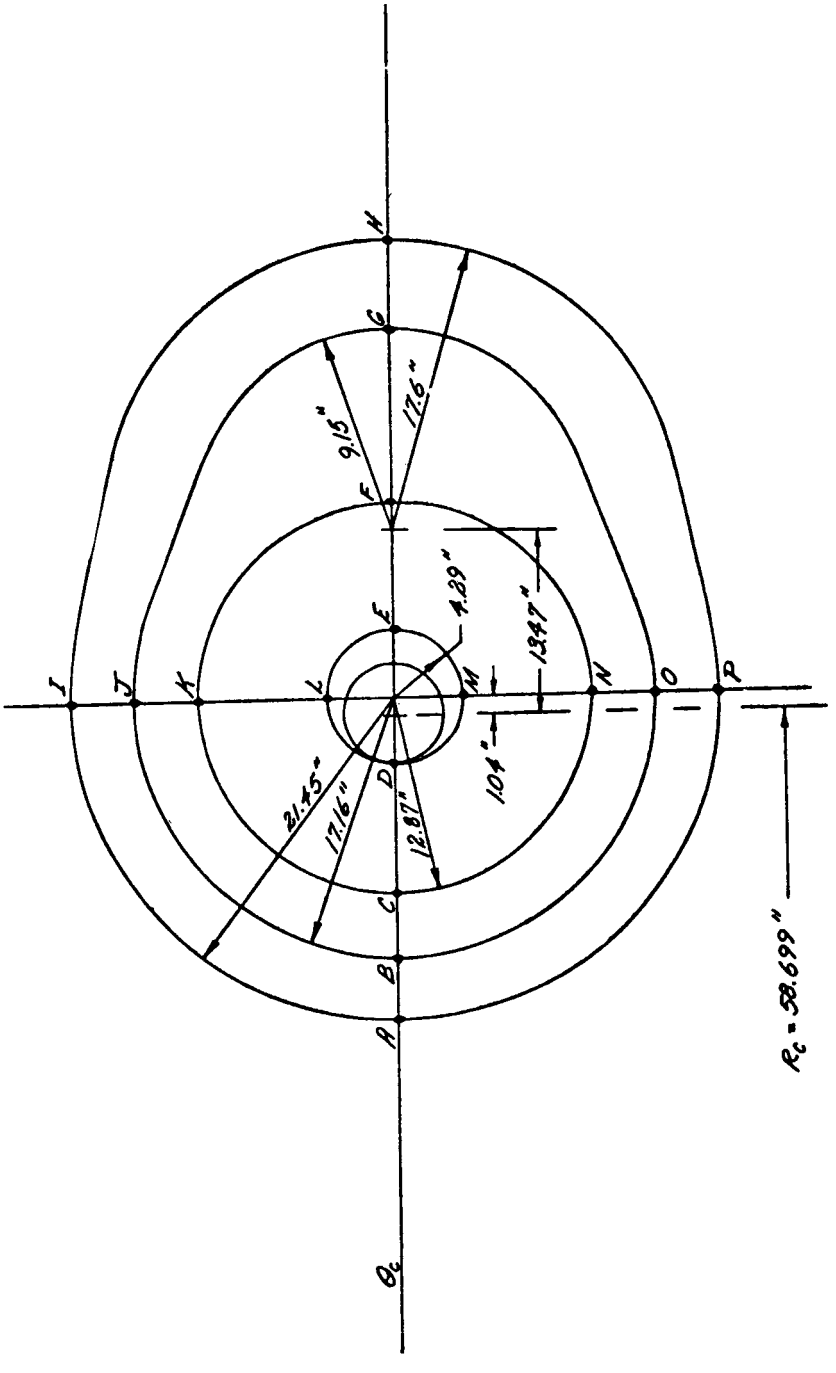

Figure 1 SHEAR COMPRESSION PAD, ABLATOR THICKNESS LOCATIONS
AVCOAT 5026-39/HC-G

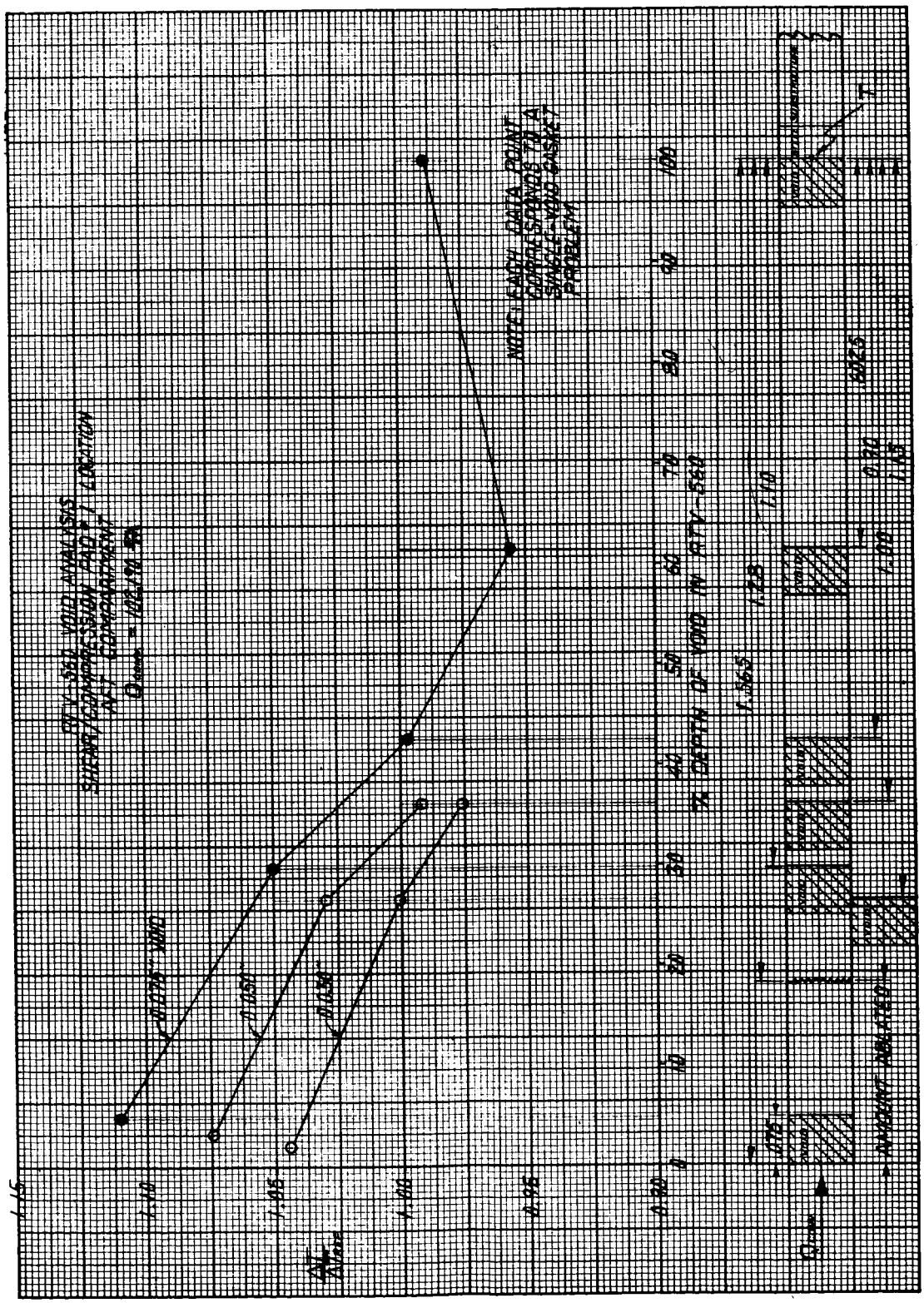

Figure 2 RTV-560 VOID ANALYSIS, SHEAR COMPRESSION PAD 1 LOCATION

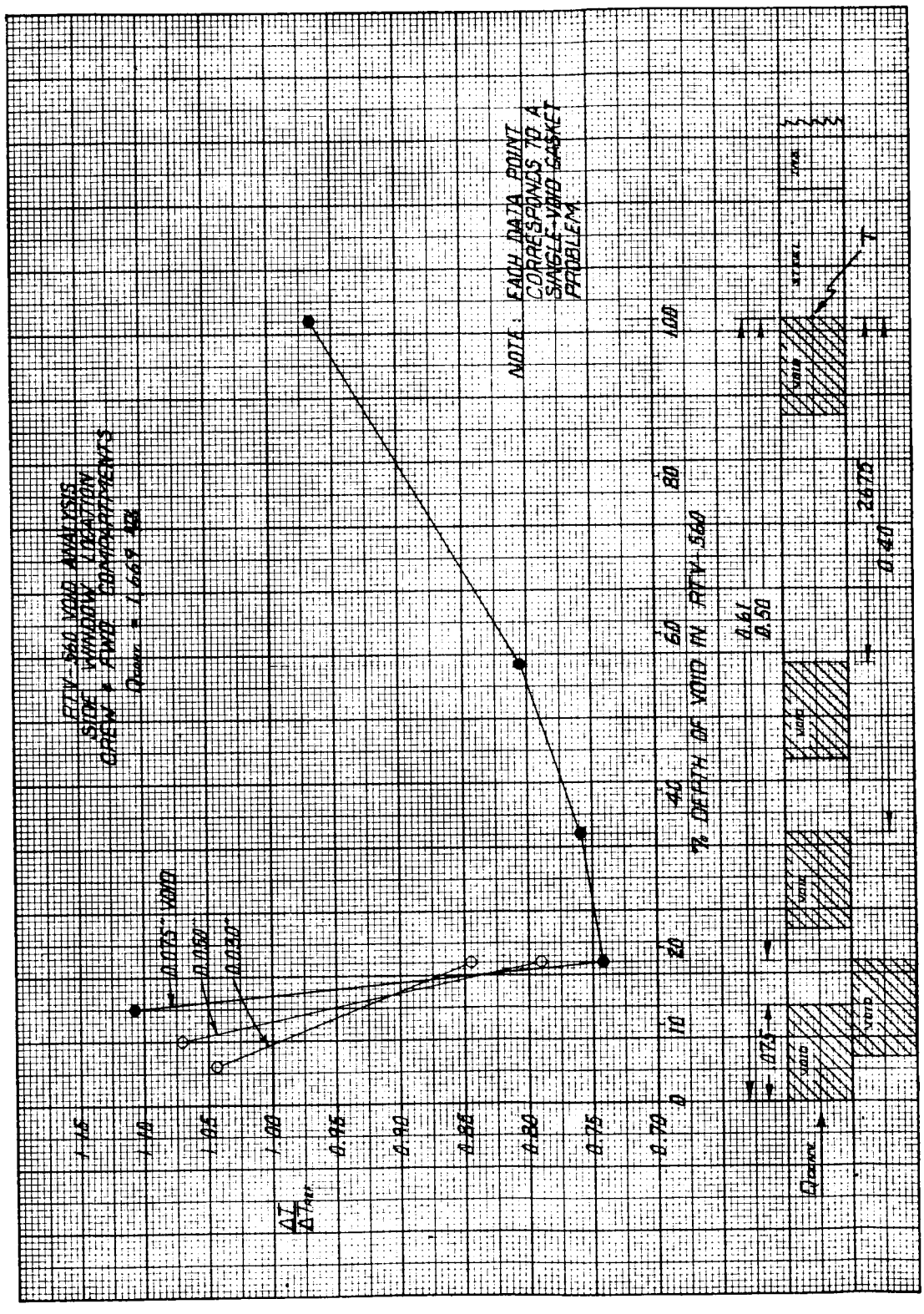

Figure 3 RTV-560 VOID ANALYSIS, SIDE WINDOW LOCATION, CREW AND FORWARD COMPARTMENT

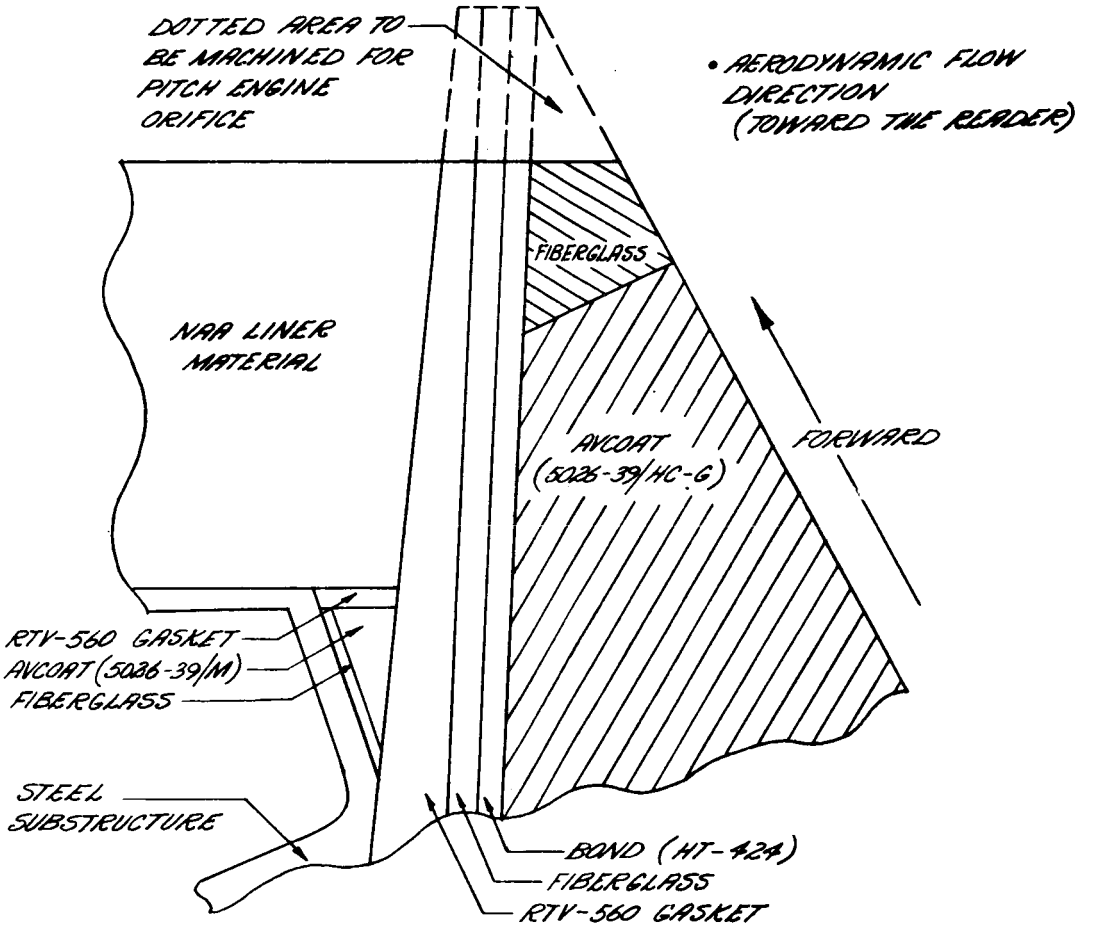

Figure 4 FORWARD PITCH ENGINE LOOSE ABLATOR PANEL

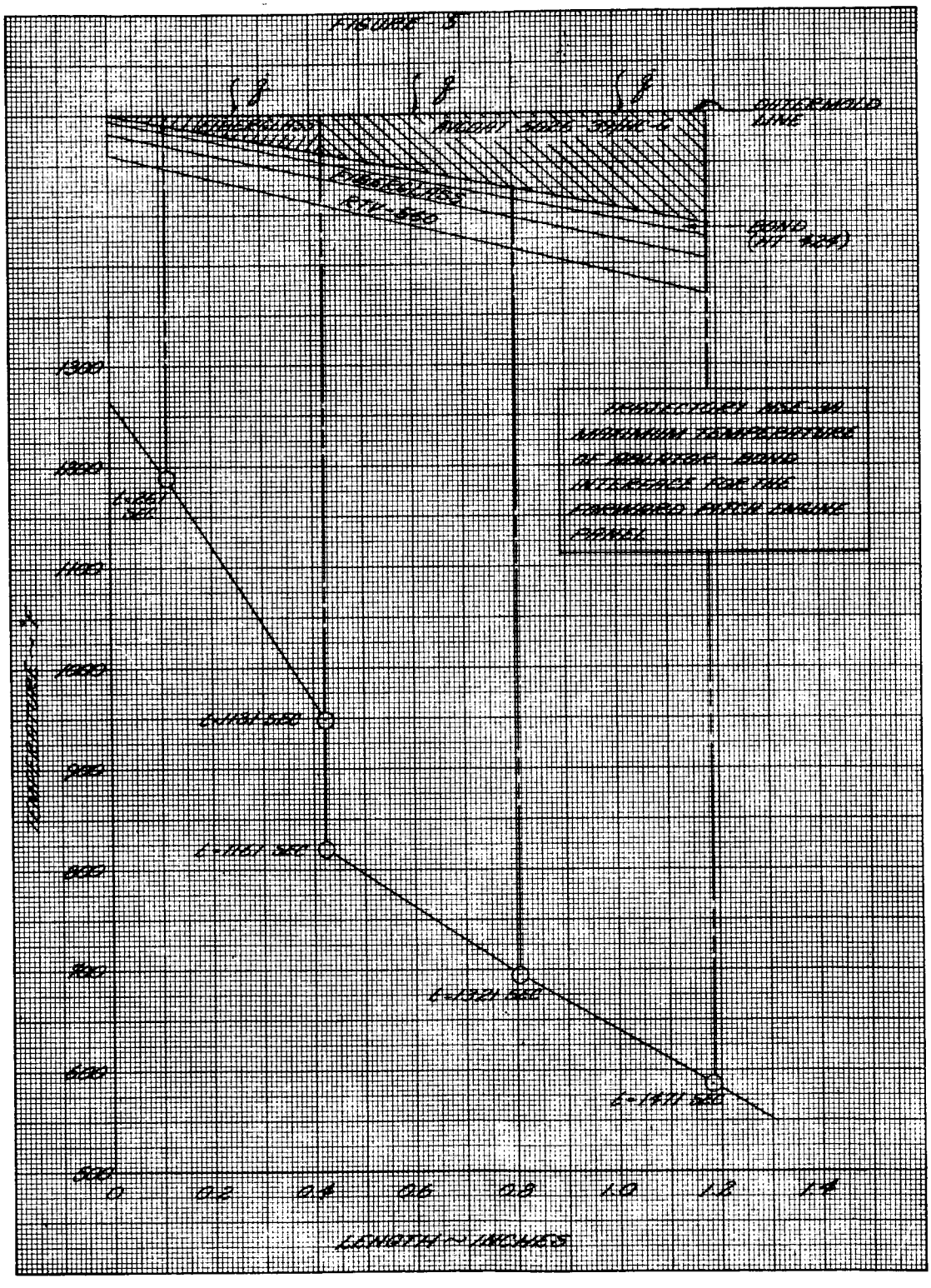

Figure 5 TRAJECTORY HSE-3A, MAXIMUM TEMPERATURE OF ABLATOR BOND

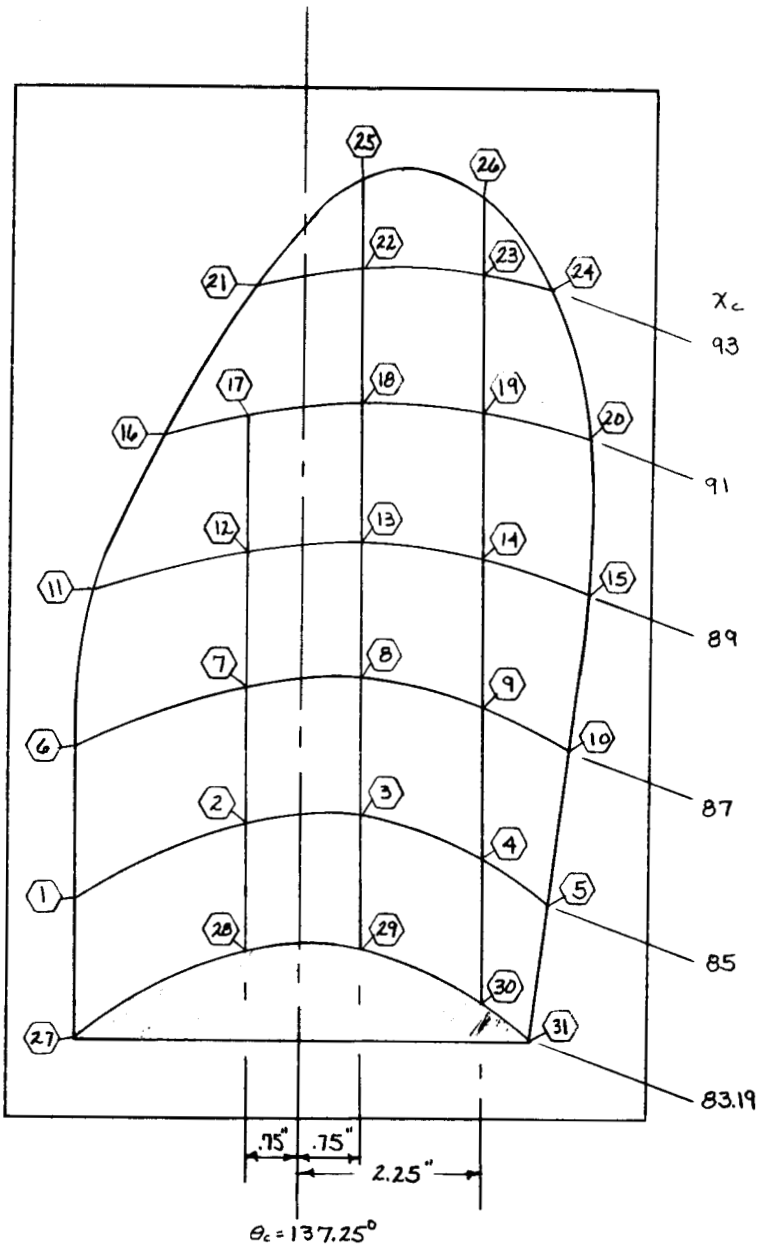

Figure 6 WINDWARD ABORT TOWER WELL

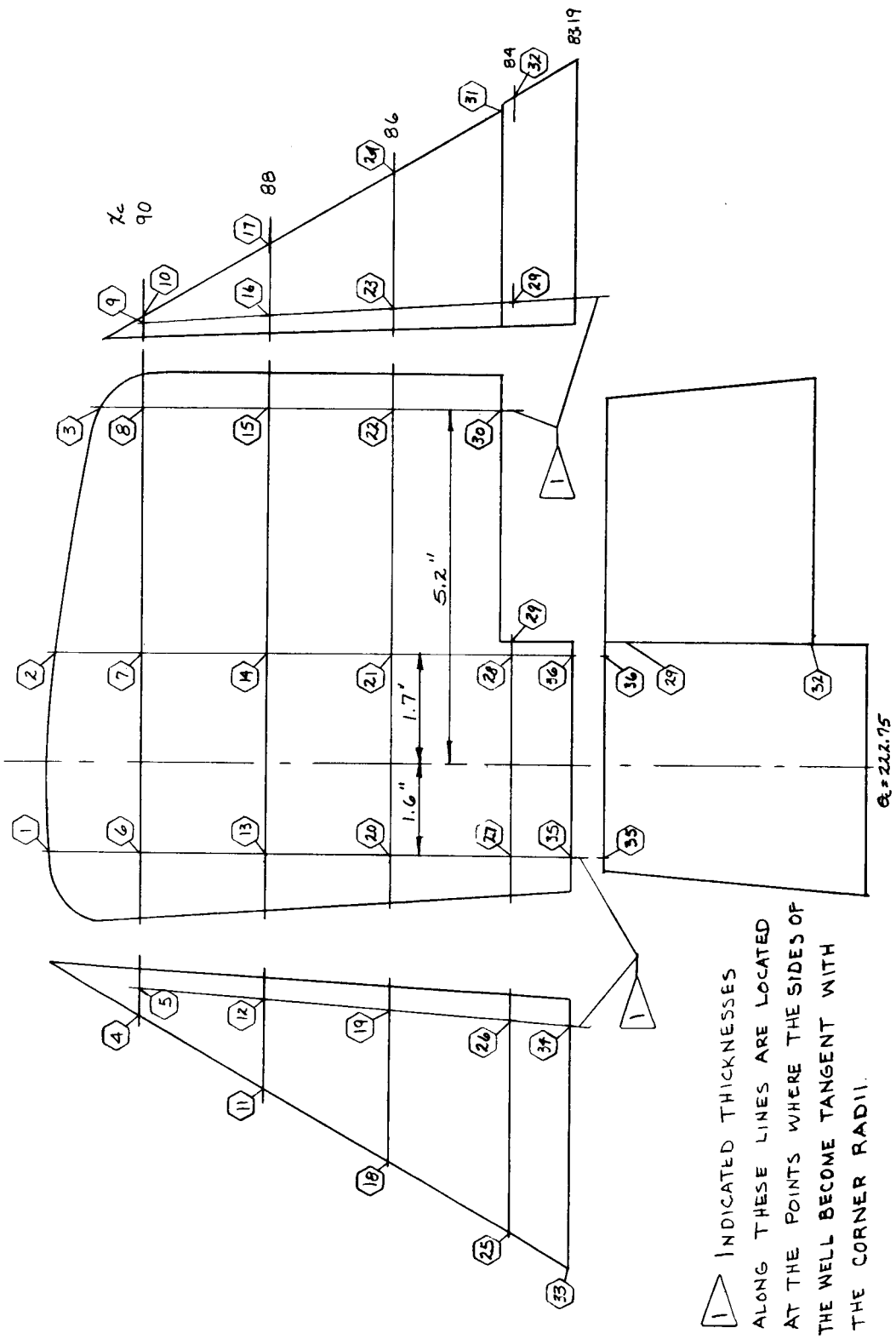

Figure 7 LEEWARD ABORT TOWER WELL

1.1.6 Ablator OML Thermal Adequacy for Airframe 006

Ablator thicknesses defined per 401098 Revision "E" were plotted at all axial locations corresponding to thermal design stations and compared to thermal requirements. It is important that the ablator fairing not only pass through (or above) the specified points but also yield a reasonable and thermally adequate contour between these points. Figures 8 and 9 show typical comparisons at X_c = 4.59 and at X_c = 58 inches, respectively. These figures, along with a series similar to them at other axial locations, ascertain the thermal adequacy of the airframe 006 ablator fairing.

1.1.7 Gasket and Edge Member Study

A two-dimensional thermal analysis of the RTV-560 gasket and the fiberglass edge member configuration was performed after one-dimensional analyses indicated structural overheating. The "E" panel door (per Revision "P") was selected for the analysis since this location experiences the highest heating of any gasket location and was the location of most severe overheating.

The problem was analyzed in two dimensions using Program 1459. The resultant substructure temperature history shown on figure 10 indicates that the additional heat capacity of the structure and edge member surrounding the gasket areas is sufficient to maintain the temperature of the structure below 600°F.

The structure beneath the gasket and edge member is basically the same at all locations on the vehicle. Since the structure does not overheat at the location of most severe heating conditions, it is concluded that no overheating will occur at locations with reduced heating.

1.1.8 Analysis of Crew Compartment Stringers

Two-dimensional heat transfer analyses were performed to investigate the effects of two crew compartment stringers. In particular, it is of interest to establish the maximum effects on substructure temperature responses and the extent of any effect surrounding each stringer.

Stringers at positions of X_c = 43.425, λ = 18° 31' and X_c = 43.425, λ = 91° 41' were analyzed. Trajectory HSE-3A loads for these positions are 8903 Btu/ft^2 and 2477 Btu/ft^2, respectively. Temperature responses at the stringer centerline were compared to responses 12 inches away from the centerline (in a region of one-dimensional heat flow). Figures 11 and 12 indicate temperature responses at the ablator-substructure interface and at the insulation backface, respectively, for the windward stringer. Similar histories for the leeward stringer are presented in figures 13 and 14.

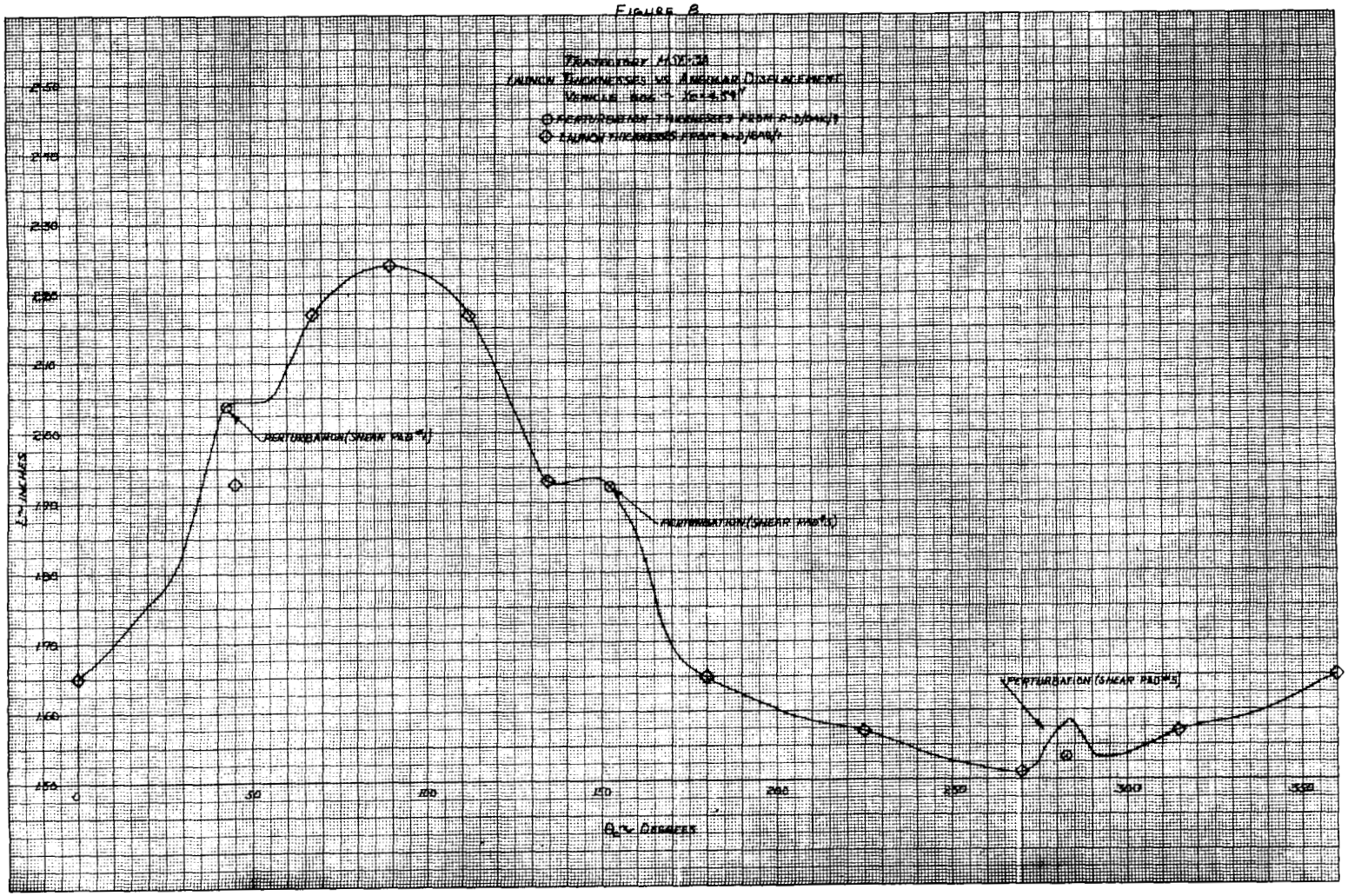

Figure 8 TRAJECTORY HSE-3A, LAUNCH THICKNESS VERSUS ANGULAR DISPLACEMENT

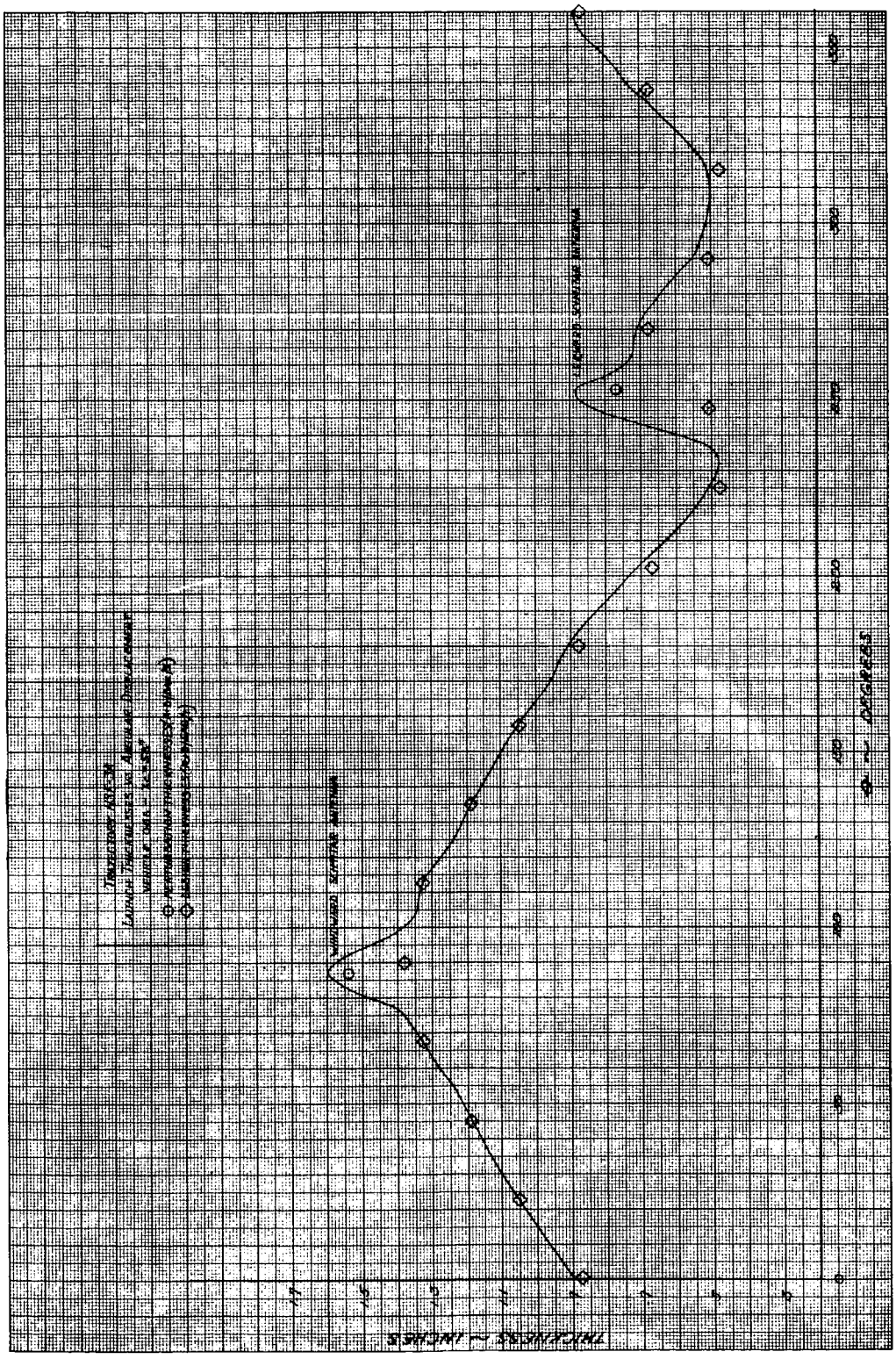

Figure 9 TRAJECTORY HSE-3A, LAUNCH THICKNESS VERSUS ANGULAR DISPLACEMENT

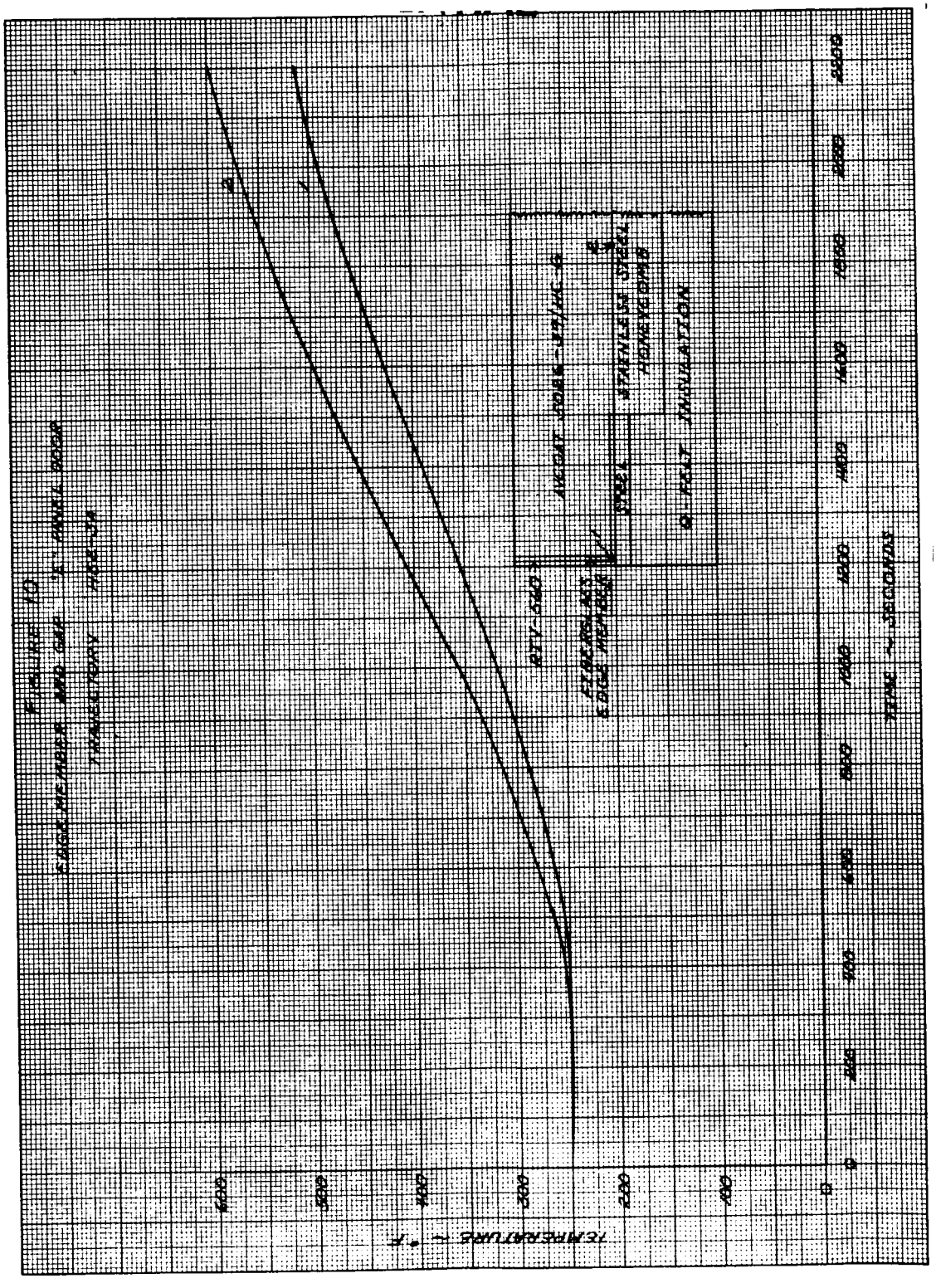

Figure 10 EDGE MEMBER AND GAP "E" PANEL DOOR

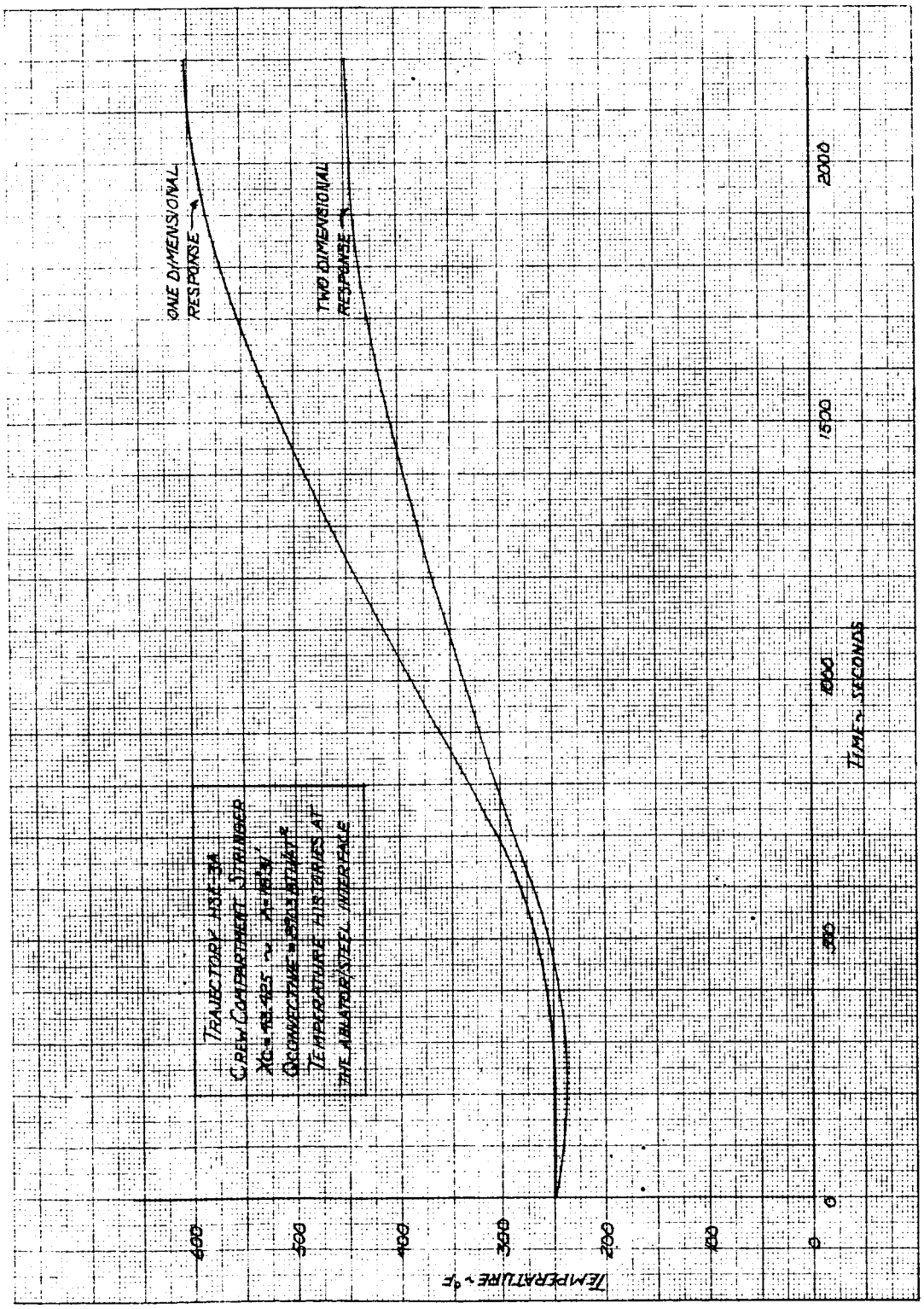

Figure 11 TRAJECTORY HSE-3A CREW COMPARTMENT STRINGER

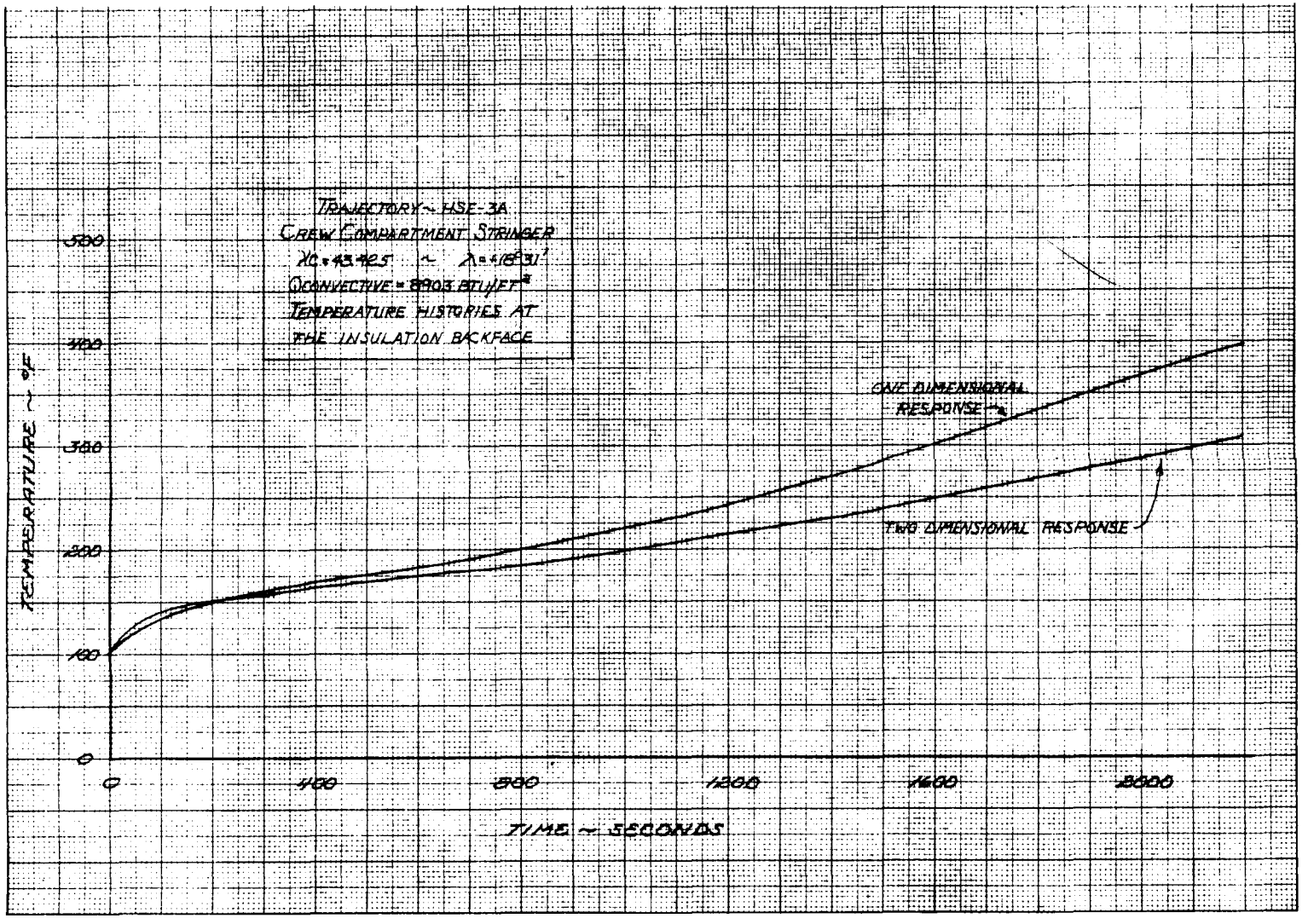

Figure 12 TRAJECTORY HSE-3A, CREW COMPARTMENT STRINGER

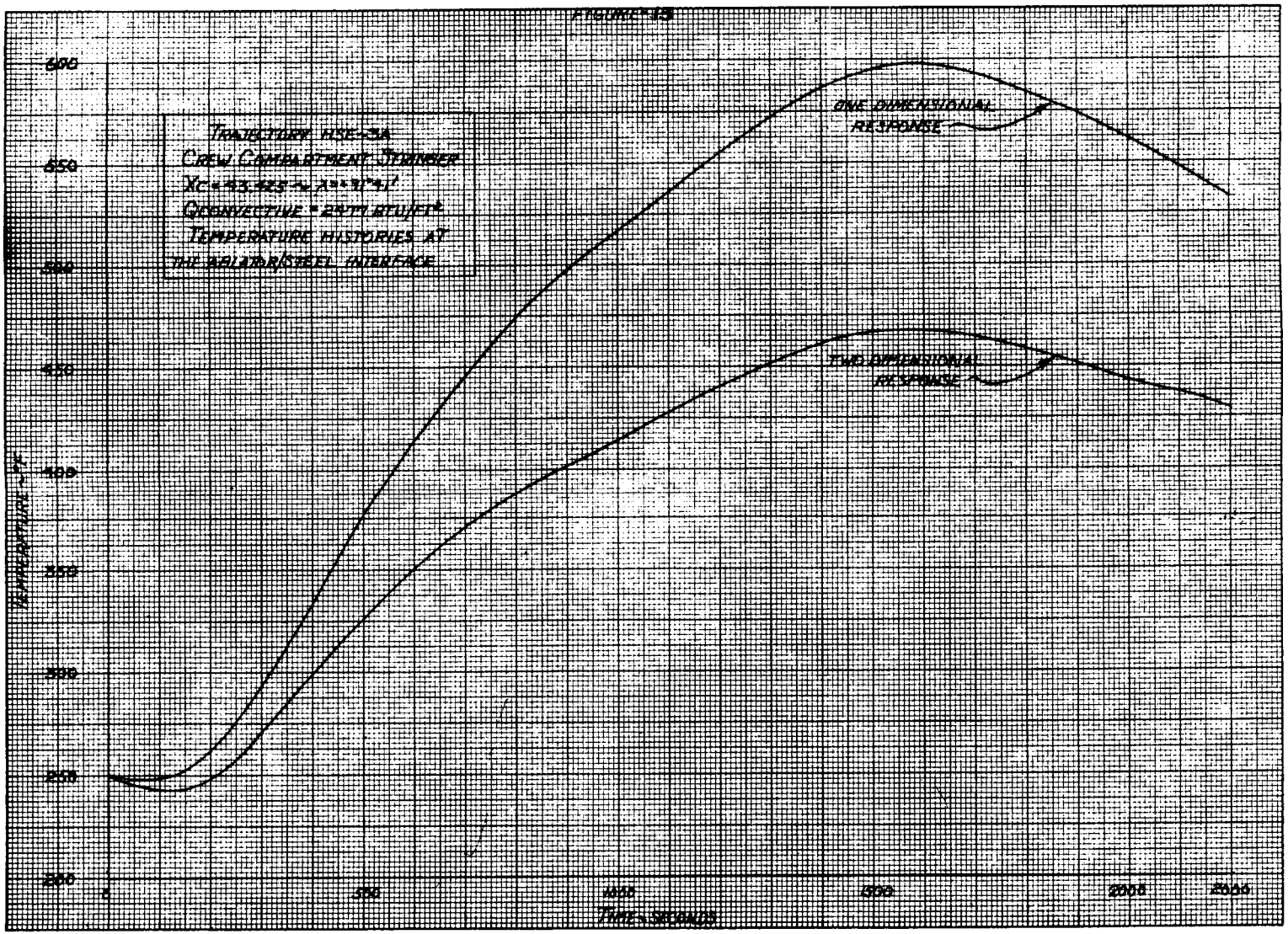

Figure 13 TRAJECTORY HSE-3A, CREW COMPARTMENT STRINGER

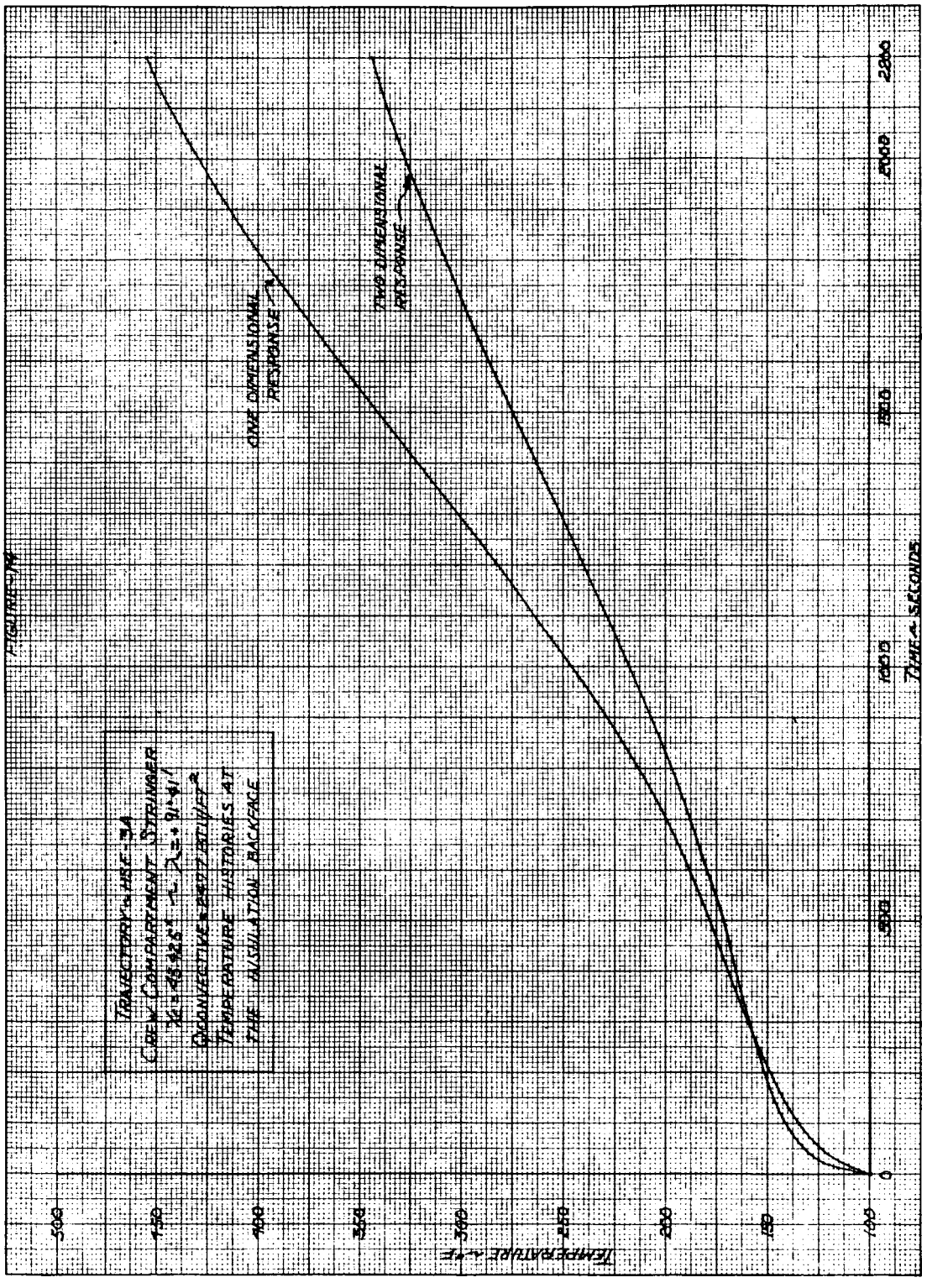

Figure 14 TRAJECTORY HSE-3A, CREW COMPARTMENT STRINGER

Since the stringer has a significantly higher thermal capacitance than the surrounding materials, it tends to depress temperature responses in its proximity throughout almost the entire heat shield composite. Figures 11 and 13 indicate that the maximum substructure temperature is reduced by approximately 130°F to 150°F. Figure 15 shows temperature gradients along the ablator-structure interface and parallel to the ablator surface which indicate that the major effect of the stringer is confined to a small distance (about 6 inches). Therefore, although the stringers produce large temperature effects, these are localized and cannot be considered as a major influence on the overall main ablator design.

1.2 Two-dimensional Areas

1.2.1 Abort Tower Well Ablator Restraints

A reanalysis of the floating ablator restraint was necessitated by the change of reference insert material from fiberglass to steel. The reanalysis was accomplished by a modification to the original mathematical model, described in the August Progress Report.

The substitution of steel for fiberglass did not significantly change the maximum substructure temperatures attained, but did increase slightly the slope of the substructure (well casting) time-temperature curve (figure 16) early in the trajectory. In comparison with one-dimensional design the structure temperatures are reduced roughly 50°F.

1.2.2 Rendezvous Window

A two-dimensional study of the rendezvous window at the aft edge of the well along the meridional centerline is complete. The configuration analyzed is shown on figure 17. Heating per SEM AVC 141 was used with the appropriate ablator reentry thicknesses. Changes in radiation view factors along the surface of the matrix were accounted for in the boundary conditions.

Substructure temperature responses, depicted on figure 18, show no overheating. These results demonstrate the effect of the heat capacity of steel members and the reinforced honeycomb face sheets which are not considered in basic one-dimensional design.

A two-dimensional analysis of the corner at the base of the rendezvous window well has been completed. This analysis, taken along the meridional centerline of the glass, when joined with previous well analyses provides a complete study of the temperatures in the well for trajectory HSE-3A. The -dimensional matrix configuration studied is shown on figure 19.

Temperature histories of the substructure (figure 20) indicate no temperature problems. It is apparent that the effect of the obtuse corner

angle is to reduce structure temperatures, as a surface area to structure area ratio of less than 1 exists. An additional reduction is produced by the well casting which has a higher heat capacity than a corresponding unit area of nominal substructure.

1.2..3 Abort Tower Attach Rod Analysis

A two-dimensional analysis of the tension tie rod was completed for a windward tower well location at X_c = 112.25 (θ = 47° 15') and a leeward well location at X_c = 112.25 (θ = 132° 45'). This analysis was performed for HSE-6 to investigate the effects of the high heat flux and associated surface recession in these areas. Results of the analysis indicate that temperatures do not reach 600° F for this trajectory.

1.3 Analytical Methods

1.3.1 Test Data Accuracy Analysis

Operating data for a variety of OVERS test runs was reduced in two different ways. In the first method, a straight-line correlation was assumed and a least squares fit obtained. In the second method, a second-order polynomial was utilized. Although the curvature is slight, the second method (figure 21) will be used for the accuracy analysis. The data points used were obtained operating with the same constant cooling water flow rate. However, they displayed considerable variation in air mass flow from run to run, inasmuch as these were normal runs and the flow rates had been chosen to produce desired environments. In order to obtain constant mass flow lines, the data was grouped about arbitrarily chosen mean values. It is apparent from figure 1 that any resultant errors in mean values are small.

1.3.2 TGA Data

TGA data reported in previous progress reports may be categorized by its temperature history. Most tests utilized a linearly increasing temperature, but three tests were made in which a linear temperature increase was followed by a constant temperature. The two resulting sets of data were analyzed separately using a constant char density. The "constant temperature" data was also analyzed using the previously reported char density-temperature function. The results of these analyses are presented in figures 22 and 23. It is readily seen that differences among the fits are small. However, at low temperatures, there is a consistent disparity between the fits and the data. Although this difference is small its effect should be investigated, since the long soak time on Apollo trajectories may make the effect significant.

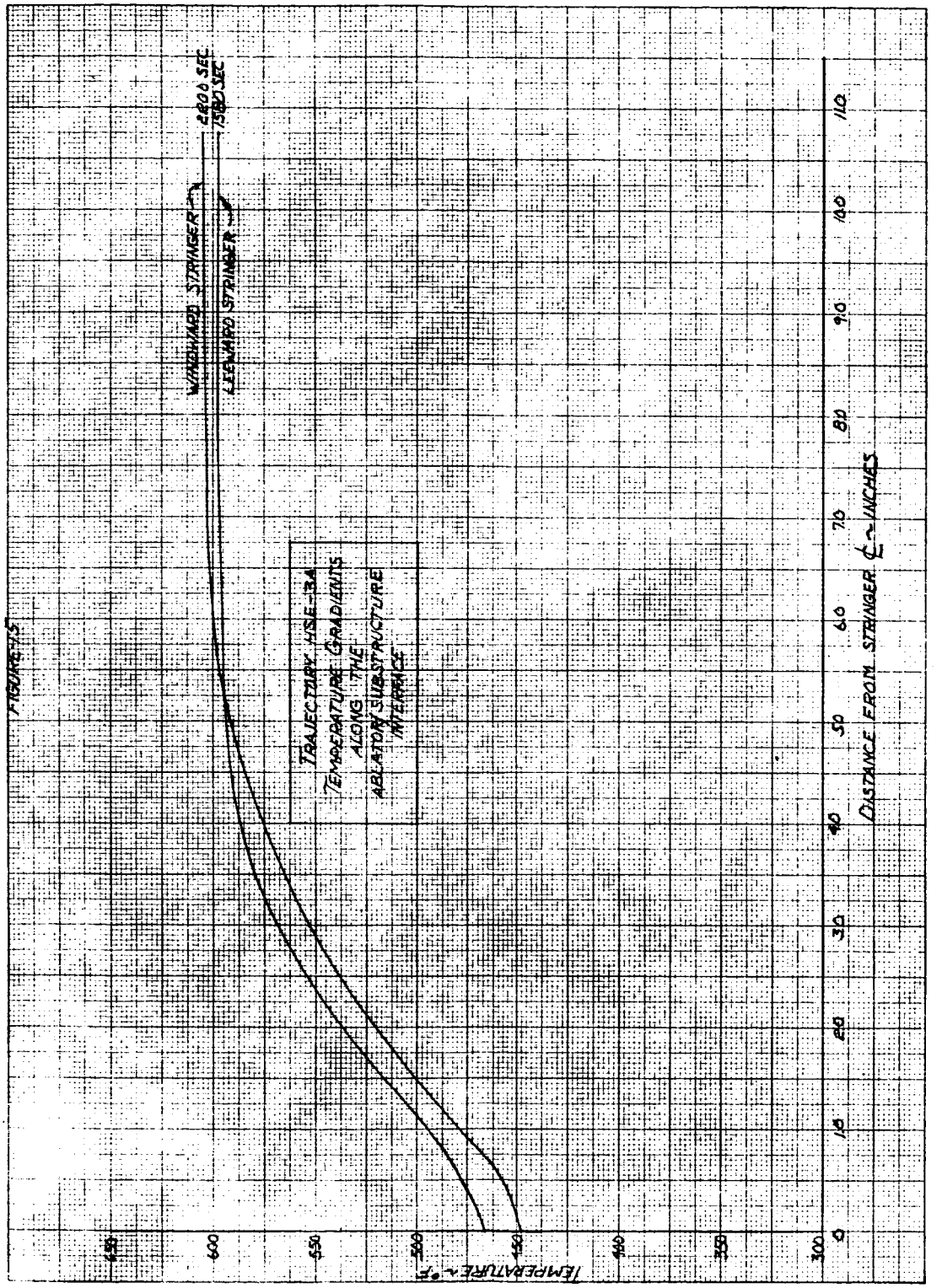

Figure 15 TRAJECTORY HSE-3A TEMPERATURE GRADIENTS

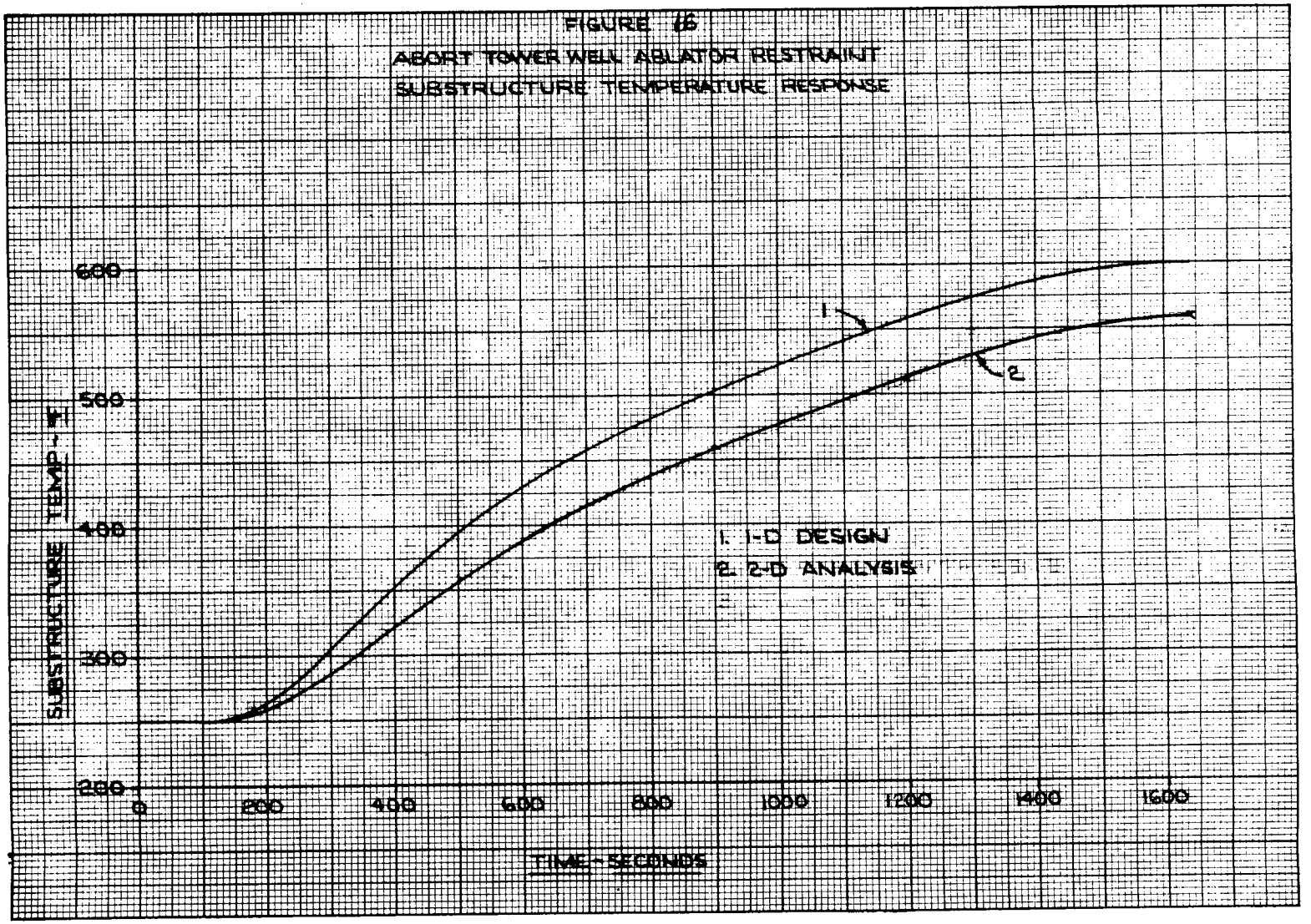

Figure 16 ABORT TOWER WELL ABLATOR RESTRAINT SUBSTRUCTURE TEMPERATURE RESPONSE

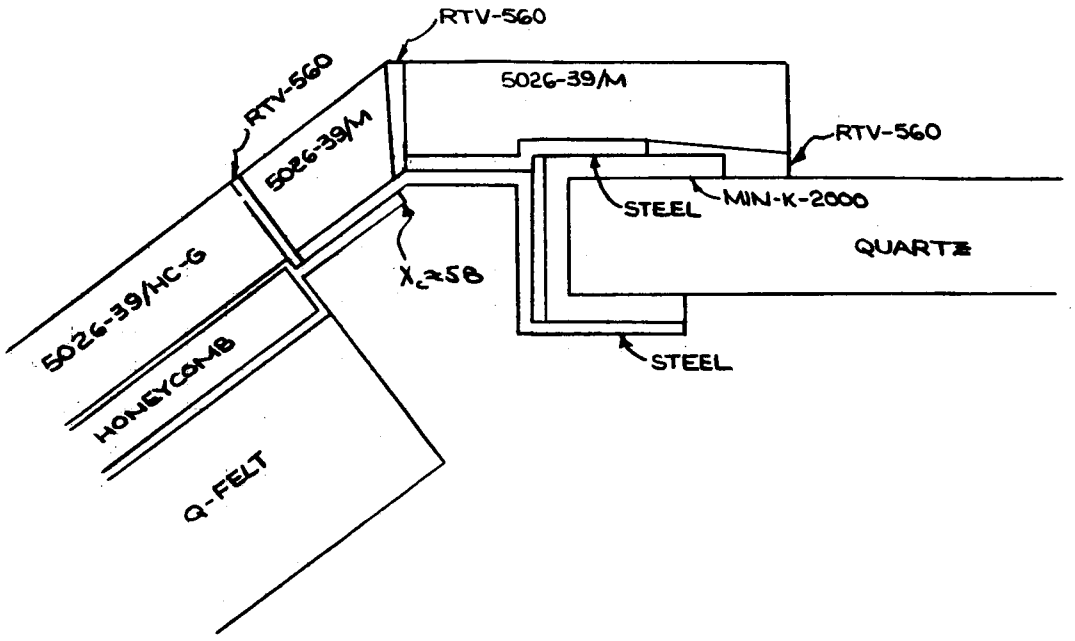

Figure 17 RENDEZVOUS WINDOW 2-D ANALYSIS CONFIGURATION

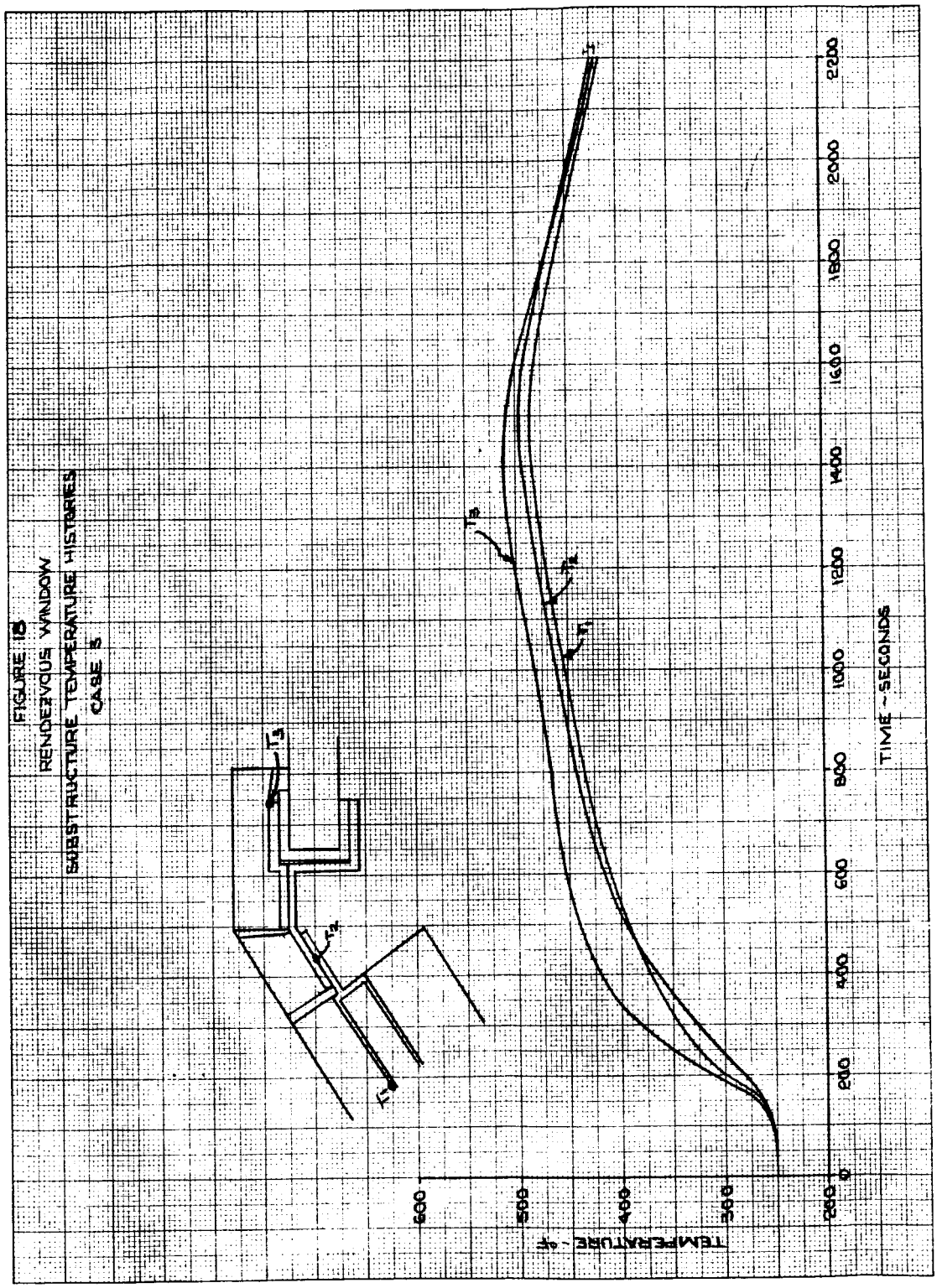

Figure 18 RENDEZVOUS WINDOW, SUBSTRUCTURE TEMPERATURE HISTORIES

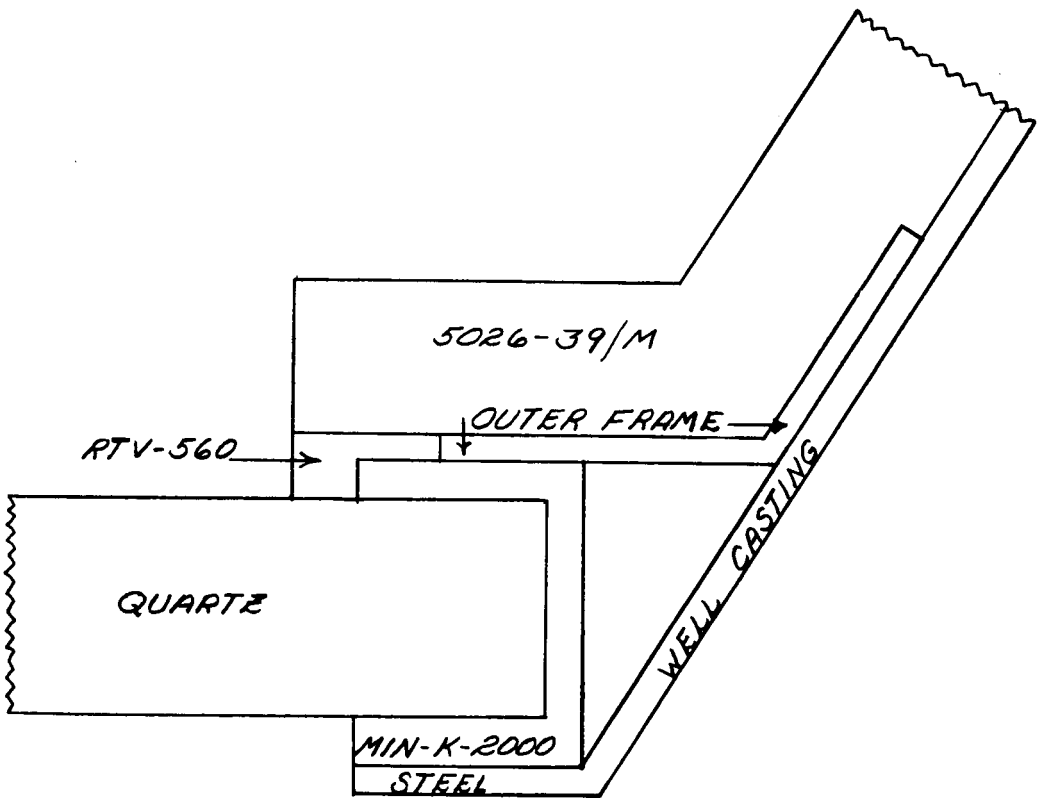

Figure 19 RENDEZVOUS WINDOW, 2-D ANALYSIS CONFIGURATION

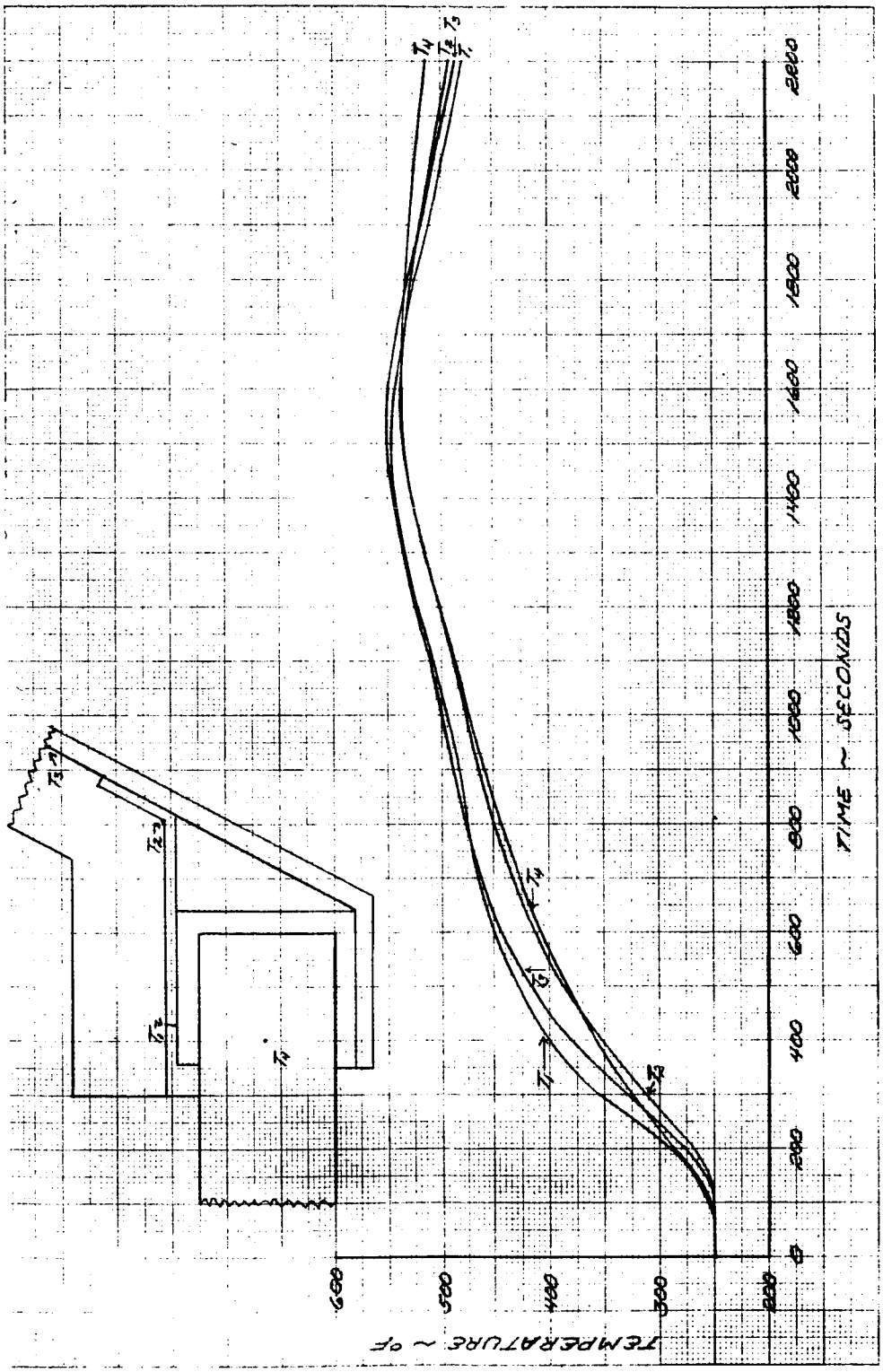

Figure 20 RENDEZVOUS WINDOW, SUBSTRUCTURE TEMPERATURE HISTORIES

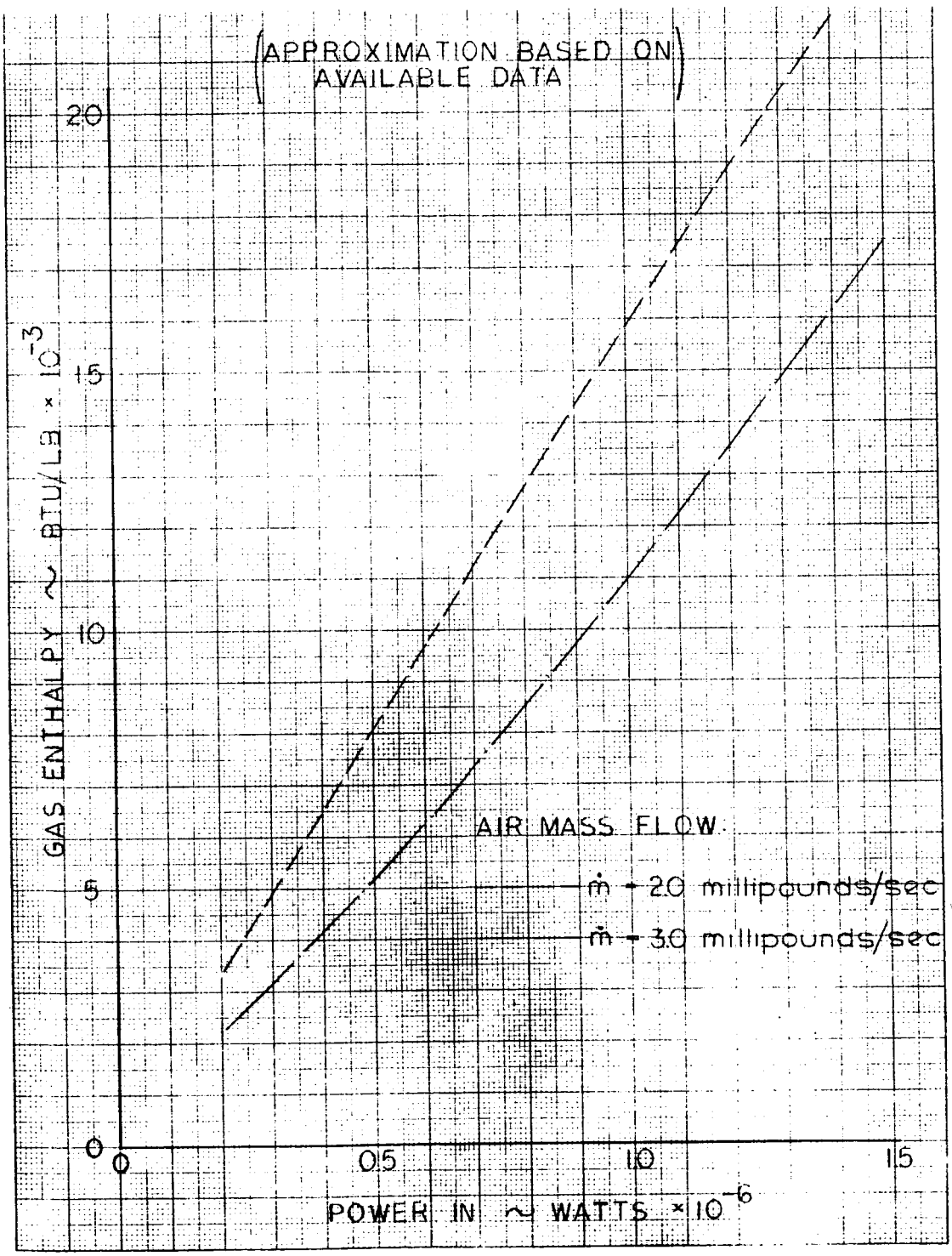

Figure 21 TYPICAL OVERS FACILITY OPERATING PARAMETERS

Figure 22 COMPARISON OF CONSTANT TEMPERATURE TGA DATA

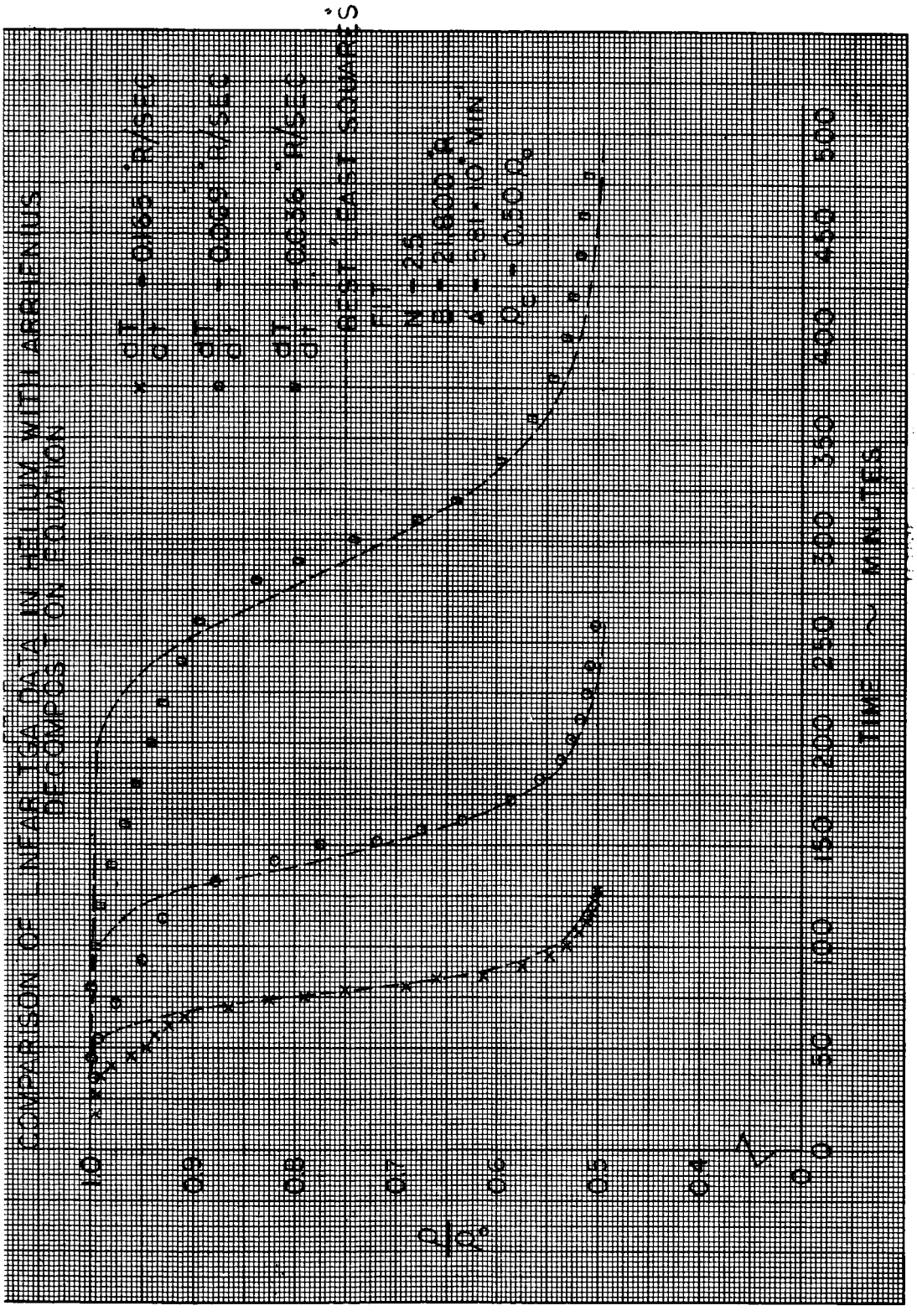

Figure 23 COMPARISON OF LINEAR TGA DATA

1.4 Test Planning and Analysis

1.4.1 Turbulent Thermochemical Heat of Ablation

Data from eleven turbulent pipe specimens tested in the 10 Megawatt facility were examined to determine the effect of varying shear levels (3 to 14 psf) on the ablation performance of Avcoat 5026-39/HC-G.

Each specimen was 4 inches in diameter, 5 inches long and had a 1.25-inch wall thickness. The 3-inch center test section of each specimen was fabricated from Avcoat 5026-39/HC-G while 1 inch on each end was Avcoat 5026-22. Weight loss measurements taken from these specimens were adjusted to account for the presence of the Avcoat 5026-22 material.

The turbulent thermochemical heat of ablation (Q_T^*) of Avcoat 5026-39/HC-G was calculated for each specimen. Figure 24 is a plot of the variation of Q_T^* with enthalpy (the small figure beside each point is the shear level in psf). Figure 24 indicates that Q_T^* decreases with an increase in shear level. A variation in shear level from 3 to 7 psf results in a 5 percent decrease in Q_T^*. A further increase in shear level from 7 to 13 psf results in a 20 percent decrease in Q_T^*.

1.4.2 Weight Loss Measurements -- OVERS Splash

A method for determining weight loss from OVERS splash specimens is being studied. Weight loss will be determined from the difference between pre- and lost-test weights of a 3/4-inch diameter core taken from the center of the specimen. The pretest weight will be determined from the measured density and pretest thickness of the specimen.

1.4.3 Radiant Lamp Test -- Oxidizer Dump

Three radiant lamp tests have been planned to verify the two-dimensional design technique used at the oxidizer dump-main ablator interface. A panel of gunned material, instrumented in depth, will serve to define main ablator one-dimensional temperature histories. A second panel, molded material instrumented in depth, will be used to supply temperature histories as defined by NAA. Temperature measurements from the third panel, a composite of the first two panels and representing the oxidizer dump area, will be used to verify the current two-dimensional design technique. Panel thicknesses have been determined using the one-dimensional design analysis (Program 1327).

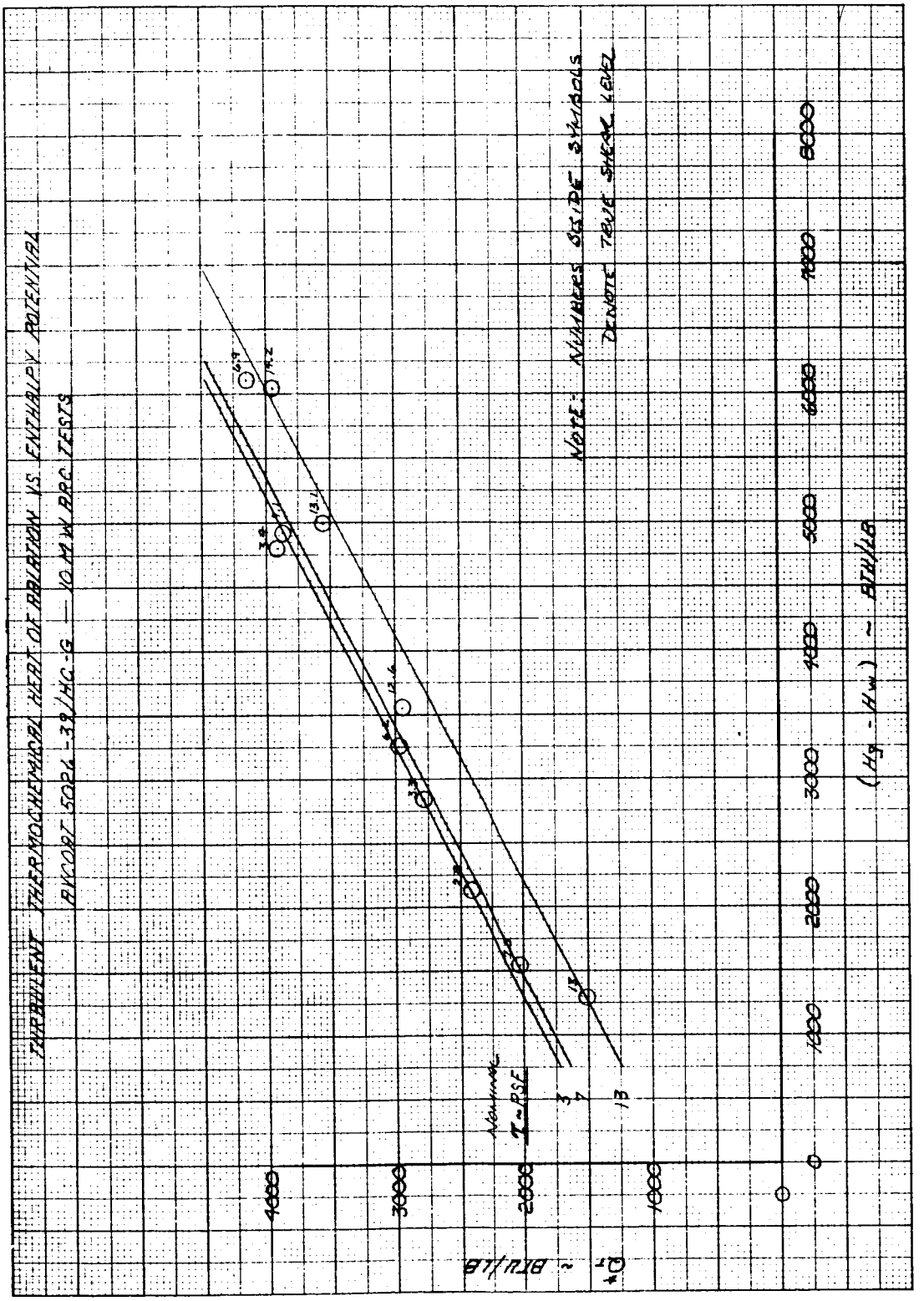

Figure 24 TURBULENT THERMOCHEMICAL HEAT OF ABLATION VERSUS ENTHALPY POTENTIAL

1.4.4 Trajectory Simulation in the OVERS Facility

The results of 2 trajectory simulation tests indicate that it is possible to closely simulate HSE-3A reentry enthalpy and convective heat flux in the OVERS facility. Because shear forces are small during this reentry trajectory, it is possible to apply the results of trajectory simulation tests directly to the Apollo mission.

Requirements for the trajectory simulator were determined after examination of the convective heat flux and enthalpy histories defined for HSE-3A reentry. It was decided that these parameters may be approximated by dividing the trajectory into four zones of constant enthalpy and varying the heat flux in 5 steps (see figure 25).

Because of the availability of 2-1.6 inche thick by 3.5 inch diameter OVERS splash specimens (instrumented in depth) the test conditions were designed to approximate those occurring at body station 103 during HSE-3A reentry. Figure 26 shows that the actual test conditions were in close agreement to those specified for the test as defined in Table III.

The test temperature and ablation data were compared with values predicted using the design procedure. Results of this comparison are plotted in figure 27 which shows that the design procedure is conservative when compared to the measured test data. Temperatures predicted by Program 1327 are consistently higher than the measured temperatures, by 10 percent at 0.3 inch to 50 percent at 1.0 inch in depth.

Length loss comparisons indicate that the average length loss from these two specimens (ΔL = 0.27 inch) is in close agreement with the length loss predicted by Program 1327 (ΔL = 0.21 inch).

1.4.5 HT-424 Tape Splice Evaluation

Two standard turbulent tube specimens were fabricated from Avcoat 5026-39/HC-G. These tubes contained a longitudinal HT-424 tape splice (reference design) and were tested to determine the performance of this type of splice under high heat flux and high shear conditions. Post-test observations of these specimens indicate that there is no serious aggravation of the main ablator cause by this type of splice.

1.4.6 Gasket Material Study -- Radiant Lamp Facility

Two flat panels, each containing three gasket materials (RTV-560, K-1205, and Teflon) were tested in the radiant lamp facility. A two-dimensional heat transfer analysis has been performed using Computer Program 1459 and the results compared with experimental data.

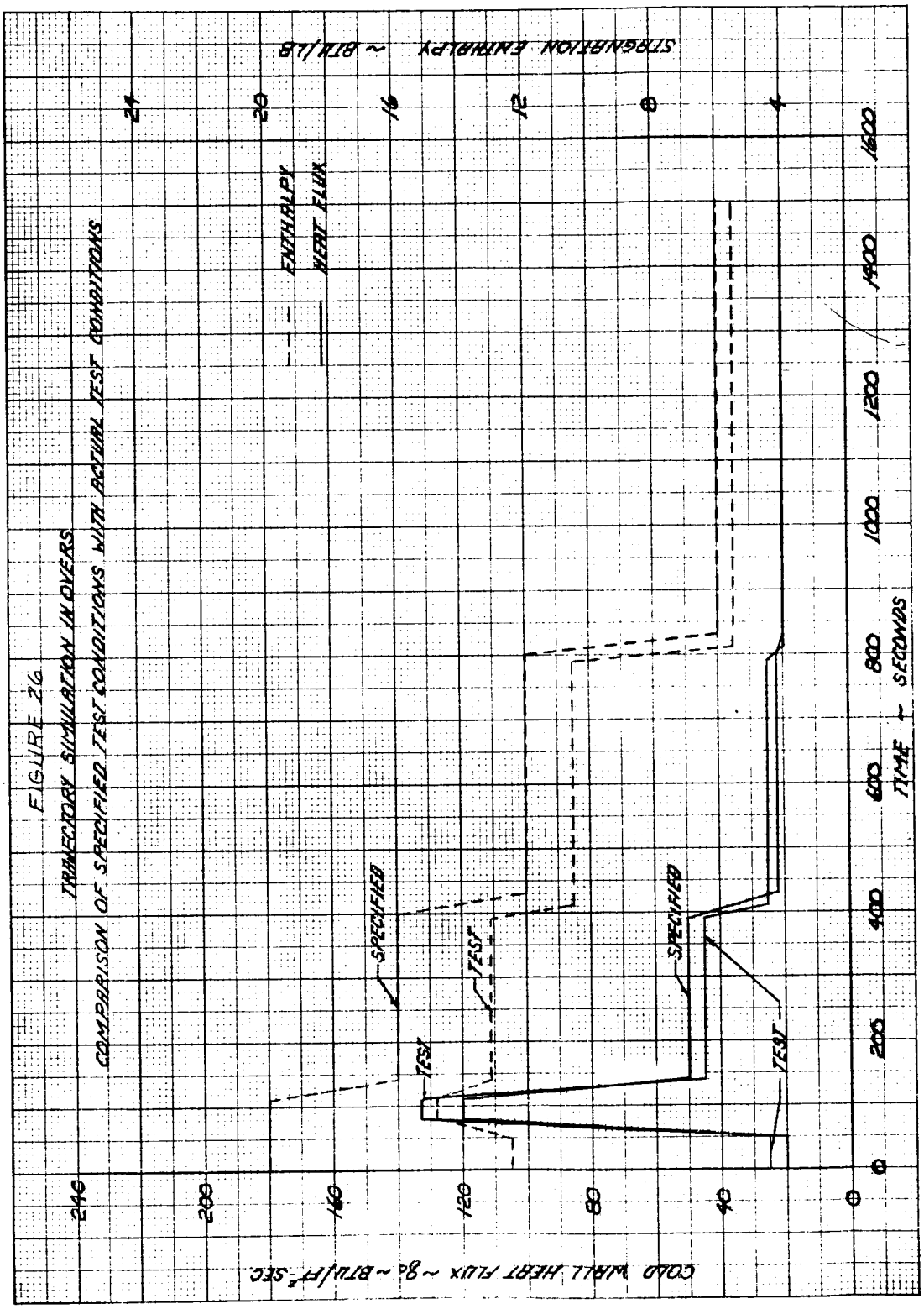

Figure 26 TRAJECTORY SIMULATION IN OVERS

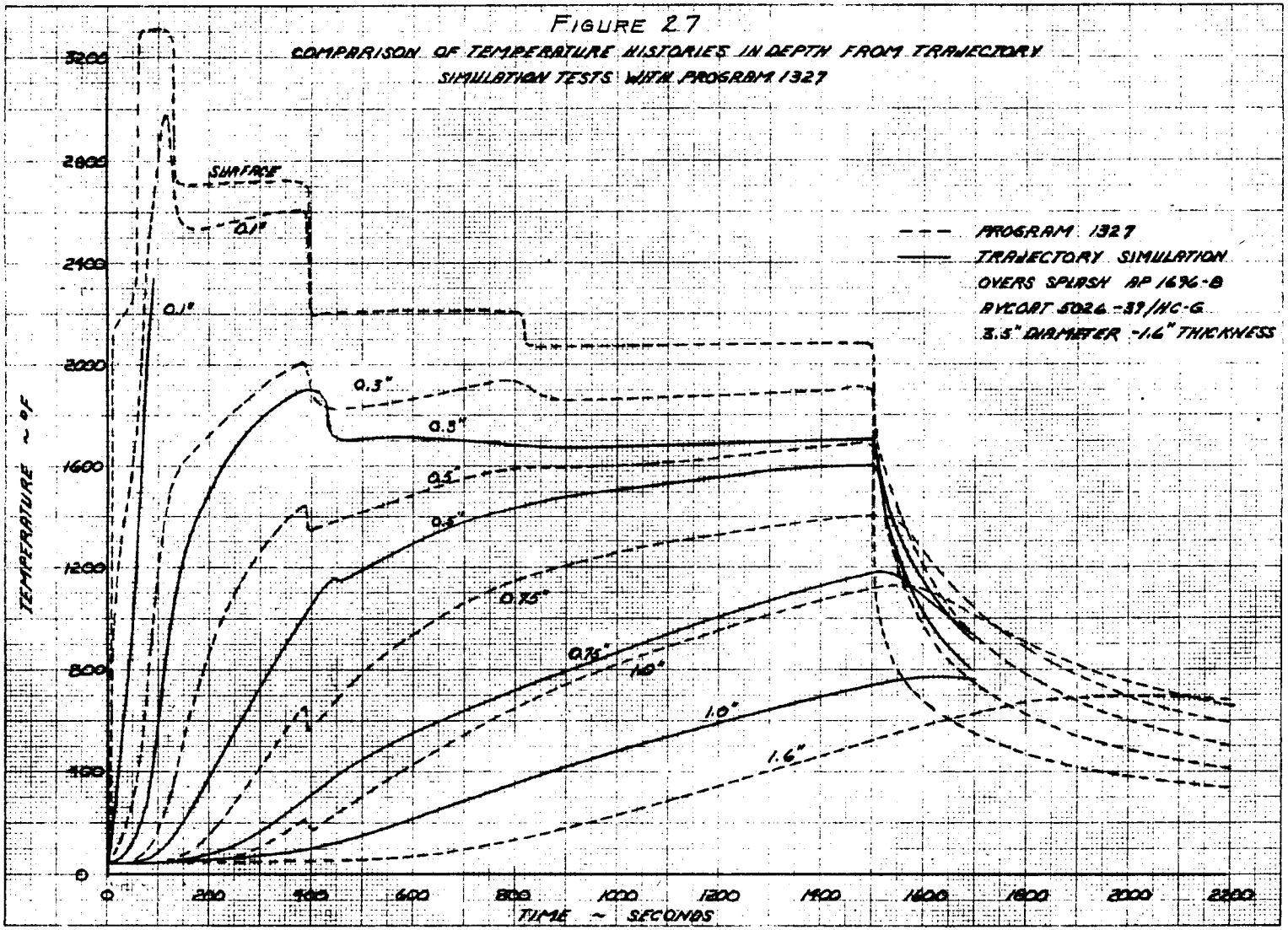

Figure 27 COMPARISON OF TEMPERATURE HISTORIES IN DEPTH FROM TRAJECTORY

Figure 28 shows this comparison for the reference gasket material, RTV-560. Analytical results are in close agreement with measurements throughout the entire trajectory. Temperature measurements below the RTV-560 show no significant increase in substructure temperature compared to the adjacent ablator material. Further analysis will be performed to evaluate the effect of RTV-560 filled-gap thickness on substructure thermal response.

1.4.7 Emissivity Data -- Avcoat 5026-39/M and Avcoat 5026-39/HC-G

An analysis has been completed of measurements of surface temperature and re-radiative flux obtained during ablation of Avcoat 5026-39/M and Avcoat 5026-39/HC-G in the OVERS arc. Measurements were made using an optical pyrometer and an Eppley Thermopile.

Emissivity values for the molded material fell with ± 8 percent of the average as shown in figure 29. The corresponding deviation for the gunned material was less than ± 15 percent. This scatter in the values of emissivity is not considered to be extreme because of the sensitivity of this parameter to the measurement of surface temperature. An example of this can be seen in figure 30. Assuming a re-radiative heat flux of 40 Btu/ft^2-sec and a surface temperature of 3000°R, an error of only 3 percent in T_s will result in a 15 percent error in emissivity. It is concluded that the scatter found in the data is within the accuracy limits of the instrumentation. Results show that the average emissivity of the molded and gunned materials is 0.89 and 0.81, respectively.

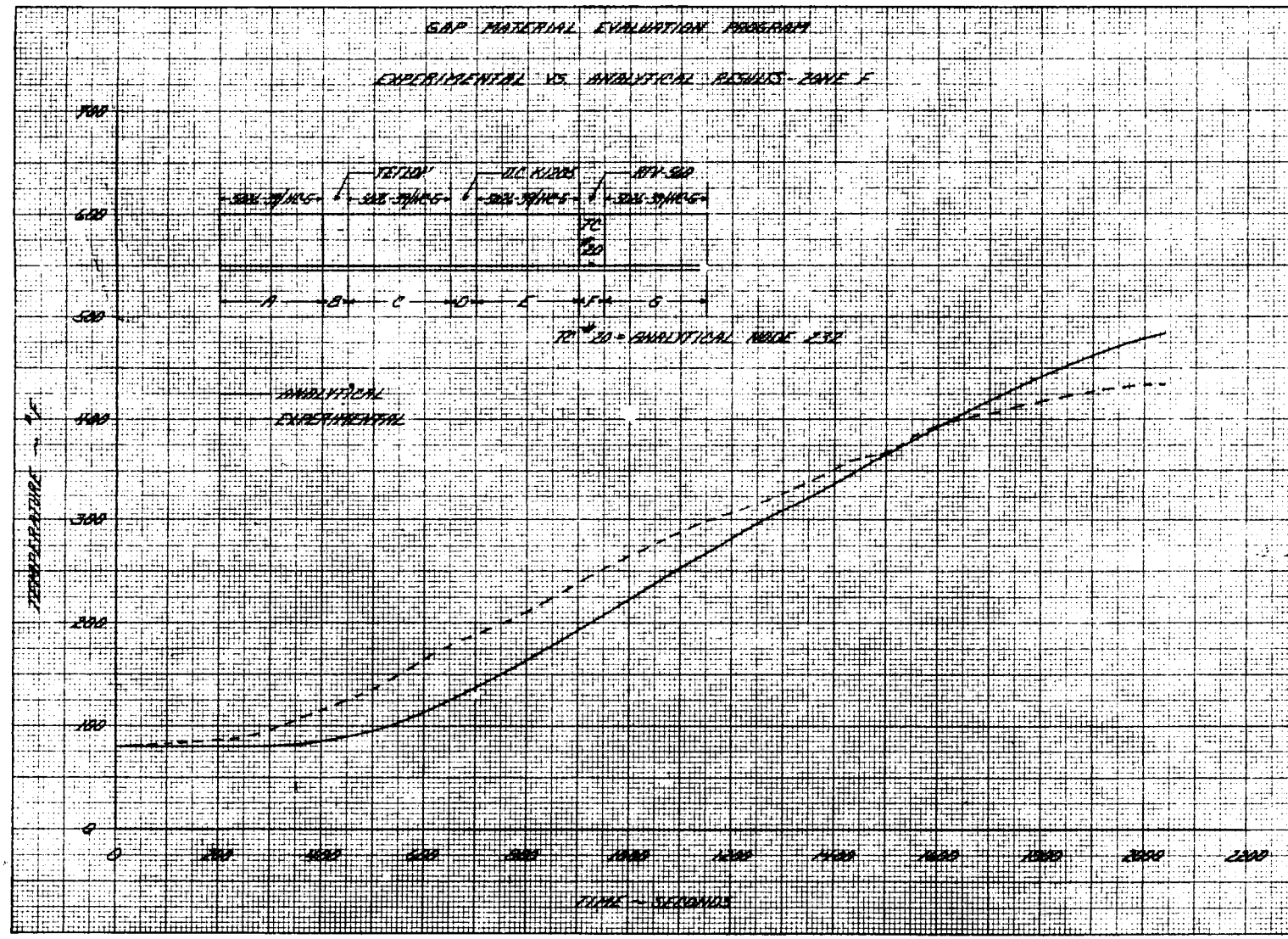

Figure 28 GAP MATERIAL EVALUATION PROGRAM

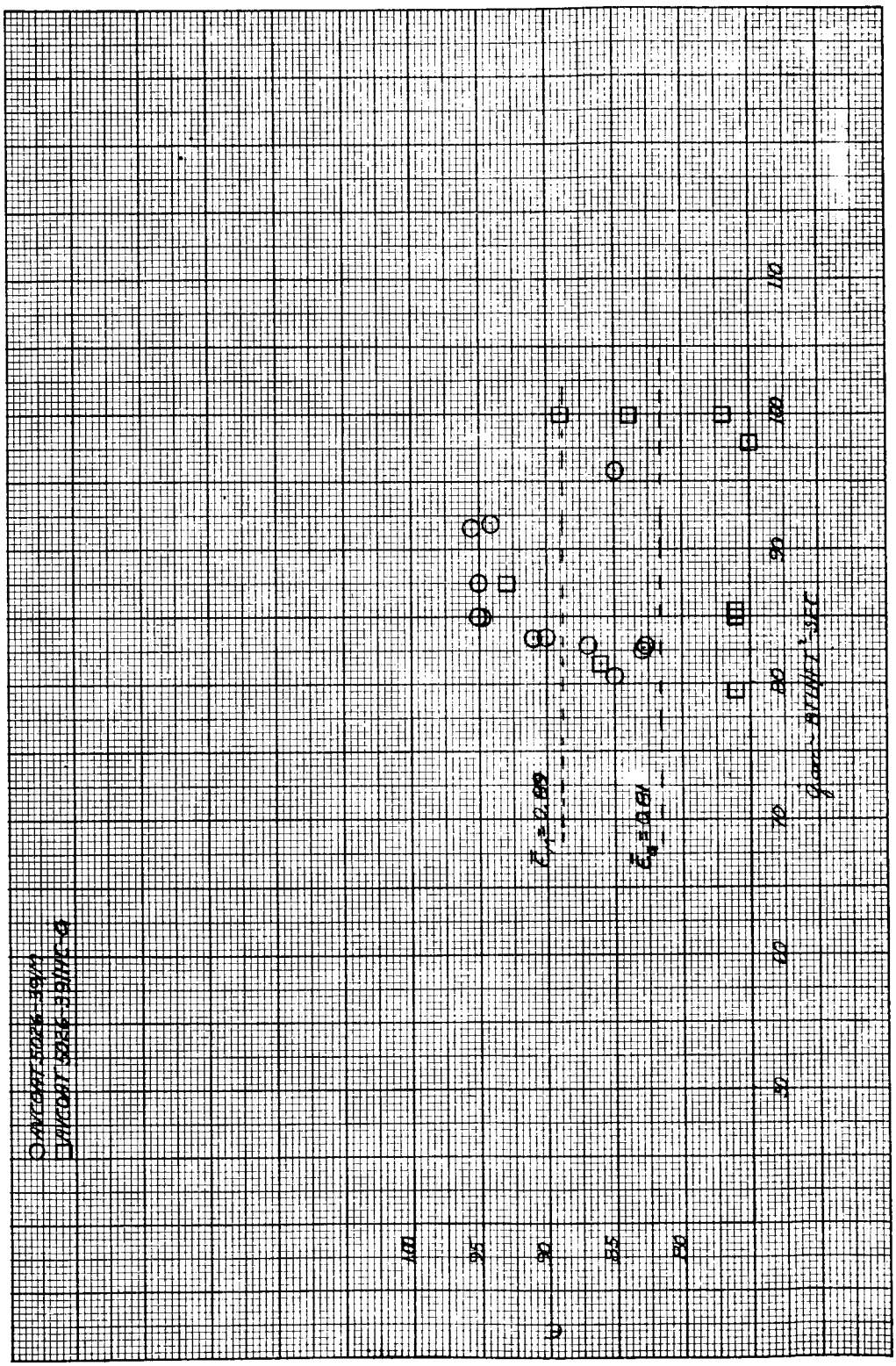

Figure 29 EMISSIVITY VERSUS HOT WALL FLUX FOR AVCOAT 5026-39/M

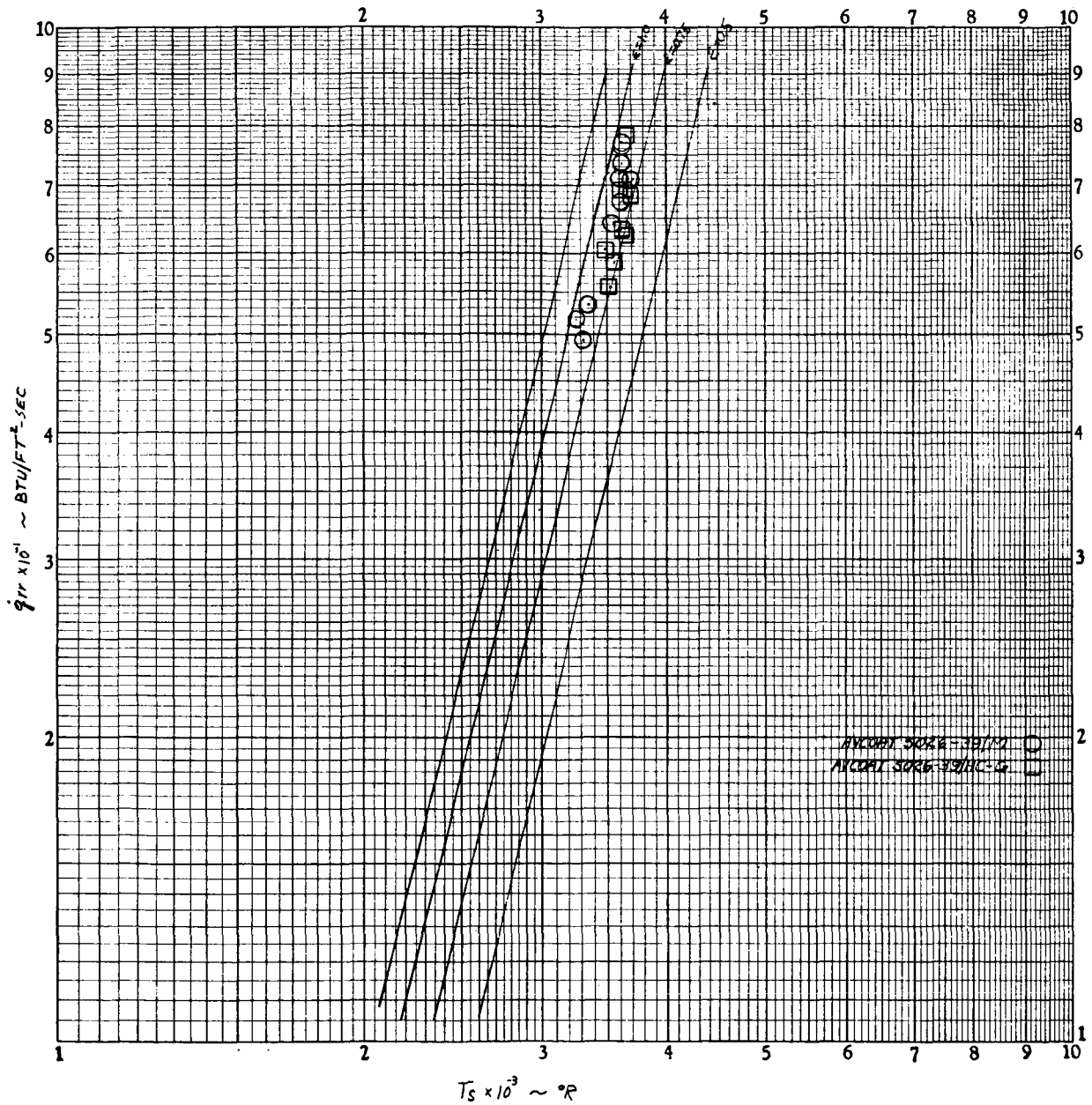

Figure 30 MEASUREMENTS OF RE-RADIATED HEAT FLUX AND SURFACE TEMPERATURE IN OVERS

B. STRUCTURES

2.0 Structural Analyses

By direction from NAA/S&ID the low temperature for the Apollo command module heat shield has been changed from -260° F to -150° F, and consequently all analyses for the -260° F environment have been stopped except for a few studies where a method of analysis is being checked. The work completed or in progress at the time of the change is described below. Current primary structural effort is concerned with completing the analyses for the final stress report on Airframes 006, 009, 008, and 011, and with providing structural support for the fabrication of the ablator on Airframe 006. Since the change in environment is so recent, no results of the current analyses are available. The analyses themselves are described below.

2.1 Forward Compartment Analyses

Thermostructural analyses of the forward compartment have been initiated for the soak environments of -150° F and +250° F to determine the deformations, stresses, and strains in the unperturbed shell. The analyses will be performed using the 1322 orthotropic shell program. The rotationally symmetric model selected consists of a closure ring at X_c = 81 and 112, 0.008 inch face sheets, and thickened lands with the 0.60 inch honeycomb core up to X_c = 133.5 for the substructure. Two ablator meridional variations will be analyzed for each condition which are intended to represent the windward and leeward sides of the command module. The meridional ablator variations are the average thicknesses for each half of the command module found on Avco drawing 401098, Revision E. The discontinuity at X_c = 112.25 between the forward compartment and the nose cone will be assumed to have only deflection compatibility since the six bolts will transfer very little moment. The analyses will reflect interactions with the crew compartment and inner structure, if they occur.

2.2 Crew Compartment Analyses

2.2.1 Rotationally Symmetric Shell Analyses

A series of investigations of the crew compartment, considered as a rotationally symmetric structure, have been started to determine general deformation behavior of the heat shield, stresses in the ablator and steel, and the interactions or gaps between compartments. Avco's program 1322 for symmetrically loaded thin orthotropic shells of revolution is being used for the investigation. Analyses are currently being performed for soak conditions of +250° F, -60° F, and -150° F. Each of the above loading conditions is being analyzed for both windward and leeward ablator thicknesses. The meridional ablator thickness distribution

representing the windward and leeward meridian was calculated at 10-inch X_c increments as the numerical average of a 60° segment on the windward and leeward sides of the vehicle. This procedure for calculating ablator thickness is used to eliminate peak thicknesses due to perturbations in the structure.

The steel substructure considered for the analyses consists of the closure rings at X_c = 23 and X_c = 81, the ring at X_c = 43, and the honeycomb panels having 0.008 face skins with thickened lands. Analyses using the leeward ablator thickness have a continuous discontinuity at approximately X_c = 31 and X_c = 43 to represent the structure along the edge of the maintenance panels.

The analyses are being performed with and without the effects of the frames in the region from X_c = 23 to X_c = 43. With the frames included, longitudinal displacement of the heat shield is assumed to be prevented by the most forward and most aft frame bolts. The resulting loads necessary to restrain the heat shield will be applied to the frames to determine maximum stresses.

2.2.2 Crew Hatch Analyses

The crew hatch analysis to determine hatch deflections, latch loads, and window interactions for -260° F soak as described in the 11 August 1964 Monthly Progress Report was continued to include the flexibility of the shell structure. Two ring analyses from X_c = 37.4 to X_c = 58.2 and from X_c = 58.2 to X_c = 81.1 were made using the 1095X ring program to determine the free deflected shape and influence coefficients for the circumferential edges of the crew hatch shell cutout. The deflections and influence coefficients for the meridional edges of the shell cutout were calculated using a beam network analysis similar to the hatch analysis for a plate fixed on two sides, free on the edge representing the meridional edge of the cutout, and of sufficient length to dampen out the edge loads. Having the free deflected shape of the hatch and the shell and a system of influence coefficients, the loads necessary to insure contact between the shell and hatch at the latch locations were solved simultaneously. The latch loads are shown in figure 31. Compared to the latch loads reported in 11 August 1964 Monthly Progress Report, which considered a rigid shell structure, the maximum tensile latch load has been reduced by approximately 280 lbs. The final deflected shape of the hatch is found by applying the latch loads and the thermal loads to the hatch using the 1630 matrix program. The deformed shape of the hatch due to cooling from 70° F to -260° F soak while restrained by the latches is shown in figure 32.

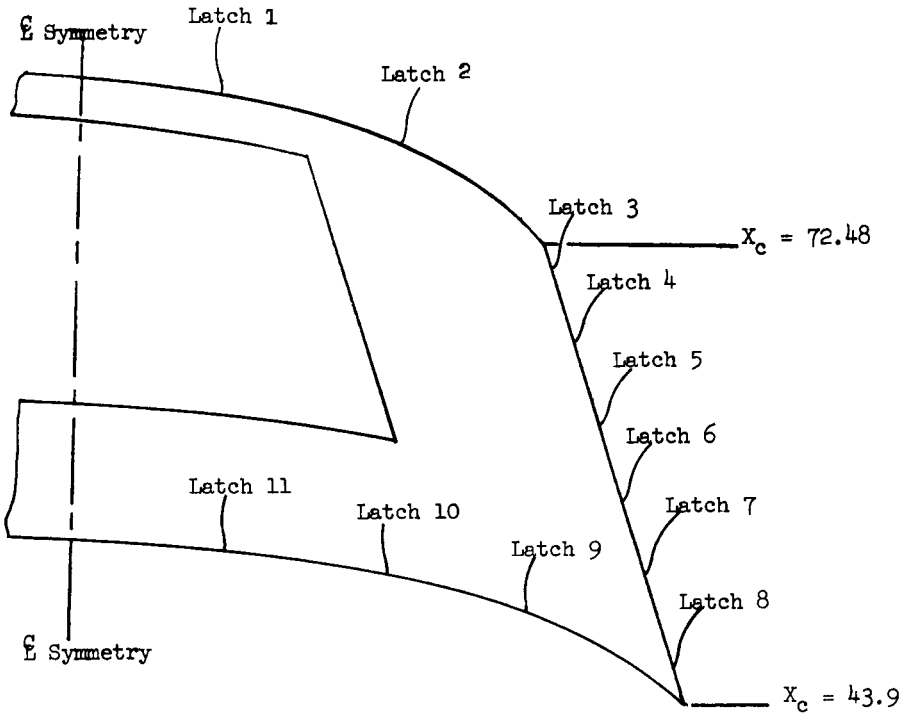

Latch	Radial Load
1	-46.26
2	-88.64
3	647.96
4	-514.52
5	40.55
6	135.92
7	-475.04
8	611.71
9	-70.7
10	-164.97
11	52.92

Positive Sign Indicates Tension

Figure 31 LATCH LOADS AT -260°F COLD SOAK FLEXIBLE SHELL

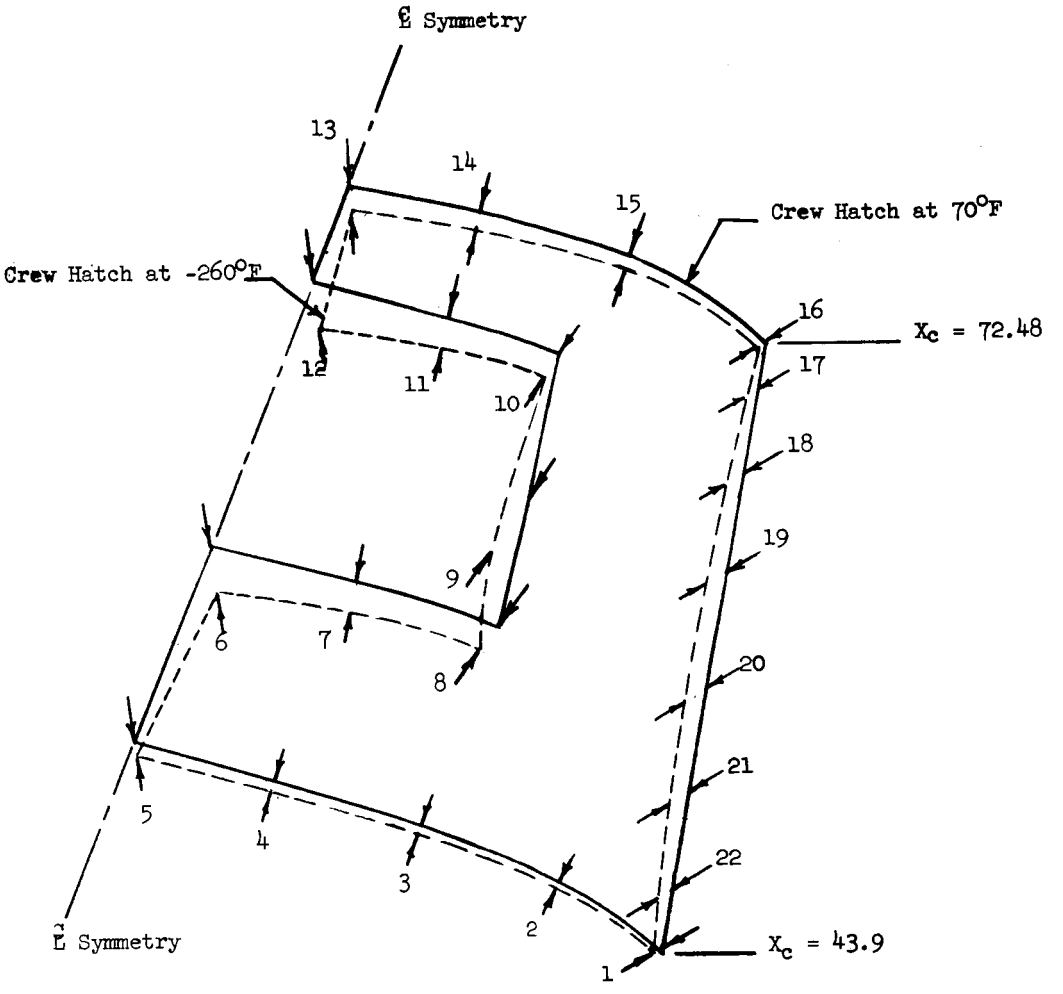

Point	Deflection
1	0.112
2	0.117
3	0.119
4	0.122
5	0.122
6	0.589
7	0.581
8	0.514
9	0.546
10	0.418
11	0.464
12	0.477

Point	Deflection
13	0.216
14	0.209
15	0.163
16	0.095
17	0.098
18	0.118
19	0.132
20	0.139
21	0.135
22	0.115

Figure 32 CREW HATCH DEFORMATION VEHICLES 006 AND 009 COOLING FROM 700°F TO -260°F SOAK

With the change in environment from -260° F to -150° F, the analyses described above are being re-done for the -150° F condition.

2.2.3 Side Window

At the time of the change in environment from -260° F to -150° F, deflections of the side window frame due to the distortions of the heat shield structure had been calculated for -260° F soak temperature and max. q tumbling abort. The analysis was for vehicles 006 and 009, in which the quartz window is mounted in a removable panel. The deflections of the window frames or the -260° F soak condition were calculated in two parts. First, the deflections of the circumferential edges of the window frame due to circumferential bending and extension were found using the 1095X ring program. Ring widths equal to the meridional length of the window panel above and below the window were used for the analysis. The ring above the window is supported by the tangential restraint of the slip stringers, while the ring below the window has infinite tangential restraint due to the shear web at X_C = 43. The vehicle was assumed to be symmetrical about the Z axis and, therefore, 180° of the structure was analyzed. The radial deflections of the rings are shown on figures 33 and 34. Secondly, the local deflections of the window frame edge were found from an analysis of an infinite plate fixed along two sides and free along the edge representing the window edge. Moments equal to the thermal edge moments were applied to the free edge and the deflections calculated using a finite difference approximation. The maximum deflection at the center of the window edge from the plate analysis was 0.011 inch radially outward. The results of the two analyses were superimposed to give the final deflected shape of the window frame, shown in figure 35. To determine the mismatch between the quartz window and the distorted window frame, the window was positioned to contact the frame at three locations. The resulting mismatches were calculated and are shown in figure 36. It is possible to rotate the window and establish contact at three other positions; however, the resulting mismatches will be of the same order of magnitude.

A similar analysis was done for the deflections of the side window frame due to max. q non-tumbling abort, and max. q tumbling abort with maximum pressure at both windward and leeward meridians. The most critical deflections of the side window occurred at max. q non-tumbling abort with maximum pressure on the leeward meridian.

Ring analyses similar to the -260° F soak condition were used for the abort condition. Ultimate pressures were used in the analysis with the pressure on the middle portion of the side window panel being carried equally by the upper and lower rings. At particular stringer locations, the deflections of the upper ring were larger than those allowed by the

slotted holes in the stringer, resulting in a bottoming condition. Using a system of influence coefficients, stringer loads were determined which when applied to the rings limited the deflections to that allowed by the slots. The deflections of the rings are shown in figures 37 and 38. The meridional edges of the window frame were assumed to remain straight but have deflections at the ends equal to the radial deflections of the rings. The final deflected shape of the window frame due to the max. q abort pressure and an ambient temperature of 125° F is shown in figure 39. With the window contacting the frame at three positions, the resulting window-frame mismatches are shown in figure 40.

2.2.4 Gaps Along Longitudinal Edges of Maintenance Panels

An analysis has been started to determine the maximum gap created at the outer surface of the ablator along the longitudinal edges of the maintenance panels due to circumferential bending of the heat shield. A unit ring at X_c = 33 is used to describe the behavior of the structure through approximately the center of the maintenance panels. The structure is assumed to be symmetrical about the Z_c axis, requiring only 180° of structure to be analyzed. The ring is being analyzed first with no restraint except bottoming in the frame slots and second with a tangential restraint representing the shearing capability of the structure back to the shear web at X_c = 43.4. Avco's 1095X ring program is being used for the analysis. Space flight environments being considered are -150° F soak and a circumferential temperature distribution varying from -150° F to +250° F.

2.3 Aft Compartment Analyses

2.3.1 Current Analyses

Analyses are now in progress for the following conditions:

(a) A linear temperature variation of -150° F at X_c = 20.0 at -85°K/X_c = 16.5

(b) Heating from low temperature distribution with sun normal to conic surface (windward side), using a temperature range of +238° F at X_c = 23.2 to -85° F at X_c = 0.

The -150° F (-85° F inside S/M) temperature variation case is being analyzed with and without eccentricity of reference surface. The solution for no eccentricity is complete and is being checked; the free thermal deformations are being calculated by computer program 1322 for the eccentricity problem.

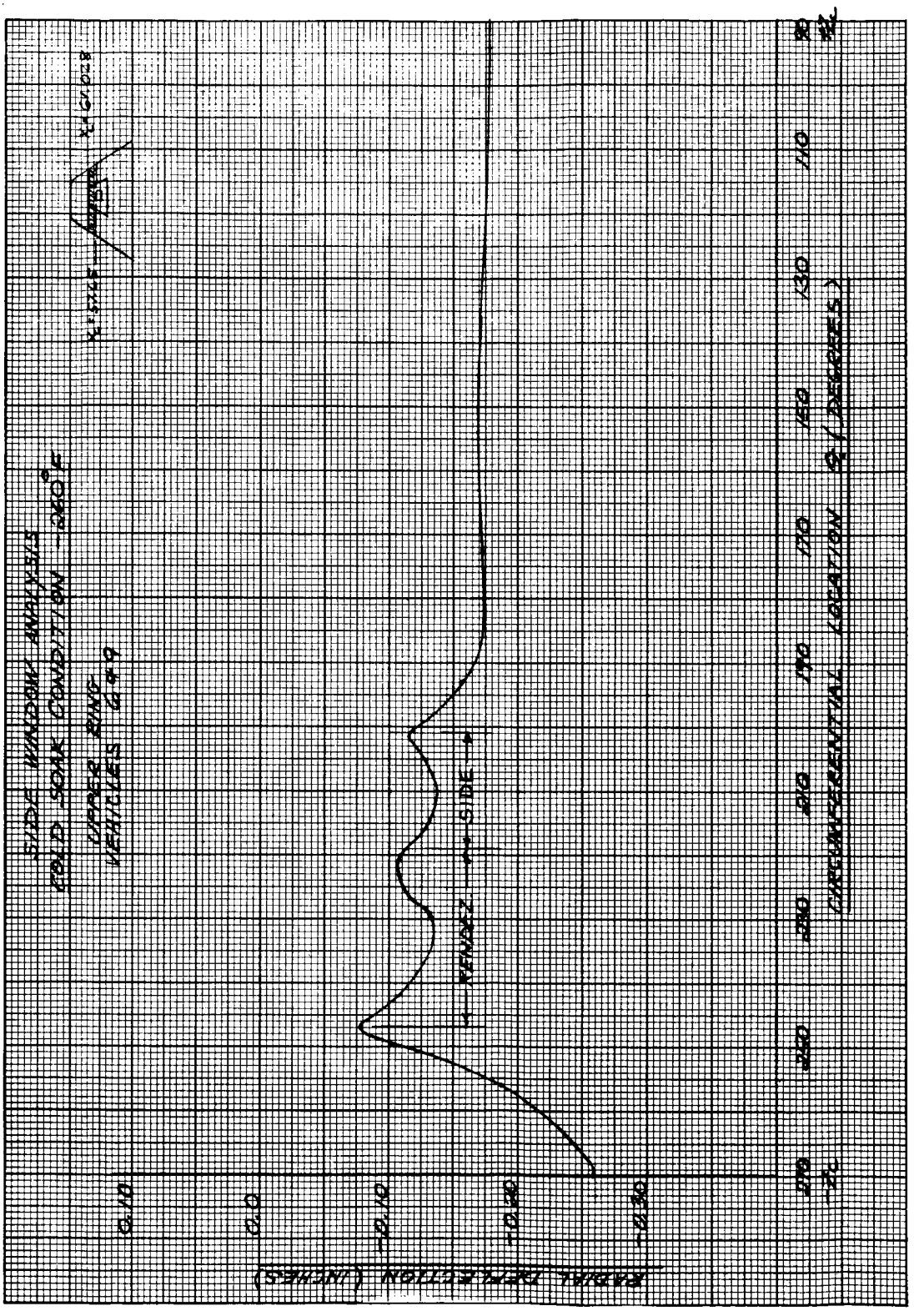

Figure 33 SIDE WINDOW ANALYSIS COLD SOAK CONDITION -260°F

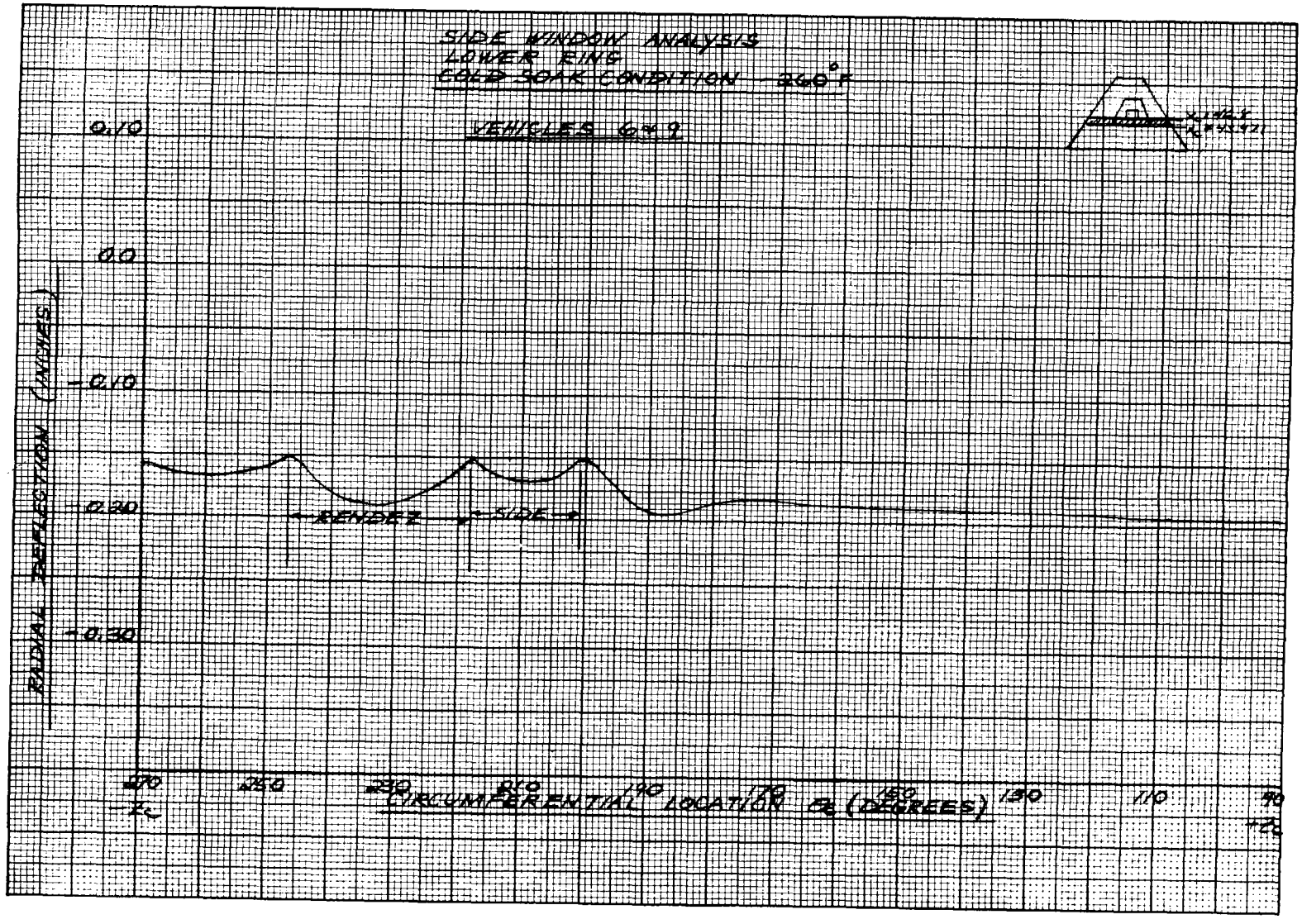

Figure 34 SIDE WINDOW ANALYSIS COLD SOAK CONDITION -260°F
LOWER RING

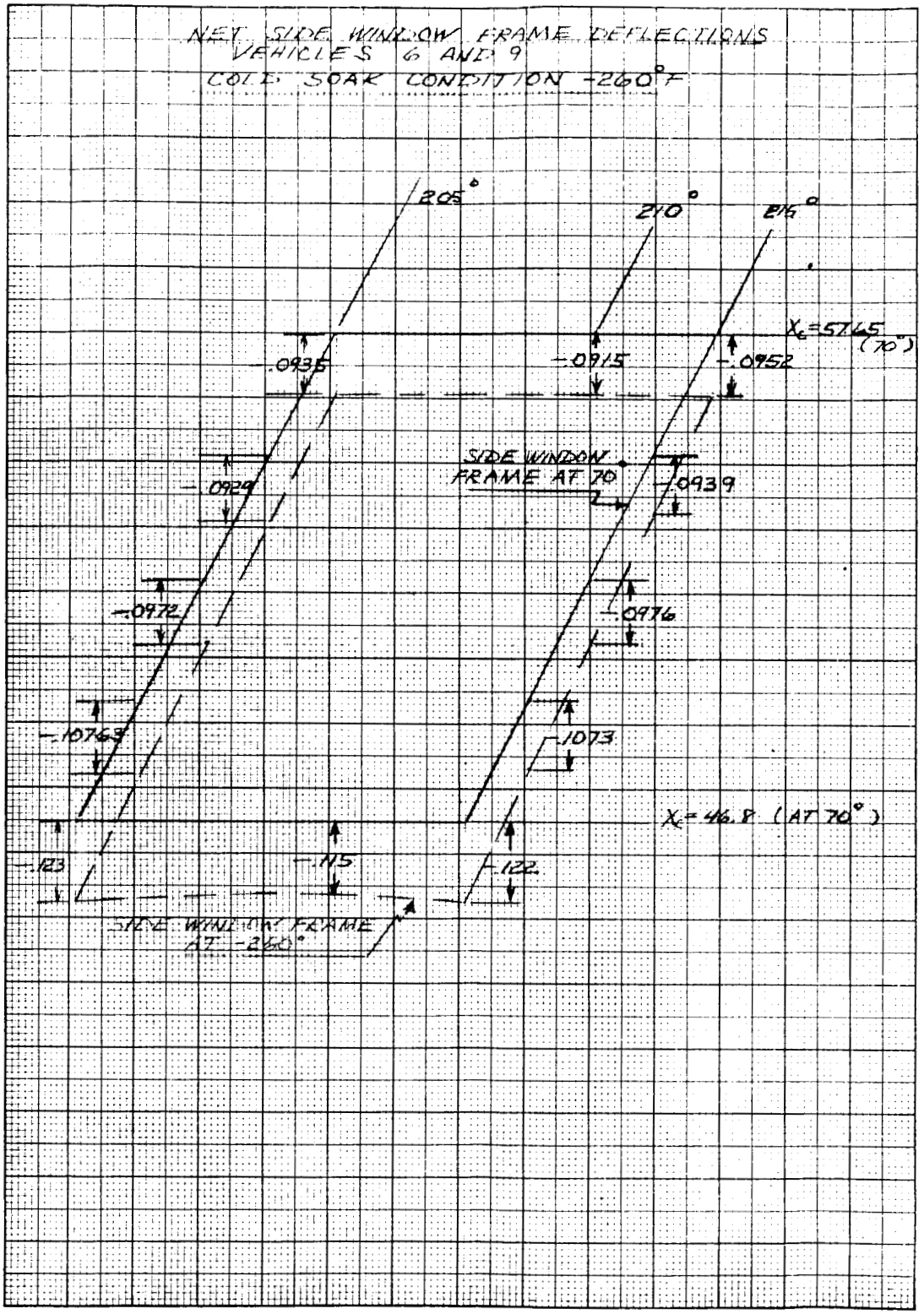

Figure 35 NET SIDE WINDOW FRAME DEFLECTIONS VEHICLES 6 AND 9

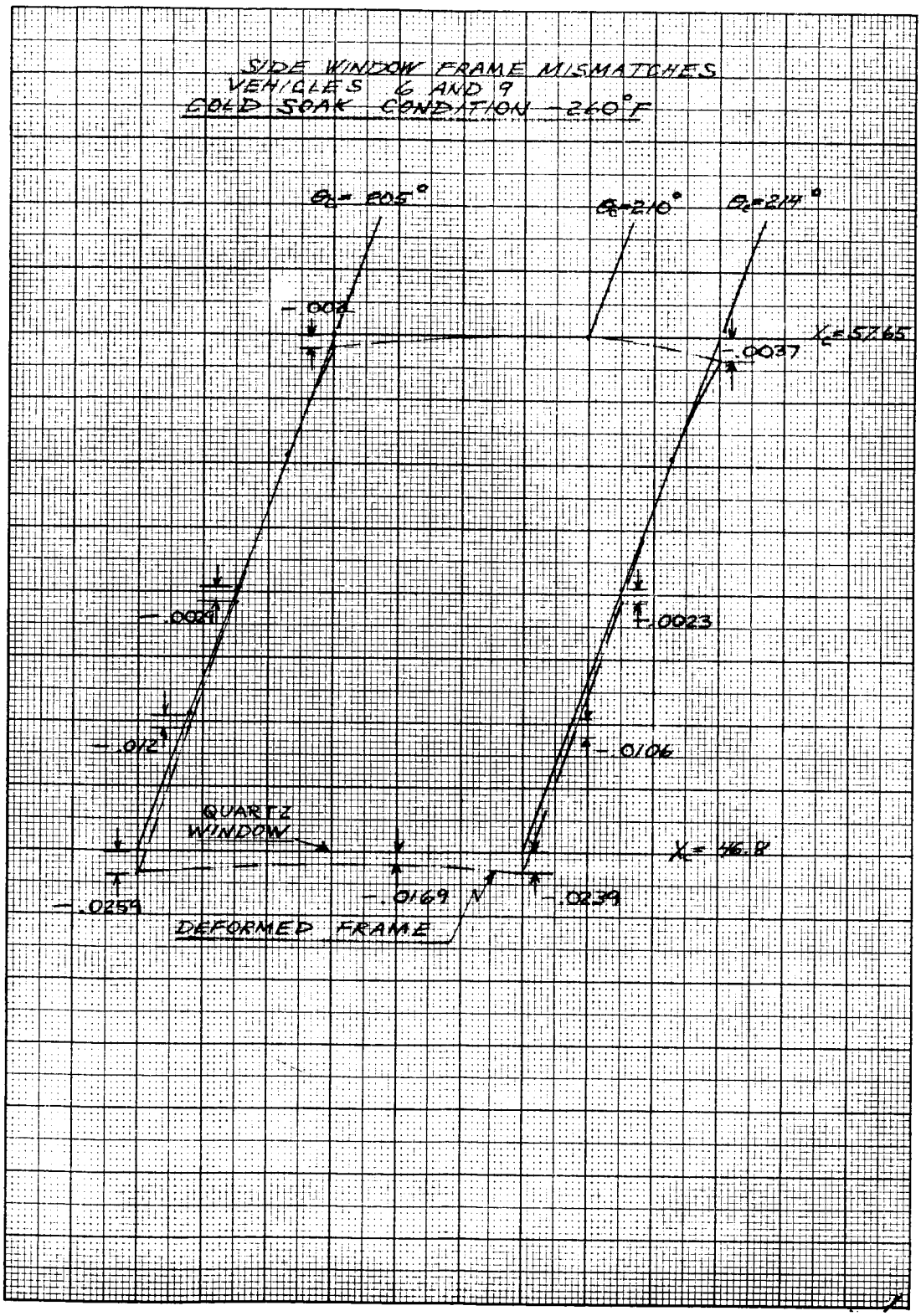

Figure 36 SIDE WINDOW FRAME MISMATCHES VEHICLES 6 AND 9

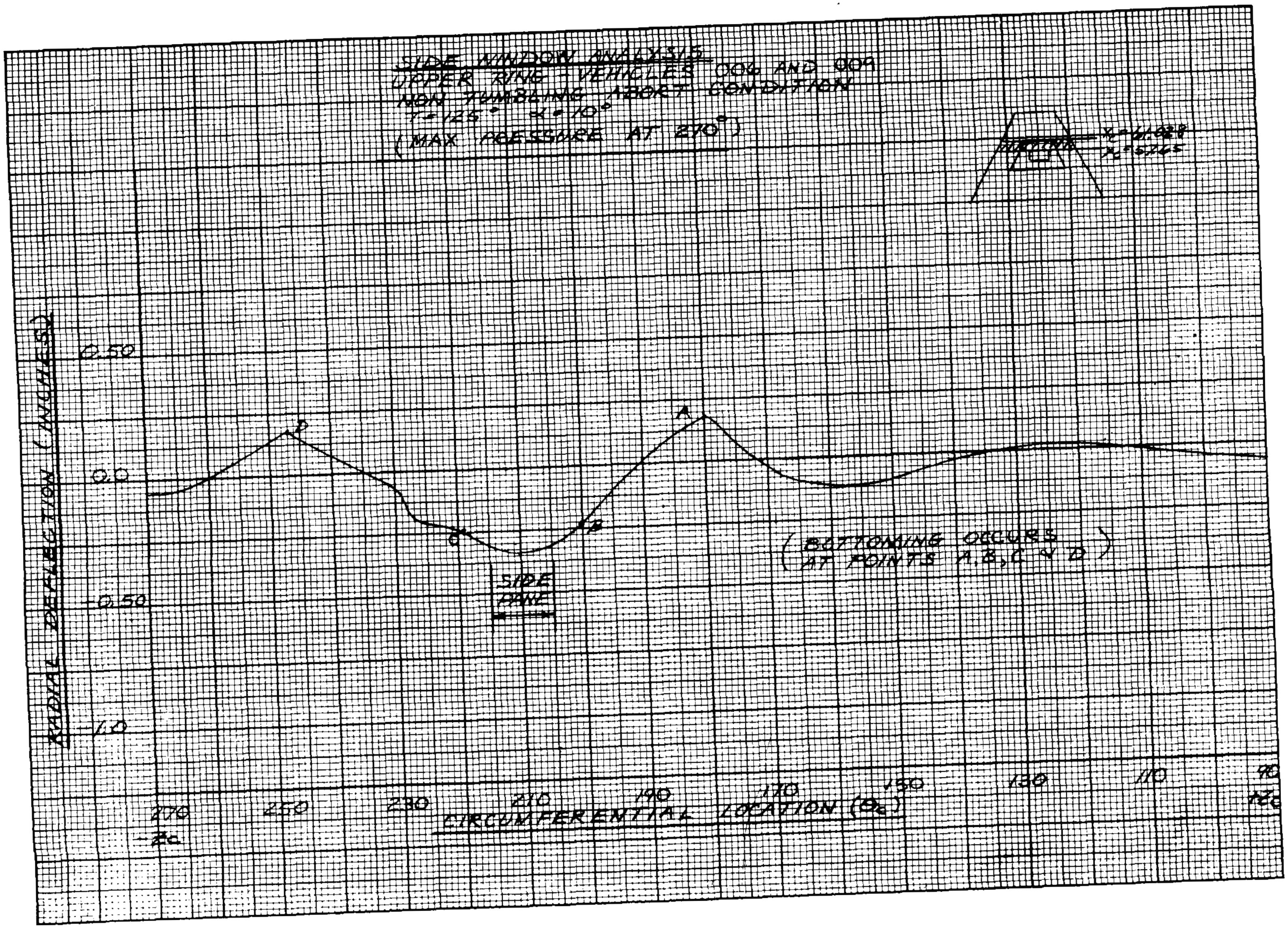

Figure 37 SIDE WINDOW ANALYSIS UPPER RING-VEHICLES 006 AND 009

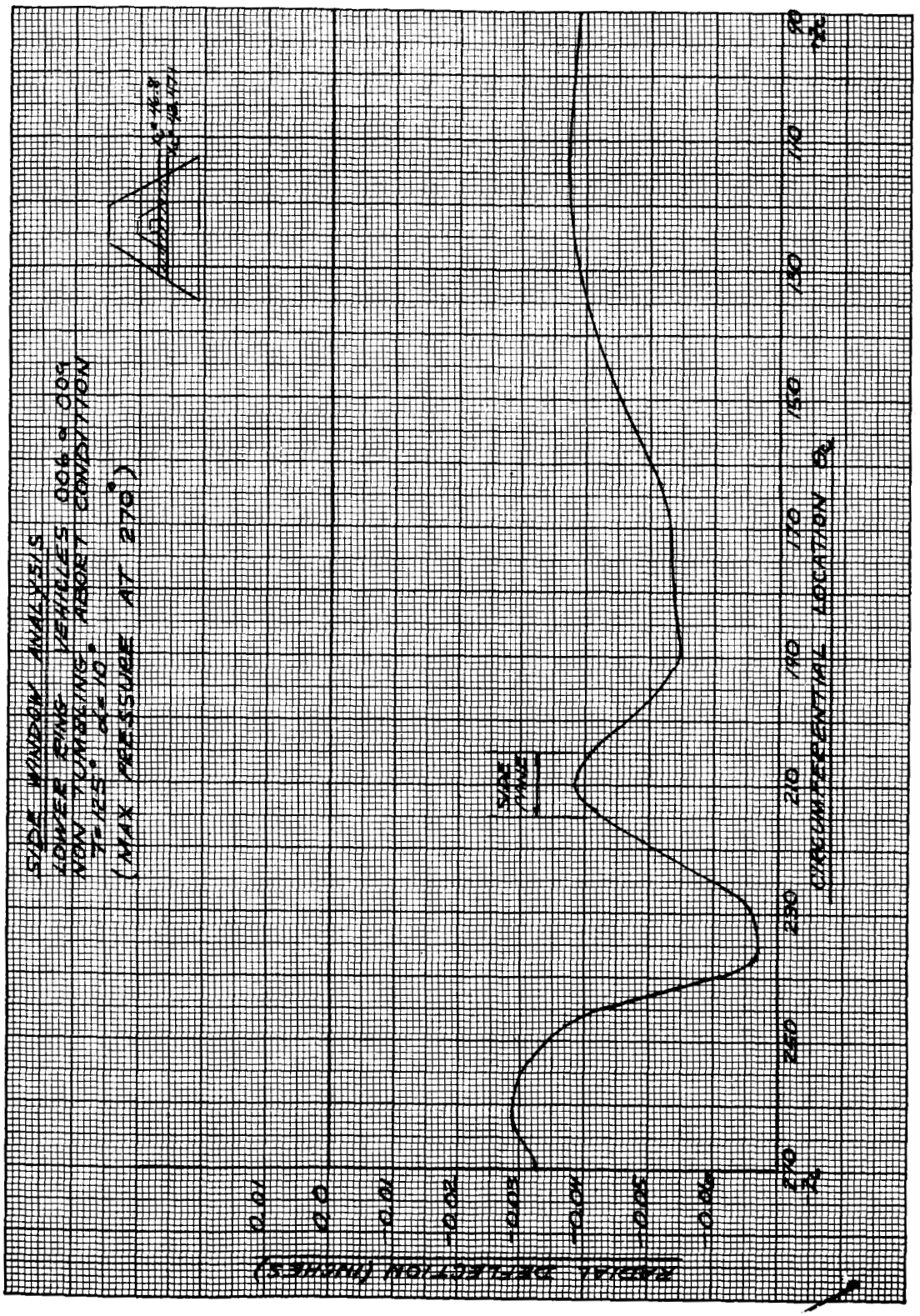

Figure 38 SIDE WINDOW ANALYSIS LOWER RING-VEHICLES 006 AND 009

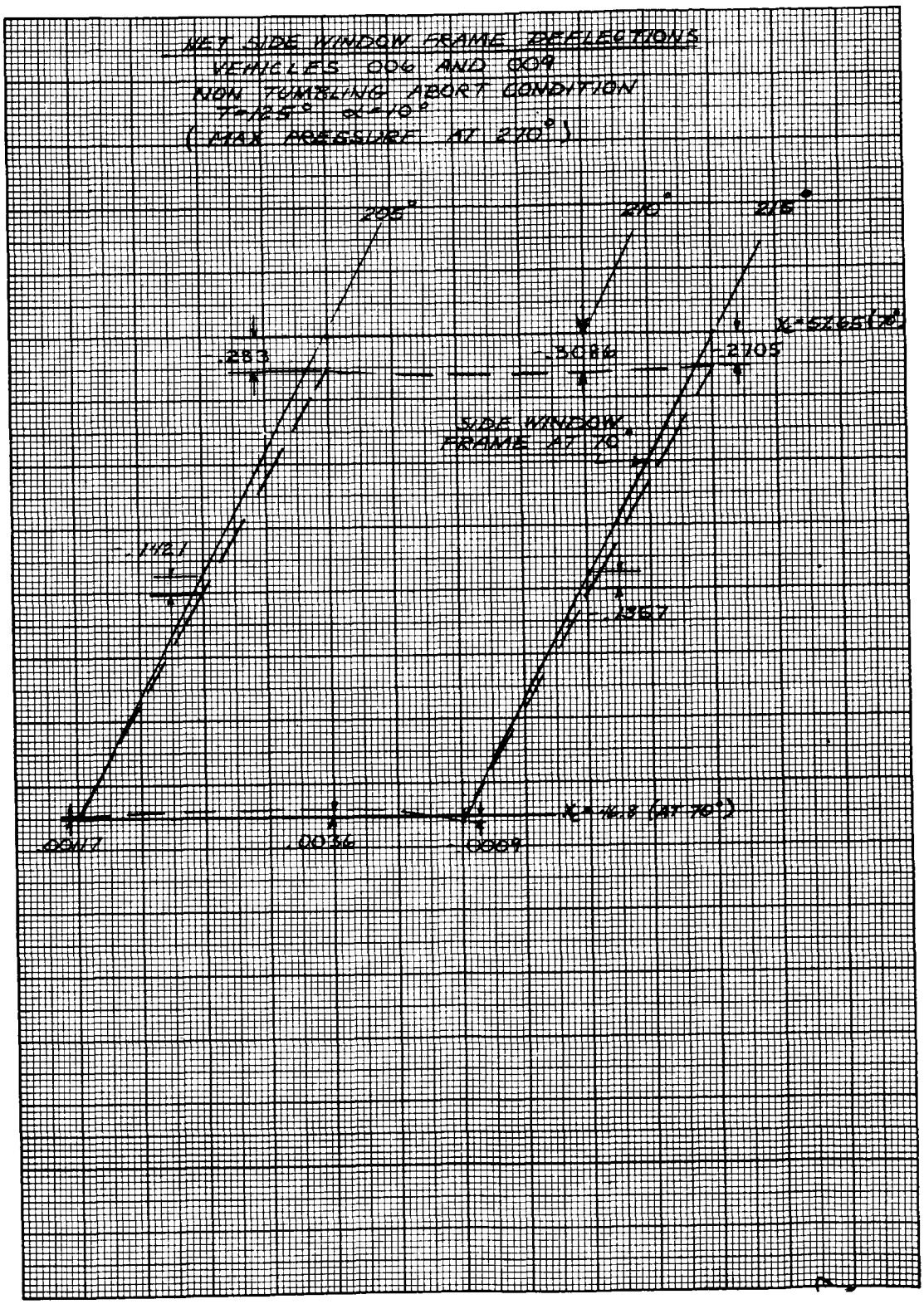

Figure 39 NET SIDE WINDOW FRAME DEFLECTIONS

2.3.2 Effects of Errors due to Short Shell Elements

A study was performed to determine the effect on short shell influence coefficients obtained by varying the number of integration points in the 1322 program. From this study, the proper number of integration points was obtained. With this new information, both the -260° F (-85° F inside S/M) and the -60° F soak environments were rerun. A comparison with the original solution presented in the 11 August 1964 Monthly Progress Report showed no significant difference. The gap analysis at $X_c = 32.0$ was also redone yielding the same negligible difference.

2.3.3 Effects of Eccentricities of Reference Surfaces

The final solutions for both the -260° F (-85° F inside S/M) and the -60° F soak environments including eccentricities have been completed and are now in the process of being checked.

2.4 Unsymmetrical Shell Analyses of Forward and Crew Compartment Heat Shields

An analysis of the crew and forward compartment heat shields with an asymmetrical temperature distribution has been initiated, utilizing Avco's computer program 1450. This program can handle asymmetrical pressure and temperature, but it is limited to an axisymmetrical shell composed of isotropic layers. Also, the physical properties (E, α) cannot vary in the circumferential (θ) direction. Since the heat shield is asymmetrical and its properties are orthotropic and temperature dependent (and thus vary with θ), the following approach is taken:

a.) The pertinent cross-sectional parameters are computed at a number of points along and around the true orthotropic shell. This yields at each point the quantities:

$(EI)_\xi$ $(EI)_\theta$

$(EA)_\xi$ $(EA)_\theta$

$(M_T)_\xi$ $(M_T)_\theta$

$(N_T)_\xi$ $(N_T)_\theta$

b.) An axisymmetric shell model is established which has the same EI and EA as the heat shield along some arbitrary meridian. To bound the solution, two models will be used; one will approximate the windward meridian and the other the leeward. Further discussion here will consider a single model assumed to match the $\theta = 0$ meridian.

Since the model is isotropic, it cannot have $(EI)_\xi \neq (EI)_\theta$ and, similarly, the other parameters cannot be directional. However, it appears that $(EI)_\xi$, $(EA)_\theta$, $(M_T)_\xi$, $(N_T)_\theta$ are more important to the shell's deflection than their counterparts, and these are the parameters that will be matched (other combinations may be investigated also). This matching is accomplished by setting:

$$h_m = \sqrt{\frac{12\,(EI)_{\xi,\ \theta = 0}}{(EA)_{\theta,\ \theta = 0}}}$$

$$E_m = \frac{(EA)_{\theta,\ \theta = 0}}{h_m}$$

$$\alpha_m = \frac{(N_T)_{\theta,\ \theta = 0}}{(EA)_{\theta,\ \theta = 0}} \times \frac{1}{T_{avg.}} \quad ,$$

where T_{avg} is the true average temperature through the heat shield.

c.) The thermal load and its effect at each point $(\xi\ ,\ \theta)$ are input by developing a dummy temperature distribution such that

$$\frac{(N_T)_m}{(EA)_m} = \frac{(N_T)_\theta}{(EA)_\theta}$$

and

$$\frac{(M_T)_m}{(EI)_m} = \frac{(M_T)_\xi}{(EI)_\xi}$$

The resulting model and load should produce the same deflections and rotations as in the actual heat shield.

C. DESIGN

3.0 Design Effort

Due to funding limitations imposed during this period and the receipt of 006 substructure, work on vehicles 008 and 011 was severly cut back. . Design support for vehicle 006 is hampered by the lack of 1) a complete set of drawings as defined by the latest NAA drawing list; 2) a complete inspection log, or equivalent, of the substructure as delivered; and 3) vehicle conformance to agreements made at T. I. M.'s. Maintenance panel bolt edge distances, external doublers, and weld bead heights are examples of areas which now require additional design effort.

The major design changes and/or additions completed during the past two months include: a) final machining of the shear/compression and compression pads will now be done at the aft compartment assembly level; b) steps in the vehicle OML will be faired for honeycomb application by using alternate layers of HT-424 tape and fiberglass cloth; c) separate honeycomb core drawings for all removable panels were released; d) instrumentation requirements for vehicle 009 were incorporated by E. C.'s; e) HT-424 tape bond replaced the soft bond holding the molded ablator to the window retainers; f) a clamping fixture for the crew compartment C-band antenna was designed to compensate for NAA's failure to provide the closeout ring per V16-932003, Revision P; and g) and RTV-560 seal was incorporated into the crew hatch latching mechanism port plug.

3.1 Weight - Ablator

The current weight of the Apollo Ablator is 1433.4 lbs ± 2 percent. This is based on the ablator fairing thicknesses corresponding to Avco drawing 401098, Revision E. Perturbated areas include shear pads, scimitar antennas, abort tower wells, fixed windows and tension tie blocks. As a result of minor refairing and incorporation of new heating inputs at stations X_C 98.00 to X_C 107.00, the weight decreased by 9.2 pounds.

3.2 Specifications

The specifications and standards effort for the report period consisted of a total of 66 Specification Change Notices being generated and released or awaiting sign off. Eight new specifications were generated and 27 revisions are in process or were relased.

APOLLO WEIGHT SUMMARY

	WEIGHT Pounds							CG (of total) (Inches)			MI (of total) (Slug Ft^2)		
Compartment	Ablator	Adhesive	Sealer	F'glass	Gasket	S & C Pads	Total	X_c	Y_c	Z_c	I_{xx}	I_{yy}	I_{zz}
FWD NOSE CONE	45.0	1.8	0.7	0.5	0.4	___	48.4	122.4	-0.1	0.5	2.1	1.3	1.2
Forward	112.2	6.2	2.5	2.1	0.9	___	123.9	93.6	-0.1	2.7	31.6	18.5	18.0
Crew	437.4	22.2	9.0	26.2	5.4	___	500.2	45.5	-0.5	14.0	445.1	264.8	245.8
Aft	685.3	20.6	8.2	6.9	10.8	29.1	760.9	8.4	0	5.3	571.3	302.0	283.0
Totals	1279.9	50.8	20.4	35.7	17.5	29.1	1433.4	32.4	-0.1	7.9	1051.7	890.1	849.7

1. ρ = 31 lb /Ft^3

2. Perturbations include shear pads, tower wells, scimitar antennas, fixed window fairings and tension tie blocks.

3. 3 per cent estimate for moisture absorption.

APOLLO ABLATOR WEIGHT

Item	Weight
Forward Nose Cone	48.4
5026-39/HC-G (Fwd Nose Cone)	45.0
Closeout - Fiberglass Station Xc 112.25	0.5
Gasket - RTV 560 Station Xc 112.25	0.4
Adhesive - HT 424	1.8
Surface Sealer (Barrier Coat BR-C-8)	0.7

APOLLO ABLATOR WEIGHT

Item		Weight	
Fwd Compartment	123.9		
5026-39/HC-G	112.2		
Fwd Compartment		100.0	
Tower Wells			9.6
Leeward (2)			4.2
Windward (2)			5.4
Fwd. Comp. Door			1.6
Pitch Eng. Panel			1.0
Closeout - Fiberglass		2.1	
Station 112.25			0.5
Station 81.13			1.0
Fwd. Comp. Door			0.2
Pitch Eng. Panel			0.1
Fwd. Compartment			0.3
Adhesive - HT 424		6.2	
Surface Sealer (Barrier Coat BR-C-8)		2.5	
Gasket - RTV 560 (Station 81.13)		0.9	

APOLLO ABLATOR WEIGHT

Item	Weight		
Crew Compartment	500.2		
5026-39/HC-G		437.4	
Crew Compt.			327.8
Crew Hatch			19.0
Crew Hatch Wind.			1.7
Side Window (2)			9.4
Rendezvous Window (2)			22.3
Sex., Teles. Door			9.3
Maintenance Doors			36.3
Type A 0°			4.5
Type A 180°			4.5
Type A 239°			2.6
Type A 301°			2.6
Type B 207° 30'			2.8
Type B 332° 30'			2.8
Type C 270°			2.8
Type E 45°			6.7
Type E 135°			6.7
A. C. Motors			11.6
Pitch			2.2

APOLLO ABLATOR WEIGHT (Cont'd)

Item	Weight		
Yaw (2)			4.8
Roll (2)			4.6
Closeout Members & Bolt Plug Sleeves (F'Glass)	26.2		
Crew Compartment		9.2	
Crew Hatch		1.1	
Crew Hatch Wind.		0.3	
Side Window (2)		1.7	
Rendezvous Window (2)		2.5	
Sex., Teles. Door		0.6	
Maintenance Doors (Fiberglass)		5.8	
Type A 0°			0.7
Type A 180°			0.7
Type A 239°			0.5
Type A 301°			0.5
Type B 207° 30'			0.5
Type B 332° 30'			0.5
Type C 270°			0.5
Type E 45°			1.0
Type E 135°			1.0

APOLLO ABLATOR WEIGHT (Cont'd)

Item	Weight	
A. C. Motors	4.7	
Pitch		0.8
Yaw (2)		1.8
Roll (2)		1.5
Scimitar Antennas (2)		0.6
Umbilical	0.3	
Gaskets - RTV 560	5.4	
Crew Compartment	3.5	
Crew Hatch	0.4	
A. C. Motors	1.4	
Pitch		0.3
Yaw (2)		0.7
Roll (2)		0.4
Maintenance Doors (Gaskets)	0.1	
Type A 239°		0.03
Type A 301°		0.03
Type C 270°		0.06
Sex., & Teles. Door	0.05	
Side Window (2)	0.02	

APOLLO ABLATOR WEIGHT (Concl'd)

Item	Weight
Adhesive - HT 424	22.2
Surface Sealer (Barrier Coat BR-C-8)	9.0

APOLLO ABLATOR WEIGHT

Item	Weight	
Aft Compartment	760.9	
5026-39/HC (Aft Compartment)	685.3	
Shear Pad (3)	20.5	
Compression Pad (3)	8.6	
Closeout - Fiberglass	6.9	
Shear Pad (3)		0.5
Compression (3)		0.4
C-Band (3)		1.0
Station 23.2		3.3
Bolt Plugs		1.7
Gasket - RTV 560	10.8	
Station 23.2		9.6
Compression Pad (3)		0.3
C-Band		0.9
Adhesive - HT 424	20.6	
Surface Sealer (Barrier Coat BR-C-8)	8.2	

D. GROUND TEST

4.0 Development Test Program

During this 2 month period the Development Test Program was sharply curtailed by reason of funding limitations. The tests that were conducted are reported below.

4.1 Structural Tests

4.1.1 Vibration Beam Tests

This past reporting period, vibration tests were conducted on beam specimens APT-483, 490, and 491.

Vibration beam specimen APT-483 consisted of 5 x 22 x 1/2 inches S. S. sandwich with 1.0 inch thick Avcoat 5026-39/HC-G ablator on one surface. This specimen, prior to vibration test, had a crack produced approximately in the center by center-point loading at -260° F. APT-491 and 492 were identical with the above except they had an ablator thickness of 1/2 inch.

The twenty-two inch-long beams were clamped over a 5 inch length at one end producing a 17 inch cantilever. Vibration input was transmitted through the clamped region of the beams. The specimens were subjected to a resonant survey at room temperature to determine the natural frequency of the first three modes at a IG input level. The test condition at each test temperature was 3 minutes of combined random and sinusoidal input per NAA Spec. MC364001C, paragraph 3.5.2.2, except that the sinusoidal sweep was started at 10 CPS rather than 5 CPS due to equipment problems. This three-minute combined input test was then followed by a two-minute continued random input per the specification (but not required by it) to allow a beam response analysis to be completed.

APT-483 was tested per the above test condition at temperatures of R. T., +250° F, -260° F, f and -100° F. APT-491 and 492 were tested at -260° F and -100° F to complete the test sequence previously reported.

APT-483 developed a crack across the beam at the root approximately 3/4 inch deep after two minutes at R. T. After completion of test, a second crack was evident which went down to the substructure.

APT-491 developed a second crack, which went to the substructure, approximately 1 1/2 inches from the pre-crack towards the beam tip. There was no change to the root crack previously reported.

APT-492 developed a root crack 1/4 inch deep and two other cracks, one of which went down to the substructure.

4.1.2 Window Frame Bond Tests

Restrained window frame specimens APT-709, 710, and 711 were tested to evaluate rigid HT-424 bond attachments for molded ablator to window frames. They consisted of 12 x 2 1/4 x 1 1/4 inch 5026-39/M bonded with HT-424 to a 12 x 1 1/2 x 1/8 inch 15-7 Mo S. S. plate. These assemblies were bolted to a 3 x 1 1/2 inch steel channel and were subjected to 3-day cold soak to -260° F followed by programmed radiant lamp heating until the bond line reached 600° F. All specimens successfully survived the cold soak test and heating with no bond failure (see figures 41, 42).

4.1.3 Abort Tower Well Mock-up Cold Soak Test

Abort Tower Well mock-up APT-608 (figure 43), which consisted of 0.96 inch -39/M ablator on a 0.096 inch thick substructure with 4 mechanical restraints, was exposed to a 3-day cold soak to -260° F. The specimen was unchanged after test.

The test objective was to proof test tower well ablator and bond for hot and cold soak conditions, and to provide a functional check of the 4 mechanical restraints. This specimen will now be subjected to hot soak testing to 600° F.

4.1.4 Tests of Sta. -81 Gap Finger Seal Specimens

Finger seal specimens APT-627-1, 628-1, and 629-1 consisted of 6 inch-long mockup sections of the RTV-560 finger seal bonded to 0.060 inch thick fiberglass and steel support blocks in a manner which simulated the proposed seal installation on the Apollo vehicle at $X_C = 81.0$.

These mockup section specimens were installed in holding adapters on a standard tensile test machine and then loaded at -260° F to failure. All three specimens failed when some of the fingers broke off near their roots. Deflections and ultimate loads are presented in the chart below.

	APT-627-1	APT-628-1	APT-629-1
Maximum Load	1208 lbs.	1340 lbs.	1510 lbs.
Maximum Deflection	0.0767 in.	0.0669 in.	0.0894 in.

Preliminary analytical predictions of required maximum deflection for the above condition were 0.050 to 0.055 inch.

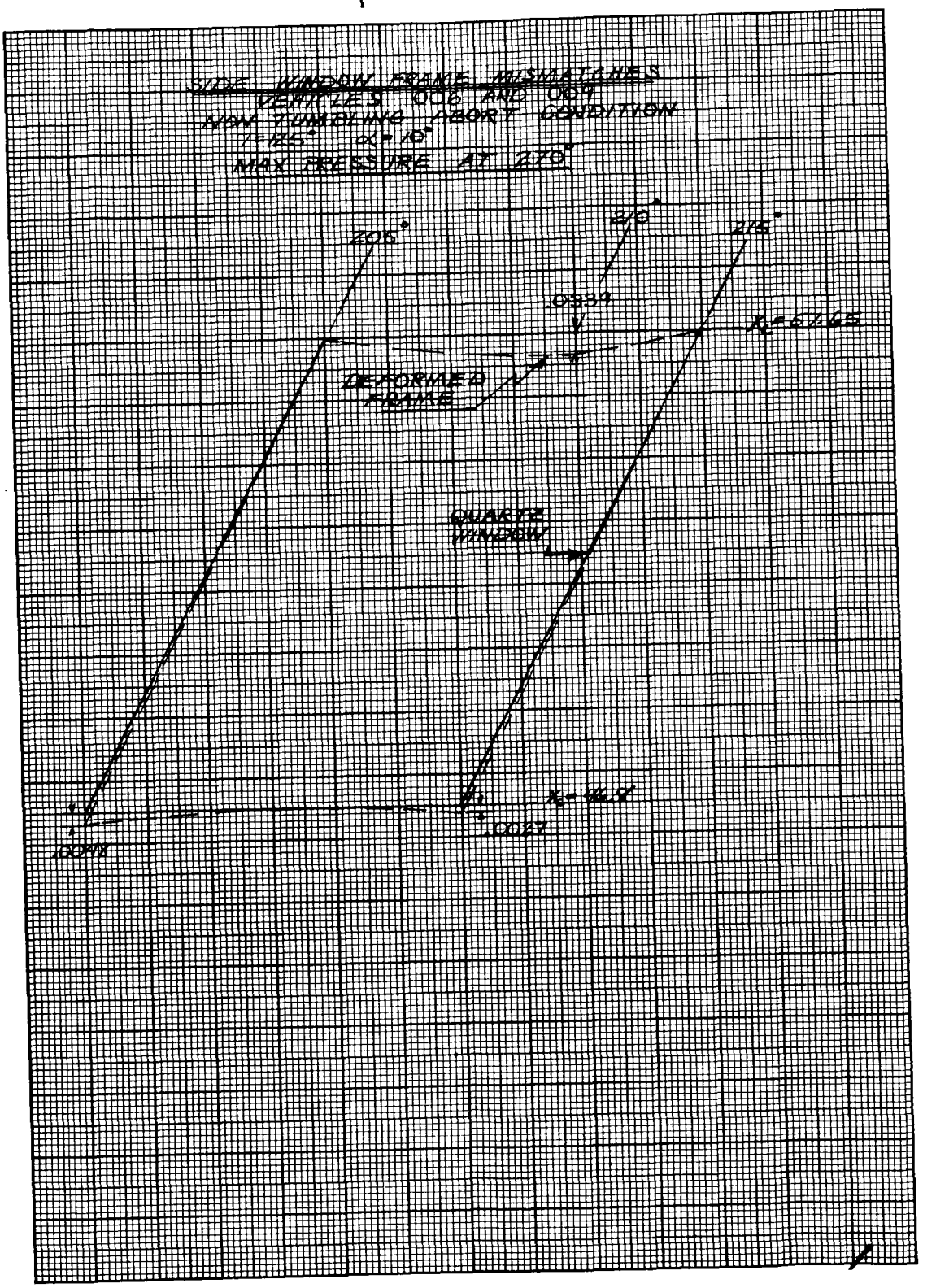

Figure 40 SIDE WINDOW FRAME MISMATCHES

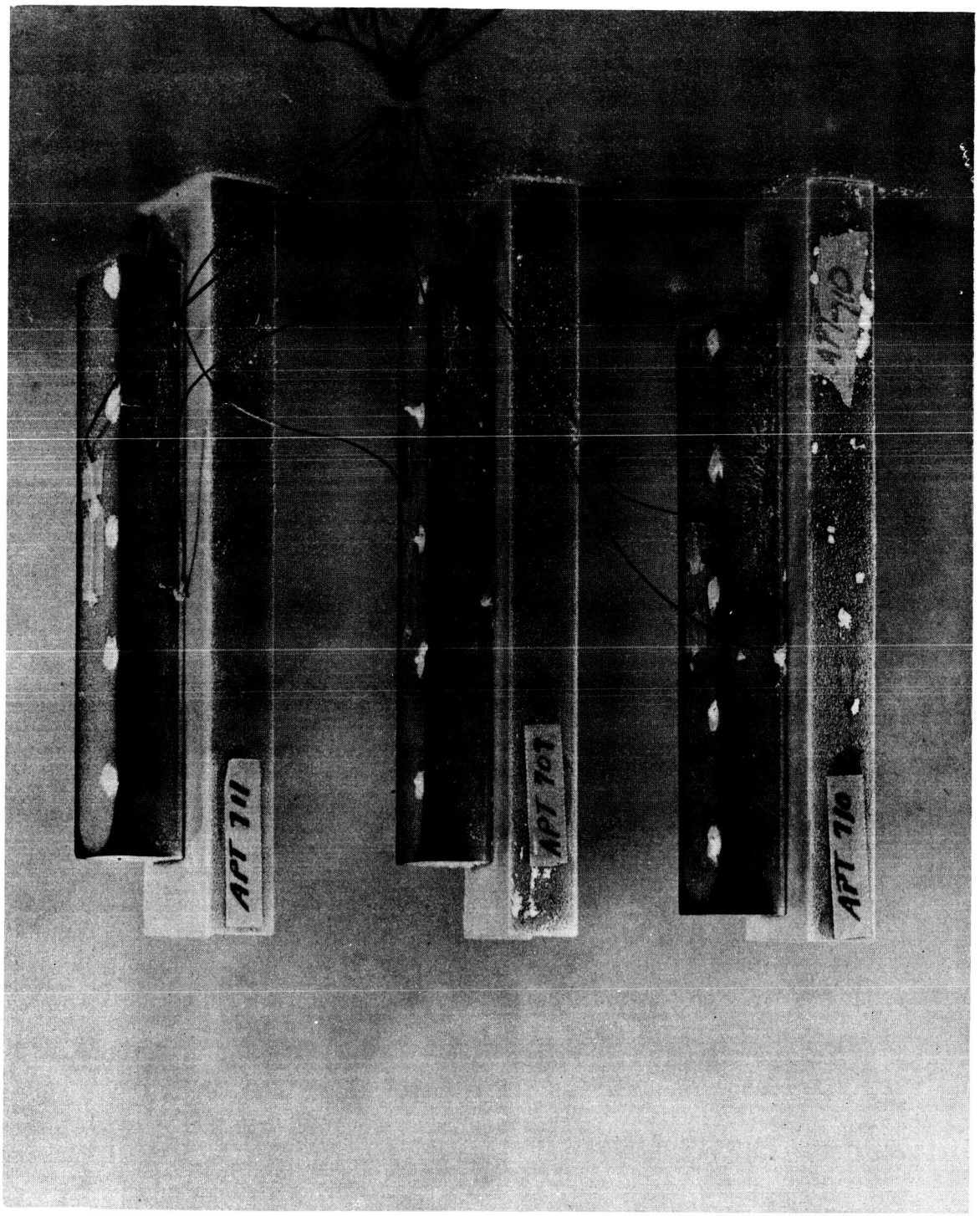

Figure 41 WINDOW FRAME BOND EVALUATION TEST SPECIMENS APT 709, 710, 711 AFTER -260°F COLD SOAK TESTING AND BEFORE REENTRY HEATING TESTING
11979-A

Figure 42 WINDOW FRAME BOND EVALUATION TEST SPECIMEN APT 711
AFTER RADIANT REENTRY HEATING TESTING
12007-J

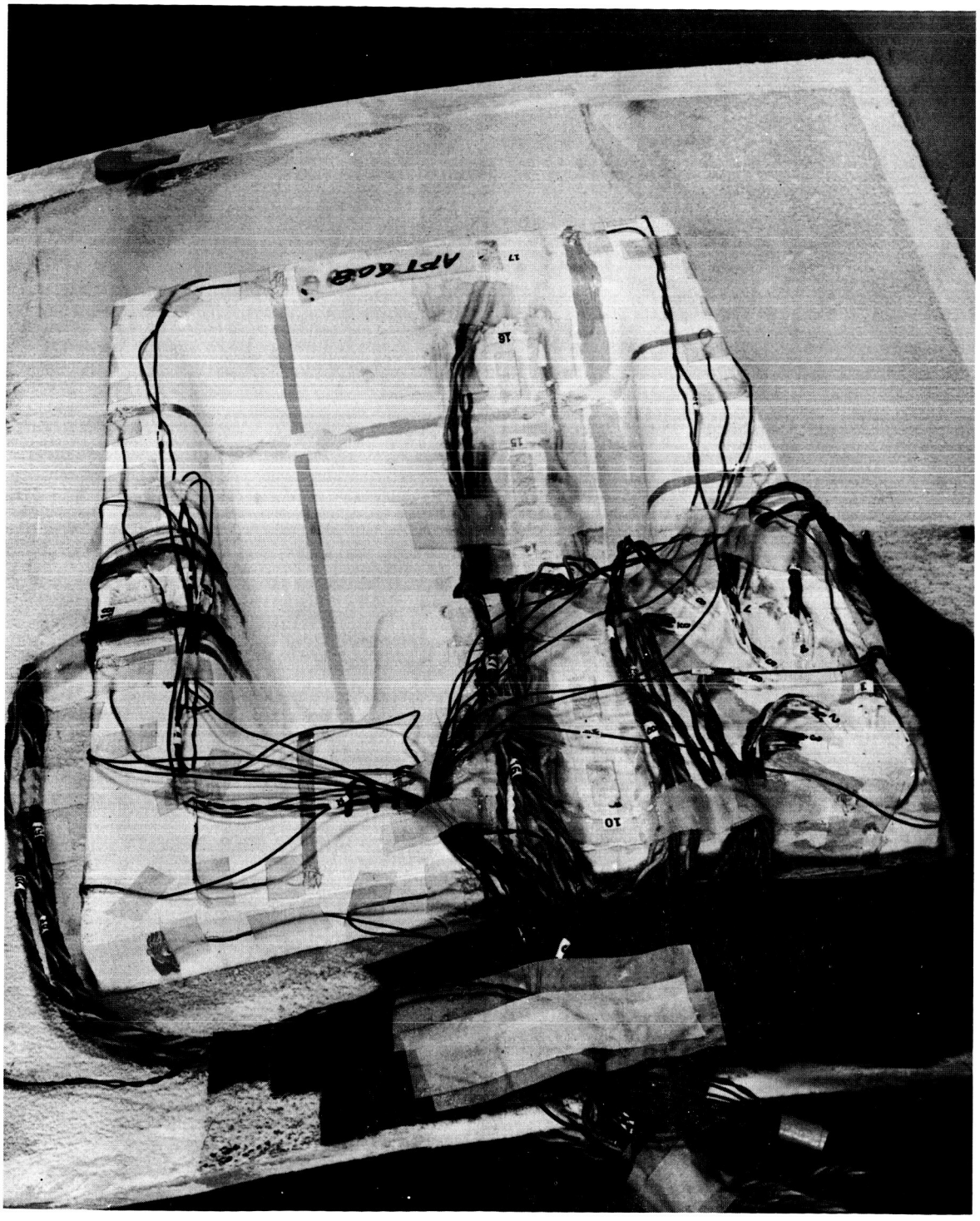

Figure 43 ABORT TOWER WELL MOCKUP SPECIMEN APT 608 AFTER COLD SOAK TESTING
11979-C

In addition, these tests demonstrated that the new bonding used for attaching the rubber seal members to the fiberglass edge members was capable of carrying more load than the seals could impose at failure. The previous series of specimens tested, as reported in the last period, all experienced bond failures.

4.1.5 Hot Soak Test of 18 x 18 Inch Back-to-Back Ablator

Specimen APT-589 (figures 44 and 45) which was previously cold soak tested, consisted of 1.0 inch-39/HC-G back-to-back on an 18 x 18 x 1/2 inch S. S. sandwich (0.015 inch face sheets). There were also edge members and bolt plug holes around the ablator edges. This specimen was subjected to a hot soak test in which the ablator-substructure interface temperature was maintained at +250° F for 4 hours. No adverse effects were found.

4.1.6 Restrained 18 x 18 Inch Ablator Panel Cold Soak Test

Specimen APT-590 was an 18 x 18 x 1/2 inch S. S. sandwich (0.008 inch face sheet) with a 1 inch thickness of Avcoat 5026-39/HC-G. It was bolted to a restraining frame providing simple support to all four edges. One-quarter of this panel was exposed to ambient conditions, the center half of the panel was insulated, and the remaining one-quarter was exposed to the standard three-day programmed cold soak to -250° F. The specimen was unchanged after test and no ill effects were observed as a result of the test.

4.1.7 Beam Tests

The beam tests completed during this reporting period were as follows:

Beam specimens APT-614, 615, 616, and 617 consisted of 5 x 22 x 1/2 inch S. S. sandwhich (0.008 inch face sheets) with 1.5 inch thickness of Avcoat 5026-39/HC-G. These specimens were previously cracked at -260° F by center-point loading. They were then cycled from R. T. to +250° F and were loaded to failure at -260° F by quarter point loading. The results are shown in table IV.

Beam specimens APT-618, 619, and 620 were tested as part of the test program to determine the effects of a thermal cycle. These specimens were tested as controls without being subjected to a thermal cycle. Test results are shown in table IV.

Specimen APT-621 consisted of 5 x 22 x 1/2 inch S. S. sandwich (0.008 inch face sheets) with 1.8 inches of Avcoat 5026-39/HC-G. The specimen was heated to +250° F in a constant moment quarter point loading fixture and loaded to failure. Test results are shown in table IV.

Beam specimens APT-637 and 638 were tested as part of the test program to evaluate the performance of a HT-424 tape splice. There were no splice failures during these tests. Test results are shown in table IV.

TABLE IV

STRUCTURAL BEAM TEST RESULTS

Apt No.	Ablator			Ultimate Load		
	Thickness (inches)	Width (inches)	Node Direction	Temp. (°F)	Moment (in. lb/in.)	Condition
614	1.5	5.0	Transverse	-260	888	F. S. B.
615	1.5	5.0	Transverse	-260	450	F. S. B.
616	1.5	5.0	Transverse	-260	675	F. S. B.
617	1.5	5.0	Transverse	-260	614	B. D.
618	1.8	5.0	Transverse	-260	720 895	B. D. F. S. B.
619	1.8	5.0	Transverse	-260	650	B. D.
620	1.8	5.0	Transverse	-260	630	B. D.
621	1.8	5.0	Transverse	+250	720	F. S. B.
637	1.4	5.0	*	-260	720	A. C.
638	1.4	5.0	*	-260	765	A. C.

*HT-424 tape splice across ablator at beam centerline and ribbon nodes 11°-15' from longitudinal centerline.

F. S. B. Face skin buckling of substructure
B. D. Bond delamination
A. C. Ablator cracking

Figure 44 SPECIMEN APT 589 FACE "A" AFTER COLD SOAK TESTING
11868-D

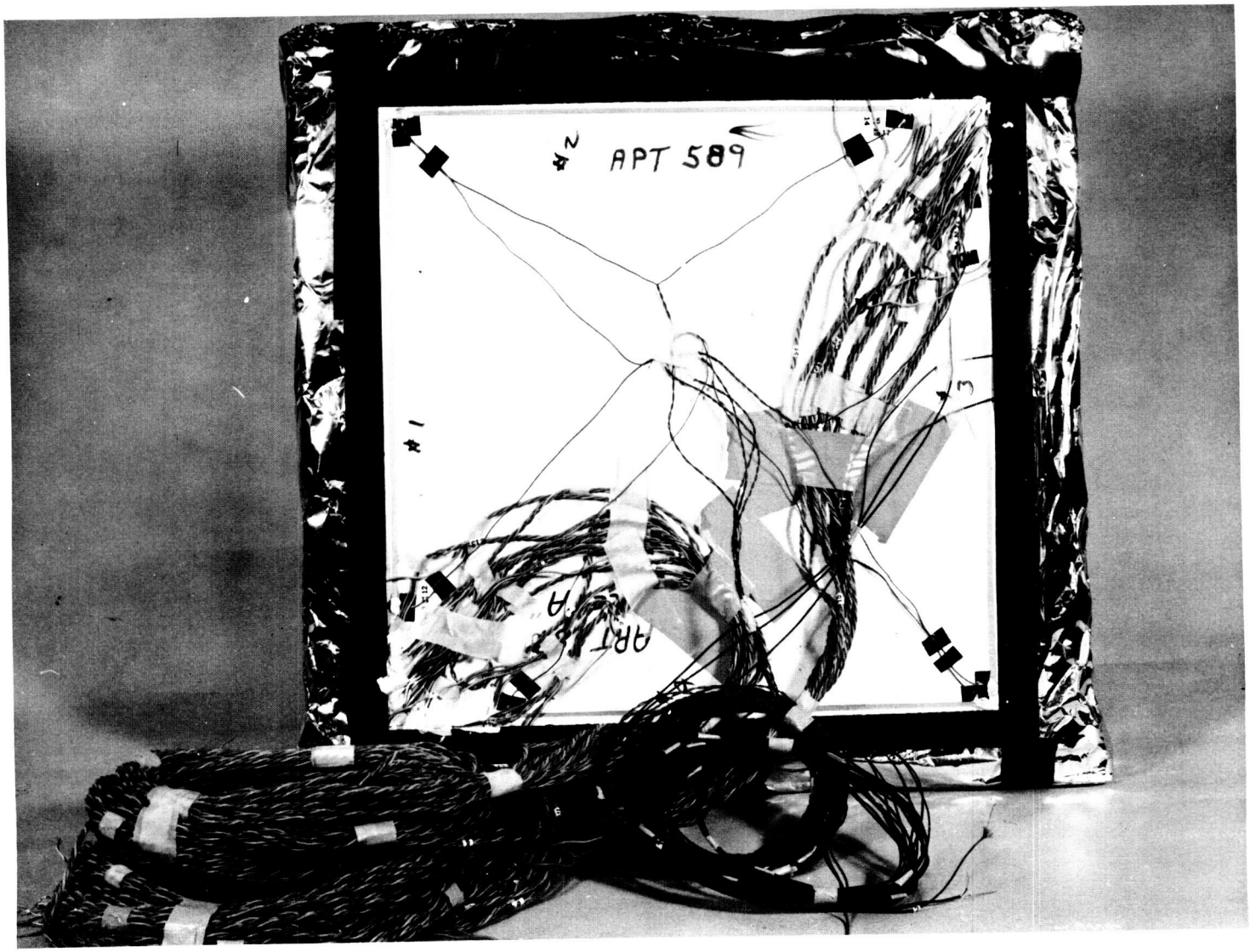

Figure 45 SPECIMEN APT 589 FACE "A" BEFORE COLD SOAK TESTING
11850-A

4.2 Thermal Tests

As previously reported, a new technique has been instituted for the measurement of front surface temperature and total radiation at the OVERS Arc facility. Surface temperatures are determined from spectral intensity measurements at 0.65 microns by an optical pyrometer and direct measurements of total radiation are performed using an Eppley thermopile-detector. The thermopile is calibrated experimentally using the Stefan equation,

$$q_r = \sigma \epsilon T_s^4 \tag{1}$$

by calculating the radiation (q_r) from surface temperature (T_s) measurements on specimen of reference material heated in the arc. The reference material is a crystalline form of silicon carbide (globar) whose emissivity is well known at elevated temperatures.

The optical pyrometer is corrected to the black body temperature associated with the measured spectral intensity (brightness temperature). Since the spectral emissivity of the sample surface is less than one, the true surface temperature will be greater than the brightness temperature. An additional correction to the brightness temperature is required to account for the reduction of radiant transmission by the plexiglass window through which the sample is viewed. The spectral intensity, i_λ, measured by the optical pyrometer may be expressed by the Wien equation for black body radiation

$$i_\lambda = C_1 \lambda^{-5} \exp(-C_2/\lambda T_B) \tag{2}$$

where

C_1, C_2 = constants

T_B = brightness temperature

λ = wavelength.

The measured spectral intensity is related to the spectral intensity of specimen radiation, i'_λ, by

$$i_\lambda = \tau_\lambda i'_\lambda \tag{3}$$

where τ_λ is the spectral transmissivity of the plexiglass window. The specimen intensity may be given by the Wien equation for a non-black body, i.e.,

$$i'_\lambda = C_1 \epsilon_\lambda \lambda^{-5} \exp(-C_2/\lambda T_T) \tag{4}$$

where

T_T = true surface temperature of the specimen

ϵ_λ = spectral emissivity of the specimen.

From equations (2-4), the difference between brightness and true surface temperature, ΔT, may be expressed as follows:

$$\Delta T = -\frac{\lambda}{C_2} T_T T_B \ln(\epsilon_\lambda \tau_\lambda). \quad (5)$$

The transmissivity of the plexiglass window is a function of the length of time it is exposed to sample testing since it is coated with ablation products generated during the course of the tests. In addition, deterioration of the window may occur as a result of interaction with the plasma. Representative transmissivity values for plexiglass windows were determined from optical pyrometer measurements of a tungsten lamp source with a dirty window both in and out of place, using the following relationship derived from the Wien equation:

$$\tau_\lambda = \left[\ln^{-1}\left(\frac{C_2}{\lambda}\frac{T_B' - T_B}{T_B T_B'}\right)\right]^{-1} \quad (6)$$

where

T_B' = brightness temperature with window out of place

T_B = brightness temperature with window in place.

Transmittance calculations were performed for windows exposed to sample testing at widely differing arc conditions and different periods of time. The resultant values are presented in a plot of transmissivity versus testing time (figure 46). The data is reasonably well correlated and it is observed that the transmissivity of the plexiglass window is insensitive to arc conditions. In conventional testing both temperature and radiation measurements are performed at a time approximately sixty seconds after the beginning of the test; therefore, a plexiglass window transmissivity of 0.85 was used in data reduction. An appropriate transmissivity was also computed for the Eppley calibration runs.

The salt (NaCl) window through which the Eppley detector views the specimen will also introduce transmission losses during sample testing. The calibration curve, however, does account for a window transmission loss and experimental data indicate a negligible difference between the

transmissivities of salt windows for typical test and calibration applications. Consequently, no correction of the measured total radiation data was employed.

Surface temperatures and total emissivities were determined simultaneously from data on the Apollo material, using an iterative procedure. The specimens were considered grey bodies and variations of emissivity with surface temperature and arc conditions ignored. The former consideration is in agreement with experimental data presented in the January 1964 Apollo Monthly Progress Report obtained from room temperature measurements of spectral reflectance on charred specimens of the Apollo material. Furthermore, a ten percent error in spectral emissivity of the specimen or spectral transmissivity of the window will introduce only a one percent error in surface temperature and a five percent error in the computed total emissivity. The latter consideration is the only reasonable one consistent with previously determined values of emissivity for the Apollo material. Equation (5) was utilized for the brightness temperature correction and Equation (1) to compute values of total emissivity from the surface temperatures and measured radiation. On the first iteration a value of spectral emissivity was assumed, and on successive iterations the average of total emissivity values from the previous iteration was employed.

Surface temperatures, radiant emission, and total emissivities for tests run in the OVERS facility are presented in tables V and VI . From the tests in which emissivity values are reported, an average value of 0.84 was obtained with a scatter band of approximately $\pm$ 0.1.

A series of 10 splash samples to evaluate performance of specimens with cracks was tested in the OVERS facility. The samples consisted of 5 cracked and 5 control specimens of 5026-39-3/8HC-G material. The specimens with tapered, staggered cracks had a nominal surface crack of 0.080 inch. Figure 47 presents a photograph of a typical sample prior to testing. Figures 44 through 52 are post test photographs of the 10 samples. Table VII presents the ablation data. It will be noted from table VII that with the exception of the pair AP1753-14 and -32 there is negligible difference in length loss for the pairs of cracked and control specimens. Samples AP1753-14 and -32 were tested at a nominal heat flux of 100 Btu/ft^2-sec while the remaining samples were tested at 12 to 50 percent of this value.

Fifteen combined radiation and convection OVERS splash tests (5026-39/HC/G, AP-1683) have been run but data reduction is incomplete. In addition splash tests on four "repair" OVERS splash samples have been conducted and the ablation data is reported, herein (AP 1752).

Arc and ablation data are presented for the four OVERS splash (AP-1752-1-4) "repair" samples in table VIII. It should be noted that true surface temperatures were obtained from brightness temperature measurements

assuming a value of spectral emissivity, $\epsilon_\lambda = 0.85$, at 0.65μ. This value is consistent with previous emissivity values determined using the new radiation and temperature measurement technique. Backface thermocouple measurements were also obtained for each sample. This data, however, is in a stage of partial reduction. Post-test photographs of the specimens appear in figures 53 and 54.

It is observed in table VIII that no appreciable difference in ablation performance between repaired and control samples occurred.

Four thermal conductivity tests were conducted in the guarded hot plate apparatus and 4 tests were conducted in the high temperature radial conductivity apparatus on 5026-39/HC-G, material. Test results are shown in table IX.

TABLE V

RADIATION AND TEMPERATURE DATA

Sample No.	Enthalpy Btu/lb	Cold Wall Heat Flux Btu/ft^2-sec	Test Time sec	Surface temperature ^oK	Radiant Emission watts/cm^2	Emissivity
AP1683-1	13400	108	300	2010	72	0.77
AP1683-13	16900	106	300	2000	79	0.89
AP1683-16	4900	101	300	1940	69	0.86
AP1683-17	7400	101	300	2030	89	0.93
AP1683-20	9400	100	300	1980	67	0.76
AP1683-29	17200	95	300	1980	--	--
AP1683-55	19200	262	400	2710	--	--
AP1683-56	16400	100	600		73	--
AP1683-57	11300	130	500	2100	--	--
AP1683-58	10200	70	800	1810	53	0.89
AP1683-59	10300	46	1200	1630	38	0.95
AP1683-60	10000	22	1500		23	--
AP1683-61	9200	7	1700	1220	11	0.86
AP1683-62	20800	217	400	2510	--	--
AP1683-88	16200	107	120	2010	79	0.84
AP1683-90	4800	101	120	2060	78	0.76
AP1683-93	7400	91	120	2020	--	--
AP1683-95	10100	94	120	1960	63	0.76
AP1683-96	17400	95	120	1950	--	--
AP1683-99	12800	106	120	2030	71	0.73
AP1684-1A	10400	21	500	1880	--	--

TABLE VI

RADIATION AND TEMPERATURE DATA

Sample No.	Enthalpy Btu/lb	Cold Wall Heat Flux Btu/ft^2-sec	Test Time sec	Surface temperature ^oK	Radiant Emission watts/cm^2	Emissivity
AP1683-31	3150	90	300	1890	74	1.00
AP1683-32	3300	110	600	2020	--	--
AP1683-33	3800	100	300	1970	77	90
AP1683-34	4200	99	600	2010	88	0.96
AP1683-35	9300	44	300	1760	42	0.78
AP1683-36	10500	46	600	1730	42	0.84
AP1683-41	11000	245	120	2560	--	--
AP1683-42	10700	253	200	2550	--	--
AP1683-47	16400	481	80	3030	--	--
AP1683-48	16700	347	120	2900	--	--
AP1683-49	17500	432	60	--	89	--
AP1683-50	17500	432	100	2220	89	0.65
AP1683-51	19000	490	60	3110	--	--
AP1683-52	18800	557	120	3090	--	--
AP1683-53	20400	564	45	3120	--	--
AP1683-54	20400	564	75	3180	--	--
AP1683-87	18900	460	100	2210	--	--
AP1683-91	18900	460	100	2210	--	--
AP1695-2	4500	102	60	1930	--	--
AP1695-13	4700	108	120	2010	88	0.95
AP1695-14	4500	102	180	1970	--	--
AP1695-3	4700	108	240	2010	88	0.95
AP1695-15	4800	102	300	1870	61	0.87
AP1695-6	6600	98	60	2000	81	0.90
AP1695-5	6700	97	120	2040	81	0.83
AP1695-27	6600	98	180	2010	84	0.91
AP1695-21	6700	97	240	2010	77	0.83
AP1695-26	7100	105	300	1820	59	0.94
AP1695-16	10300	89	60	1970	73	0.85
AP1695-24	10300	89	120	--	76	--
AP1695-9	10100	85	180	--	66	--
AP1695-35	10300	89	240	--	73	--
AP1695-25	10600	105	300	1850	56	0.85
AP1695-10	14100	104	60	1895	--	--
AP1695-11	14100	100	120	1870	--	--
AP1695-23	14100	104	180	1890	--	--
AP1695-1	13100	98	240	1785	55	--
AP1695-4	12800	94	300	1835	61	--
AP1695-8	17200	102	60	1910	--	--
AP1695-20	17200	102	120	1890	--	--

TABLE VI (Concl'd)

Sample No.	Enthalpy Btu/lb	Cold Wall Heat Flux Btu/ft^2-sec	Test Time sec	Surface temperature ^oK	Radiant Emission $watts/cm^2$	Emissivity
AP1695-12	17200	102	180	1930	--	--
AP1695-22	16700	132	240	1860	76	--
AP1695-7	17000	122	300	1870	71	--
AP1695-32	19000	118	60	1760	--	--
AP1965-33	19000	113	120	1780	--	--
AP1695-28	19000	118	180	1780	--	--
AP1695-30	19200	132	240	1950	81	--
AP1695-29	19200	132	300	1920	74	--
AP1696-9	10400	27	1500	1470	22	--
AP1696-10	9700	46	1200	1600	37	--
AP1696-11	10300	65	700	1670	43	--
AP1696-12	17500	278	250	2140	89	--
AP1696-7	11200	25	50/30	1450	--	--
AP1696-7*	15600	133	30/30	1860	57	0.84
AP1696-7*	12200	45	250/20	1620	31	0.80
AP1696-7*	10500	25	380/20	1470	20	0.77
AP1696-7*	6300	20	690	1430	16	0.69
AP1696-8*	12500	25	50/30	1420	18	0.78
AP1696-8*	14800	133	30/30	1850	62	0.94
AP1696-8*	13100	45	250/20	1610	31	0.82
AP1696-8*	10500	25	380/20	1440	18	0.75
AP1696-8	5500	20	690	1420	16	0.72

*The second value of time refers to the transition period accompanying the change in heating.

TABLE VII

OVERS SPLASH TEST ABLATION DATA

Sample No.	Specific Gravity	Mass Flow lb/sec x10-^{3}	Impact Pressure mm Hg	Enthalpy Btu/lb	Cold Wall Heat Flux Btu/ft^2-sec	Time sec	Length Loss inches
AP1753-14	0.4771	5.7	15.5	3900	99	110	0.15
AP1753-32	0.4673	5.7	15.7	4100	95	110	0.40
AP1753-11	0.4795	5.7	12.2	3300	52	220	0.19
AP1753-30	0.4720	5.7	12.1	3300	49	220	0.19
AP1753-9	0.4845	0.8	1.0	3400	12	1100	0.08
AP1753-19	0.4790	0.8	1.0	3500	12	1100	0.03
AP1753-2	0.4968	0.65	1.4	13,200	55	220	0.05
AP1753-20	0.4875	0.65	1.3	14,300	55	220	0.05
AP1753-1	0.4974	0.6	1.0	6000	12	1100	0.07
AP1753-22	0.4946	0.6	1.0	6500	12	1100	0.10

TABLE VIII

OVERS SPLASH TEST DATA

Sample No.	Specific Gravity	Mass Flow lb/sec x 10^{-3}	Impact Pressure mm-Hg	Enthalpy Btu/lb x 10^{-3}	Cold Wall Heat Flux Btu/ft^2-sec	Test Time sec	Length Loss inches	Surface Temperature °K	Comments
AP1752-1	0.493	0.8	2.1	12.5	54	300	0.09	1640	Bonded plug
AP1752-2	0.499	0.8	2.3	13.1	53	300	0.13	1700	Control sample
AP1752-3	0.500	0.8	---	12.5	52	300	0.09	1630	Regunned cells
AP1752-4	0.528	0.8	1.9	13.8	60	300	0.11	1690	Bonded slice

TABLE IX

THERMAL CONDUCTIVITY TESTS

Test No.	AP No.	Material	Density virgin/pre-charred	K	Temp °F
046	1723-2	5026-39/HC-G, 800°F prechar	30.23/19.25	0.037 0.034	250 800
049	1723-3	5026-39/HC-G, 800°F prechar	30.46/20.12	0.037 0.032	250 800
052	1723-4	5026-39/HC-G, 1200°F prechar	30.16/21.31	0.070 0.080	250 1000
043	1723-1	5026-39/HC-G, 800 °F prechar	30.21/20.09	0.035 0.030	250 800
061	1710-6	5026-39/HC-G, 2000°F prechar Radial K	30.47/20.67	0.182 0.218 0.252 0.288	500 1000 1500 2000

Note: Density is in Lbm/ft^3 and K is in Btu/hr°F units

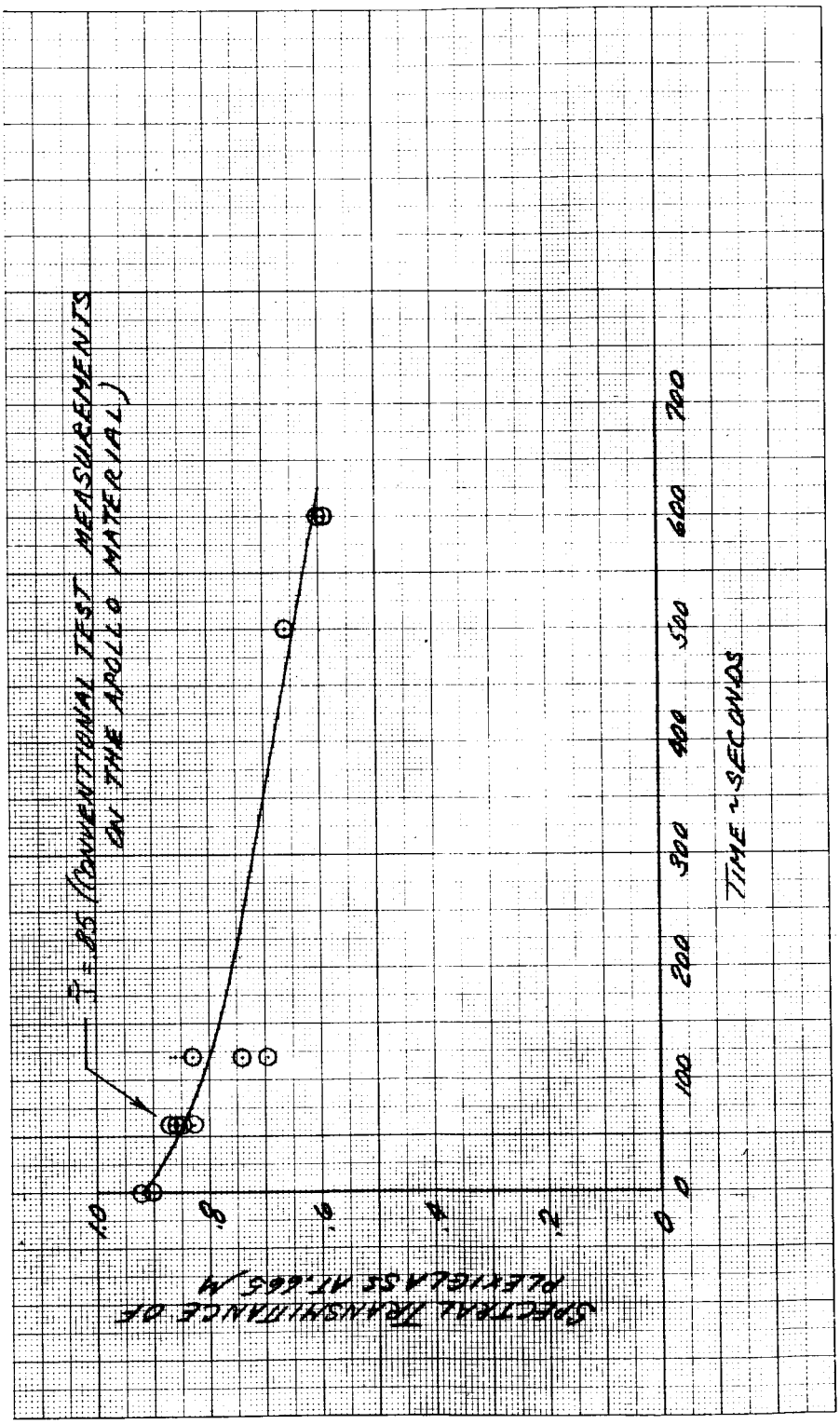

Figure 46 SPECTRAL TRANSMITTANCE OF PLEXIGLASS WINDOW (NEW) AT 0.665/M VERSUS OVERS TESTING TIME

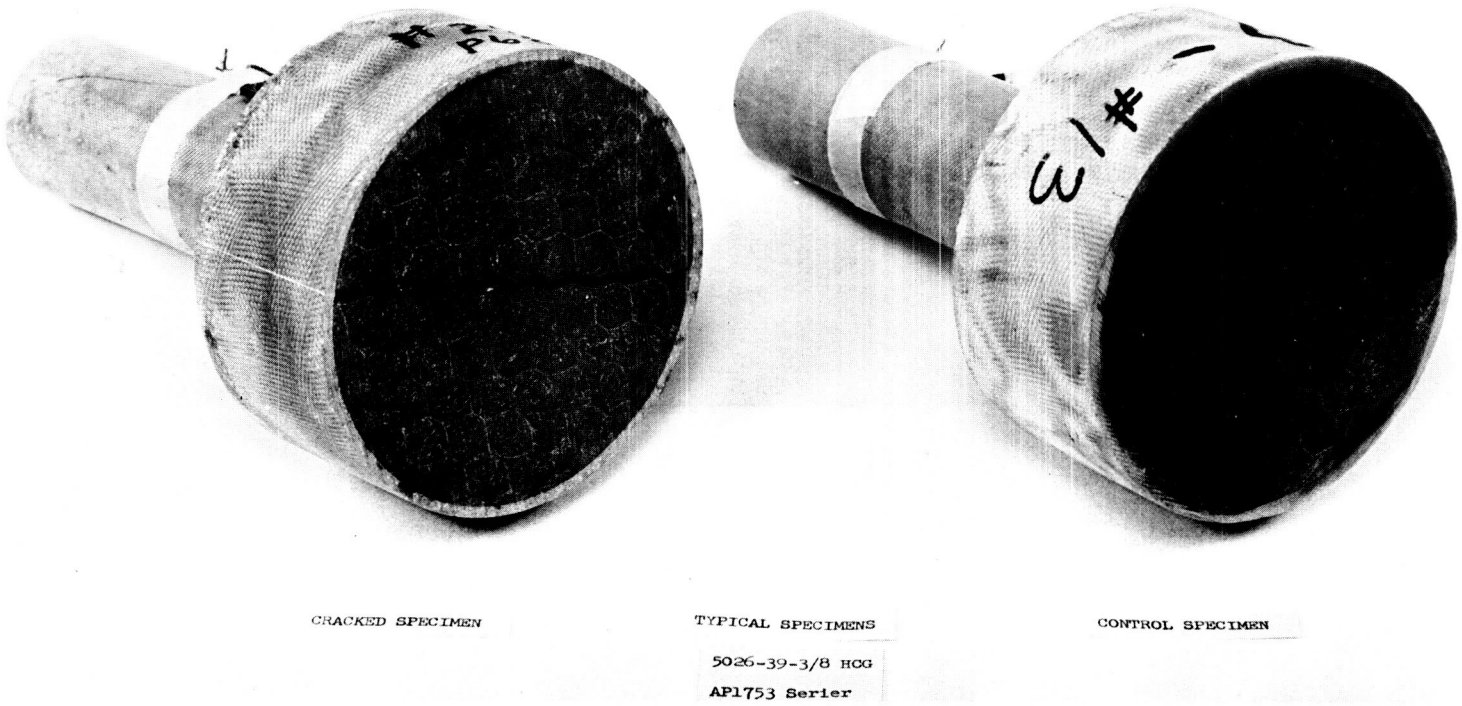

Figure 47 TYPICAL SPECIMEN AP 1753 PRIOR TO TESTING
11786-F

Figure 48 THREE-QUARTER VIEW AP 1753-1 AND -2
11786-E

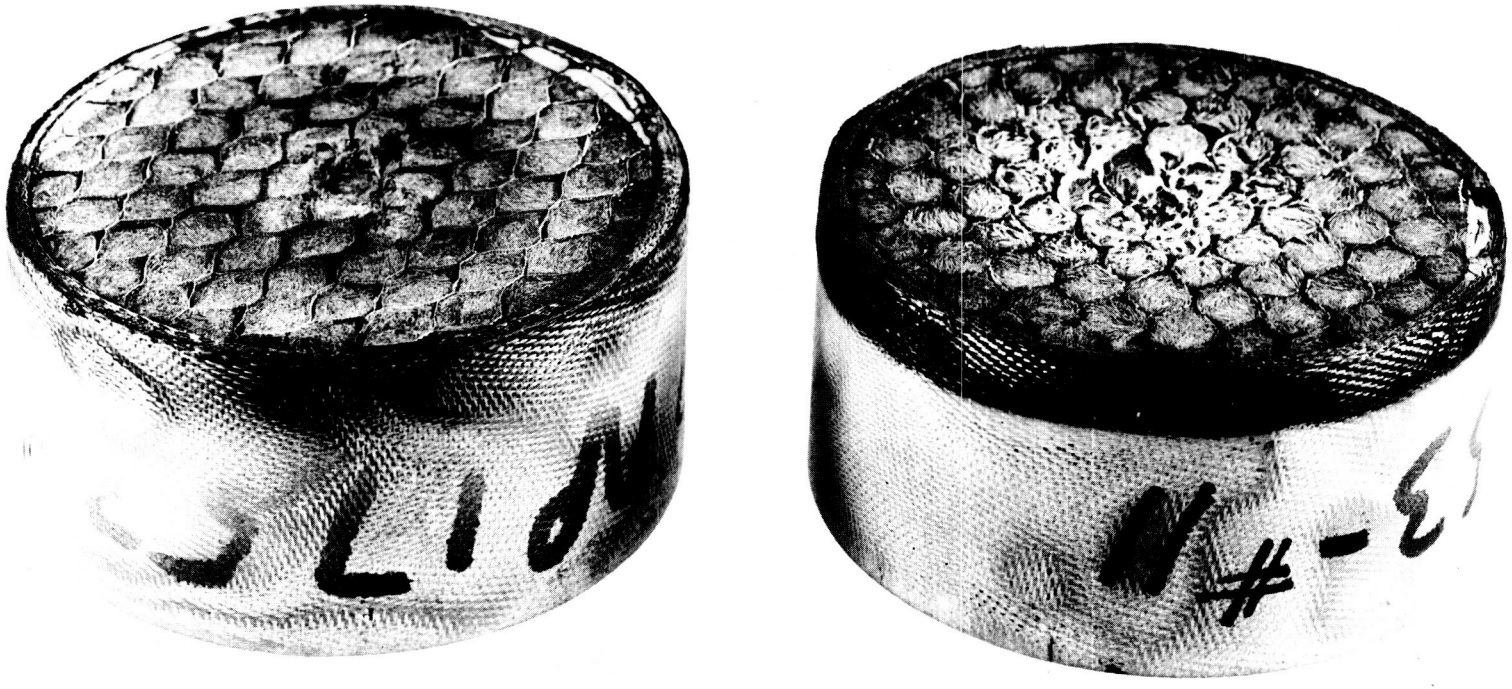

AP1753-9 AP1753 Series AP1753-11

Figure 49 THREE-QUARTER VIEW AP 1753-9 AND -11
11786-C

Figure 50 THREE-QUARTER VIEW AP1753-14 AND -19
11786-D

Figure 51 THREE-QUARTER VIEW AP 1753-22 AND -30
11786-B

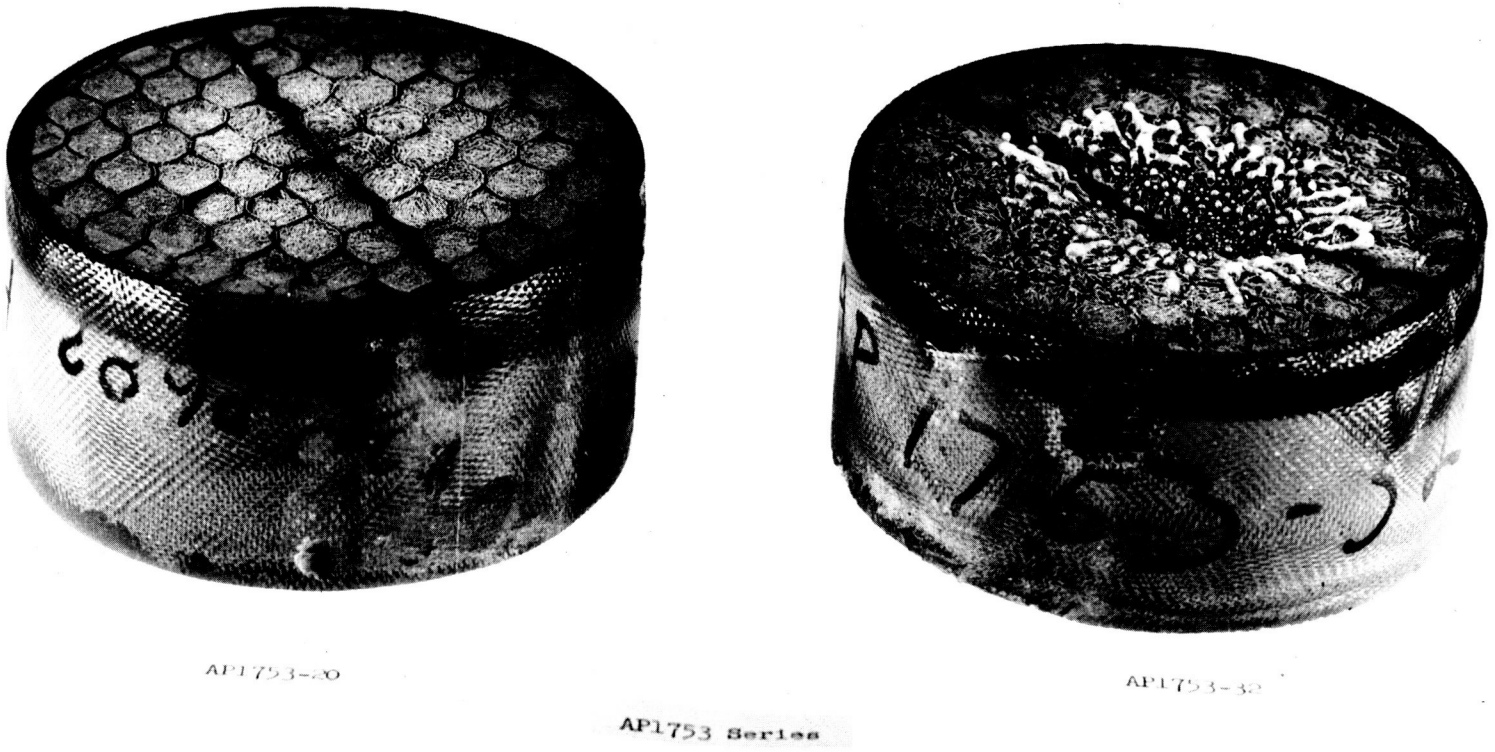

Figure 52 THREE-QUARTER VIEW AP 1753-20 AND -32
11786-A

CONFIDENTIAL

Figure 53 REPAIR SAMPLE
12166A

CONFIDENTIAL

Figure 54 REPAIR SAMPLE
12166F

II. MATERIALS DEVELOPMENT AND MANUFACTURING

A. MATERIALS DEVELOPMENT

All variables that were thought to be pertinent to "hockey puck" density changes in the 5026-39 ablator have been carefully evaluated. These included (1) operator (2) equipment (3) environment (4) processing (5) raw materials and (6) testing.

Equipment and environmental conditions were quickly shown as non-contributing to any gross differences in physical properties of the ablator when other conditions were kept constant. Operators (with proper training and experience) did not account for density variability. Testing results were found to depend upon the conditions under which the test mold was prepared. The relationship between mold size, mold pressure and ablator weight was standardized to eliminate this variable. The batch processing is fairly complicated and must necessarily allow somewhat loose specifications so that on the spot compensations may be made for uncontrollable reactions. Still, density changes could not be directly related to process variables.

Raw materials used in each batch were tabulated and correlated with density changes over a large number of runs. It was found that both glass fibers and phenolic microballoon properties could be varied within their specification ranges so as to result in widely varying molded plug densities. Fiber diameter, length and bulk density are important to final molded plug density. Also phenolic microballoon density and wall strength affect the mold plug density. All of these properties are controllable except balloon wall strength.

Microballoon breakdown during the mixing operation results in density increases. Pre-breakdown before mixing is limited by the specification allowing a minimum of sinkers. This still does not provide a means for guaranteeing high strength or even non varying strengths of balloons. It is however possible to compensate for balloon breakage by varying the fiber properties. Keeping all other properties constant, changes in the fiber bulk density can be made to compensate for balloon strength variability.

Chart I shows the density variation effects when glass fiber bulk density is increased. Three batches of phenolic microballoons have been used while all other ingredients and processing techniques have been kept constant. All materials were well within specification limits and the processing did not deviate from the prescribed procedure.

CHART I

5026-39M ABLATOR DENSITY VARIABILITY

Glass Fiber Lot No.	Bulk Density, g/cc	Phenolic Microballoon Lot No.	Total Batches Mixed	Density	
				Bad >0.59 g/cc	Good 0.52 - 0.59 g/cc
707511	0.051	466A	10	9	1
707511	0.051	466D	7	6	1
707511	0.051	466F	22	17	5
710177	0.065	466A	8	2	6
710177	0.065	466D	4	1	3
710177	0.065	466F	10	5	5
714260	0.074	466A	41	0	41
714260	0.074	466D	16	0	16
714260	0.074	466F	20	5	15

The following conclusions are evident from these data: (1) As the bulk density of the fiberglass increased the percent of good batches (within ablator density specification) increased. (2) Microballoon lots with respect to providing acceptable batch densities were A> D> F. Lot A gave 81 percent good batches, lot D gave 74 percent good batches and lot F gave 48 percent good batches. (3) All bad batches were too high in density, none were below the specified density range.

It would appear that raising the glass fiber bulk density compensated for an increase in fragility of phenolic microballoons. Four test batches shown in Chart II were prepared keeping all variables constant except phenolic microballoons and using a glass fiber with a bulk density of 0.088 g/cc.

CHART II

VARIATION OF ABLATOR DENSITY WITH FILLER CHANGES

Glass Fiber Bulk Density g/cc	Phenolic Microballoon Lot No.	Density Molded Plug, g/cc
0.088	466A	0.50
0.088	466D	0.56
0.088	466F	0.56
0.088	421E	0.53

The results shown in Chart II agree with predicted decreases in mold plug densities using higher bulk fiber. The 466F microballoons which consistently gave high ablator densities when used with lower bulk glass fiber gave ablator densities well within specification when used with the higher bulk glass fiber. Also the 466A microballoons which gave lowest ablator densities using lower bulk glass fiber dropped below specification ablator density when higher bulk glass was used. The 421E microballoons have been giving an average ablator density of 0.57 g/cc (10 batch avg.). Using these same microballoons with the higher bulk glass the ablator density dropped as expected (to 0.53 g/cc).

It was found that the presence of cured RTV 560 silicone rubber gaskets inhibits the cure of Sylgard 182 adhesive. These two materials contact each other in the vicinity of the abort tower well. Coating formulas were evaluated by brushing onto the cured RTV silicone and then casting Sylgard next to the coated RTV. An effective barrier coat was developed using epoxy / Versamid resins. A specification for this material has been written.

Two bond tensile specimens were fabricated with HT 424 tape adhesive and were held 7 days before cure (4 days at room temperature, and 3 days at 100°F). These two specimens were then cured and tested with results of 3880 and 4570 psi, both of which exceed the 3600 psi minimum strength in the applicable specification. This indicates that some time is available for minor repairs, adjustments, etc. before cure of the adhesive.

To maintain a smooth transition across depressions and/or patches on the substructure surface so that fiberglass honeycomb would give a continuous bond it was necessary to devise a method to achieve a faired surface. Several tests were made using HT 424 tape alone and interlayered with glass cloth. A suitable fairing with minimum bubbling was accomplished using a bottom and top layer of HT 424 tape and a center layer of glass cloth. The filled area was feathered out some 2 to 3 inches.

B. MANUFACTURING

AFRM 006 was received at Avco at the beginning of this reporting period. Damage to the shipping container for the crew compartment was evident. On uncrating, it appeared that the compartment had shifted off the support ring provided for its base and had sustained some damage to stringers and to the base ring at Station 23 through contact with the container. Figure 55 shows the compartment as uncrated, while figures 56 and 57 show typical areas where the base ring has been nicked by contact with screws and where internal stringers have been bent by contact with the support ring. There was no apparent shipping damage to the other compartments.

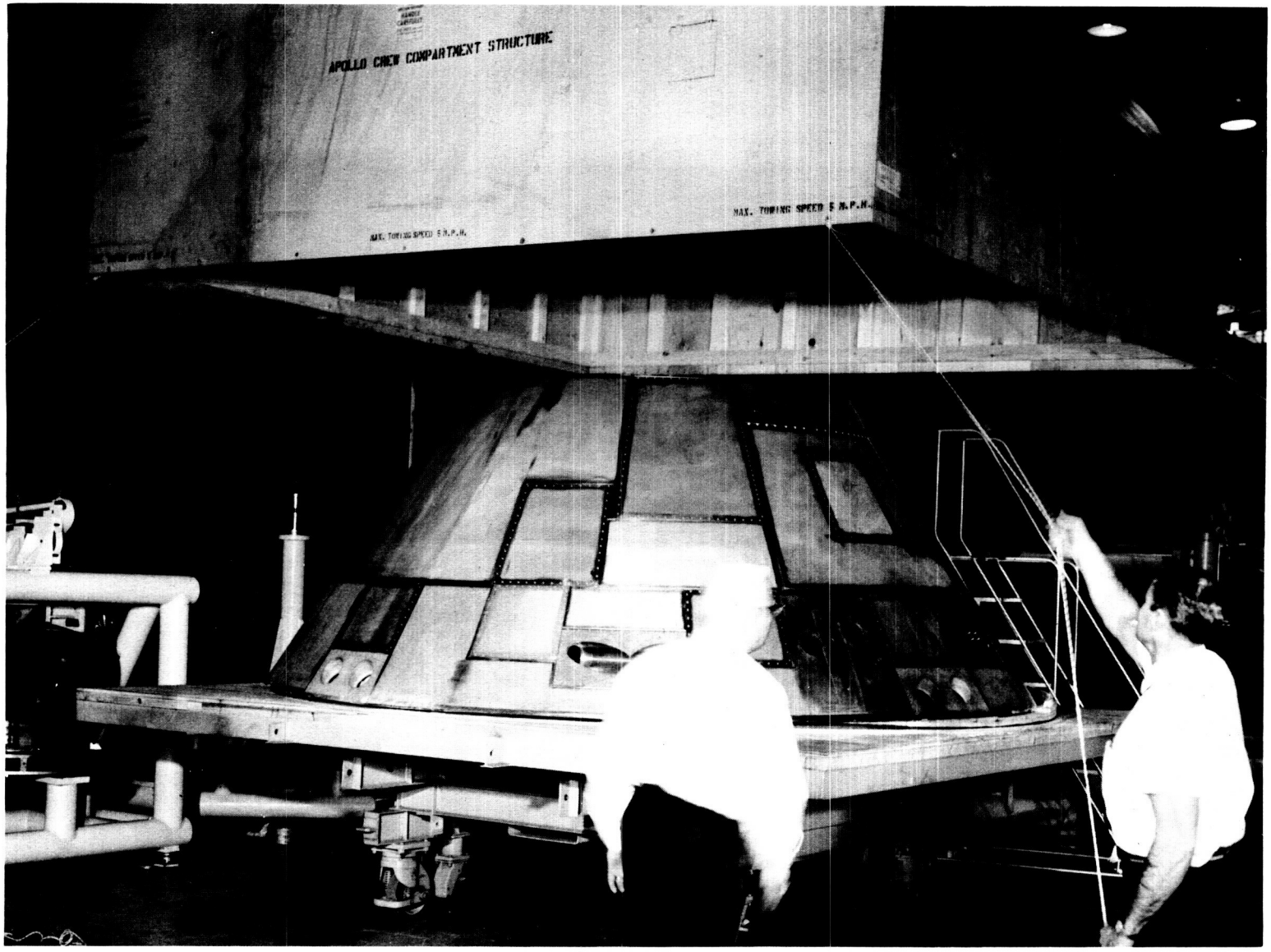

Figure 55 CREW COMPARTMENT (AFRM 006) AS RECEIVED SHOWING SHIFTING OF COMPARTMENT OF SUPPORT BASE IN SHIPPING CONTAINER
11807-D

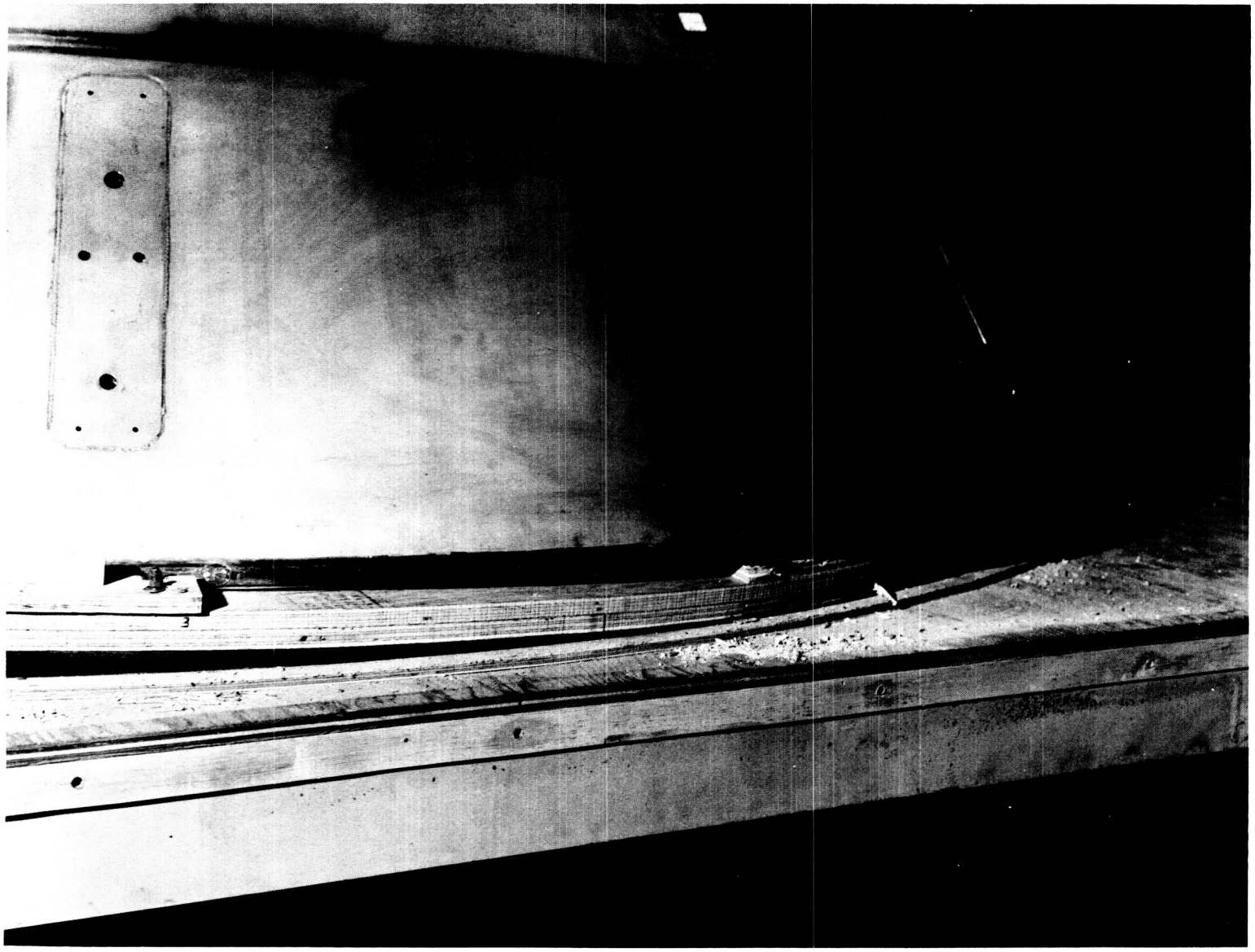

Figure 56 BASE RING OF CREW COMPARTMENT (AFRM 006) SHOWING DAMAGE FROM CONTACT WITH SHIPPING CONTAINER
11807-K

Figure 57 INTERNAL VIEW OF CREW COMPARTMENT (AFRM 006) SHOWING DAMAGE TO STRINGERS FROM CONTACT WITH SHIPPING CONTAINER 11807-J

NAA/S&ID representatives surveyed this damage and direction was given to proceed with the compartment, using 400 grit abrasive paper to dress the machined surfaces of the base ring so as to minimize the effects of the damage. Subsequent direction was given for the removal of a portion of the damaged stringer at Frame 5. These actions have been accomplished.

Application of the ablative heat shield to AFRM 006 is currently in progress in the Avco Manufacturing area. The following summary covers those operations which have been accomplished on each compartment to date:

Operation	AFRM 006 Compartment			
	Nosecap	Forward	Crew	Aft
Weight and CG Determination	complete	complete	complete	complete
X-Ray	complete	complete	complete	complete
Dimensional Inspection	complete	complete	complete	complete
Edgemember and Honeycomb Prefit	complete	complete	In process	complete
Cleaning and Priming Substructure	complete	complete	--	In process
Bonding of Edgemembers and Honeycomb	complete	complete	--	--
Contour Machining of Honeycomb	complete	--	--	--
Inspection of Honeycomb Bond	complete	In process	--	--
Repair of Defective Bond Areas	In process	--	--	--

Figures 58 and 59 show the crew and aft compartments on the weight and CG fixtures.

In addition to the operations indicated above on the substructures themselves, fabrication of detail parts has also progressed. Essentially all fiberglass parts for AFRM 006 have been fabricated and inspected. The exceptions are in the many areas on the vehicle where dimensional deviation of the substructure from NAA/S&ID drawings has necessitated re-design and modification of the existing

part. In some cases, this is the result of the presence of doublers and other repairs in the stainless steel panels, while in others, the problem results from significant contour deviations in the structure itself. In either case, the required modification of the existing design has been time consuming and has required much hand fitting and rework of parts and tooling.

Moldings of 5026-39M have been processed for abort tower wells, rendezvous window wells, and bolt plugs. These are currently being machined.

All raw materials for the mixing of 5026-39 for the AFRM 006 heat shield are in house. This operation will be scheduled as necessary to supply the material for gunning into the various compartments.

Continued process development and prove-out has proceeded with the partial completion of the crew compartment and nosecap mockups. Sufficient area was loaded by gunning in each case to insure an adequate quantity of ablator for checkout of the machining operations for each compartment. Figure 60 shows the crew compartment mockup as bagged for the ablator cure. In addition, RTV silicone gaskets are being cast in the door openings of the crew compartment mockup to perfect techniques and to train Manufacturing personnel in this operation.

The Betts numerically controlled vertical boring machine has been installed and operated with trial tapes. Some difficulty was encountered with the table drive. This has been modified and is back in operation. Adjusting and de-bugging operations are proceeding. Tapes are being prepared to machine a 30 degree sector of each compartment mockup. These tests will further check the depth of cut and the ability of the machine to follow tape instruction.

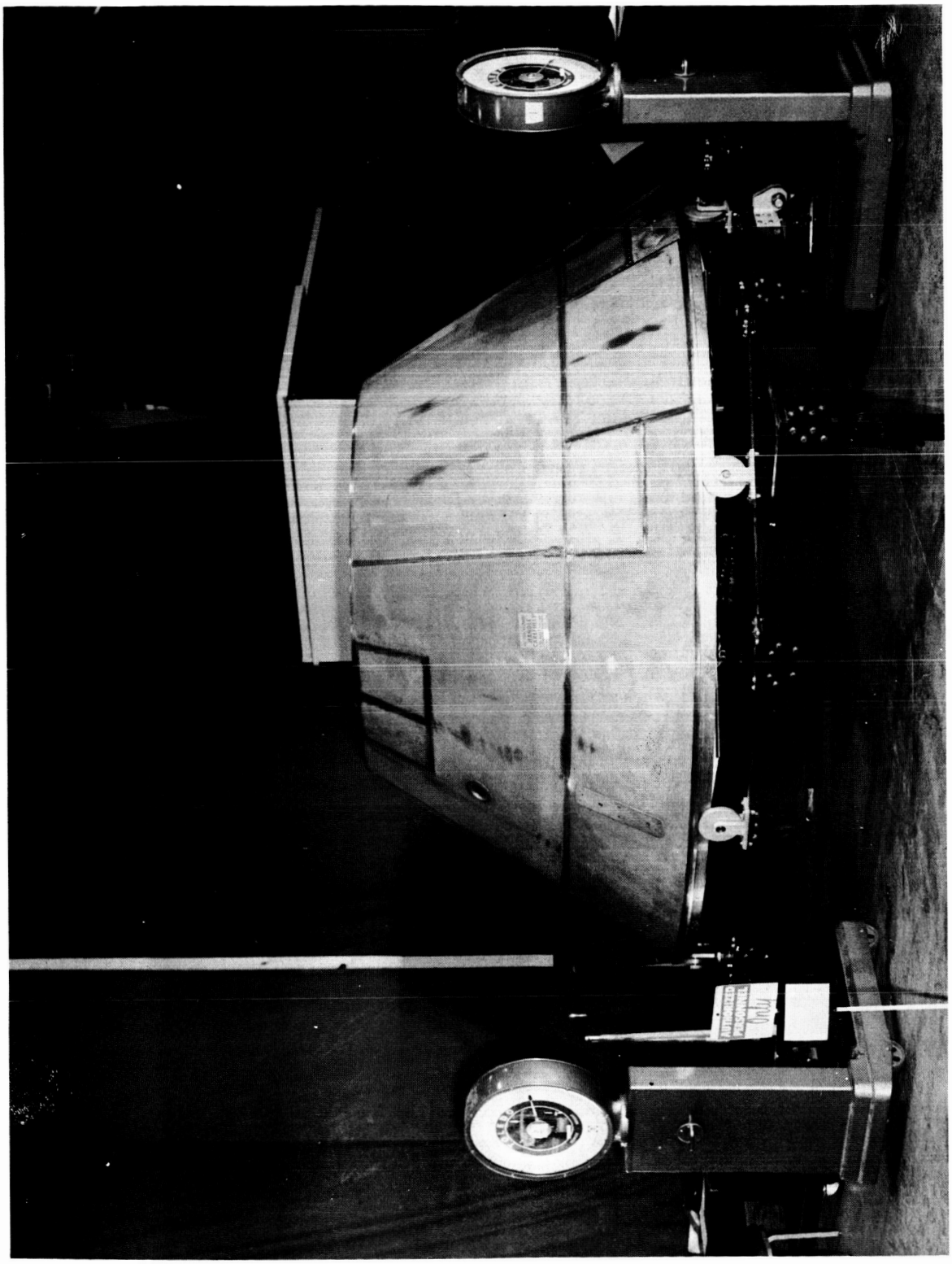

Figure 58 CREW COMPARTMENT (AFRM 006) ON WEIGHT AND CG FIXTURE

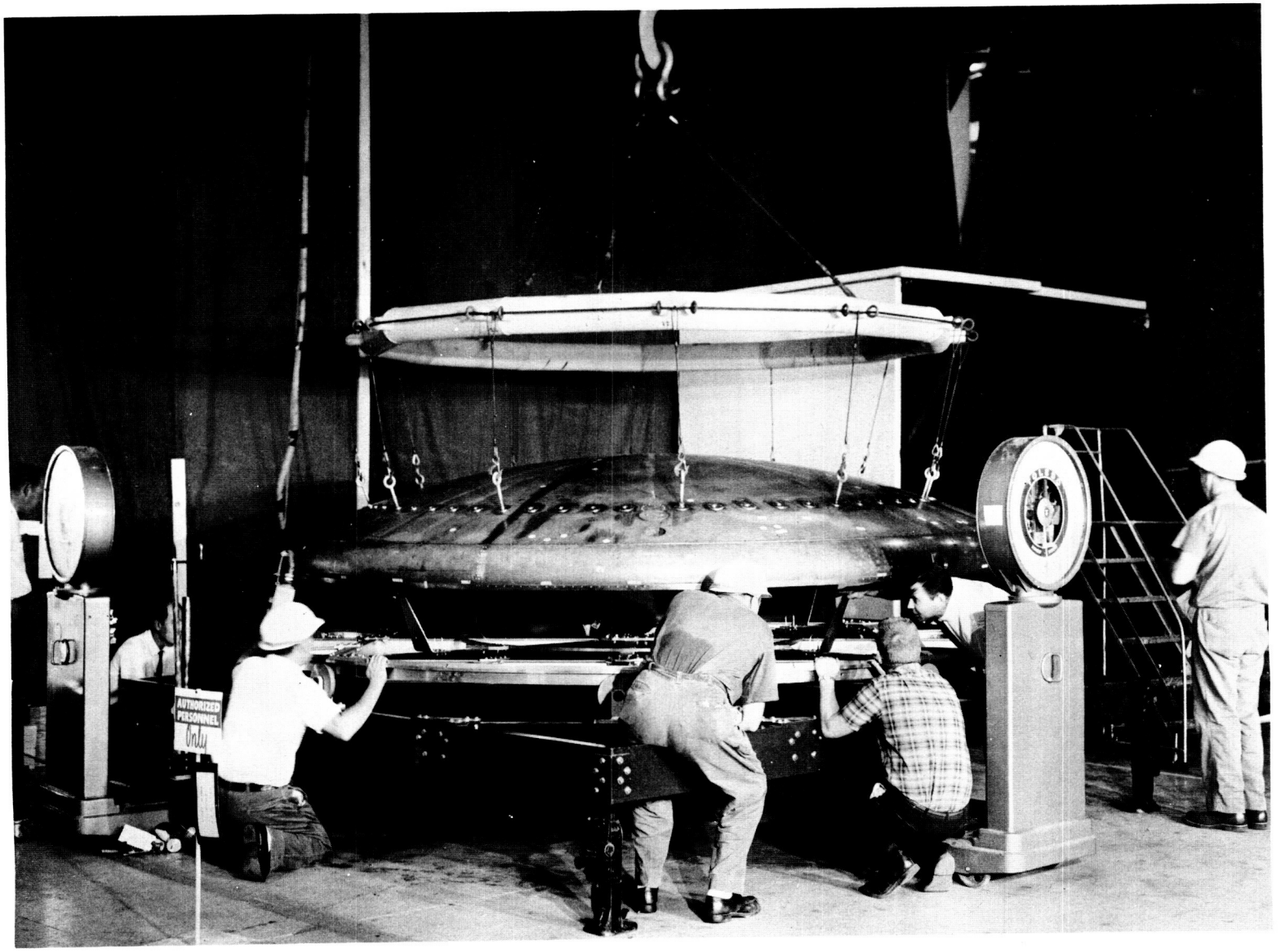

Figure 59 AFT COMPARTMENT (AFRM 006) BEING PLACED ON WEIGHT AND CG FIXTURE
10710-R-2

CONFIDENTIAL

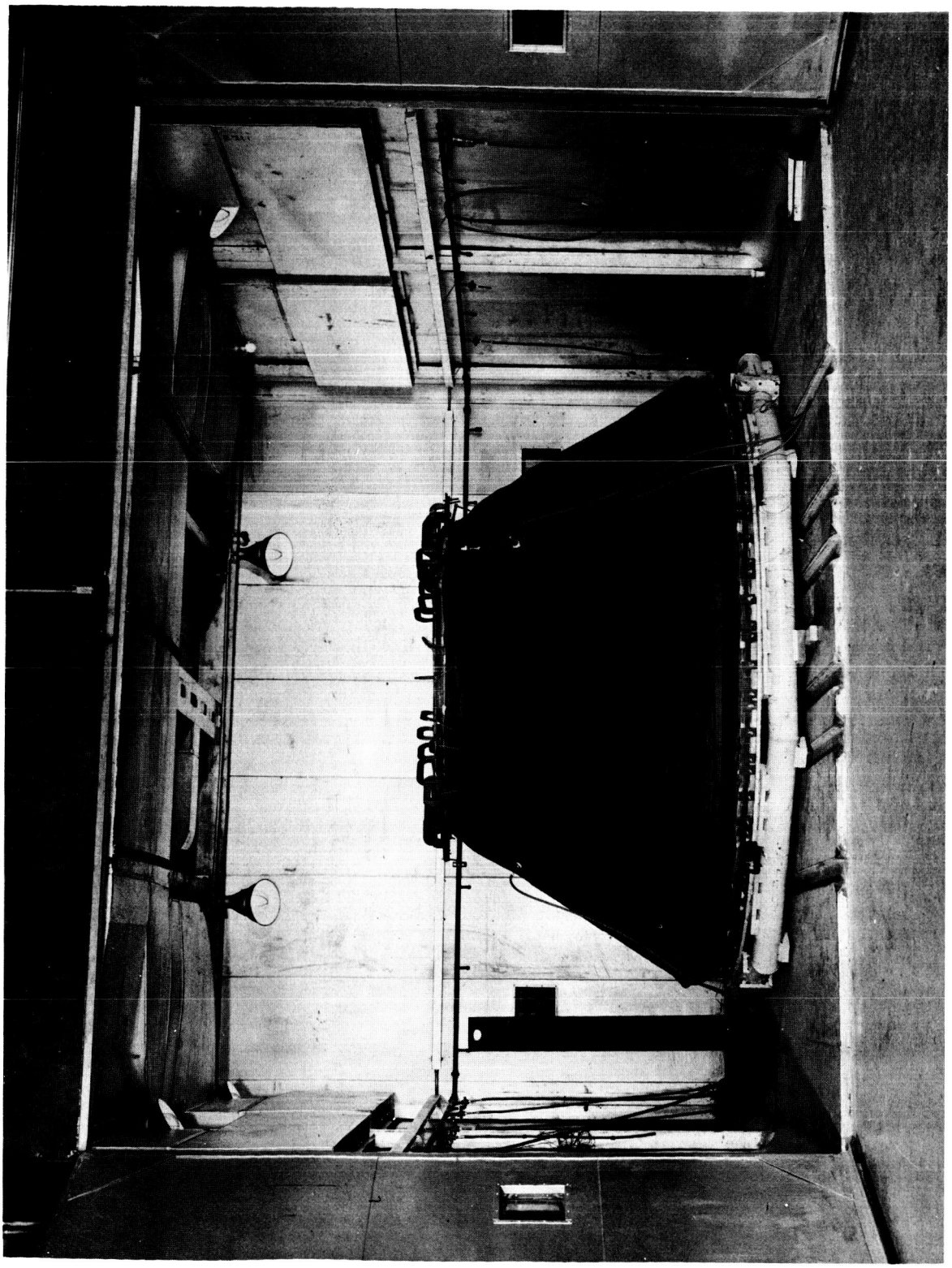

Figure 60 CREW COMPARTMENT MOCKUP IN VACUUM BAG FOR OVEN CURE OF ABLATOR 10710-W

III. QUALITY

Detail parts for the first two structures, 006 and 009 have been inspected and submitted to stores.

Inspection is being maintained to support all newly fabricated parts to replace spoilages.

Raw materials received in preparation for the formulation of 5026-39 for AFRM 006 is inspected and in stores.

Inspection of all four compartments of the 006 structure has been completed.

The results of these inspections have been submitted to Design Engineering, and release of the structures for fabrication were formally made by E. C.

At the request of NAA, a dye penetrant inspection of all visible dents, dimples, and bulges on the FWD/Nose Section was performed and the results of this inspection indicated no surface cracks. A formal report was made to the Apollo Project Office for transmittal to NAA.

The prefit of detail parts for the Nose, and Forward Section has been completed prior to bonding on the structure.

In-process inspection during the prefit of detail parts to the crew and aft sections are currently being maintained.

On 31 August 1964, during fabrication, damage to the crew compartment was discovered (see figure 61). The manner in which the damage was inflicted is unknown. A Non-Conformance Report was prepared by NAA Quality Assurance Representative and disposition was made for repair by NAA. A detail inspection plan has been prepared for all inspection required in accordance with NAA disposition made. Inflicted damage is illustrated on the attached photograph.

The inspection of the bond of Honeycomb Core to the Nose Section is complete, and all deviations were reported on MRB. A disposition for repair was made and completed. Inspection of the repairs will be accomplished during the week.

Because of the out of tolerance dimensions on all sections, a great amount of inspection time was expended to report all deviations to Engineering for the purpose of making the required changes on parts.

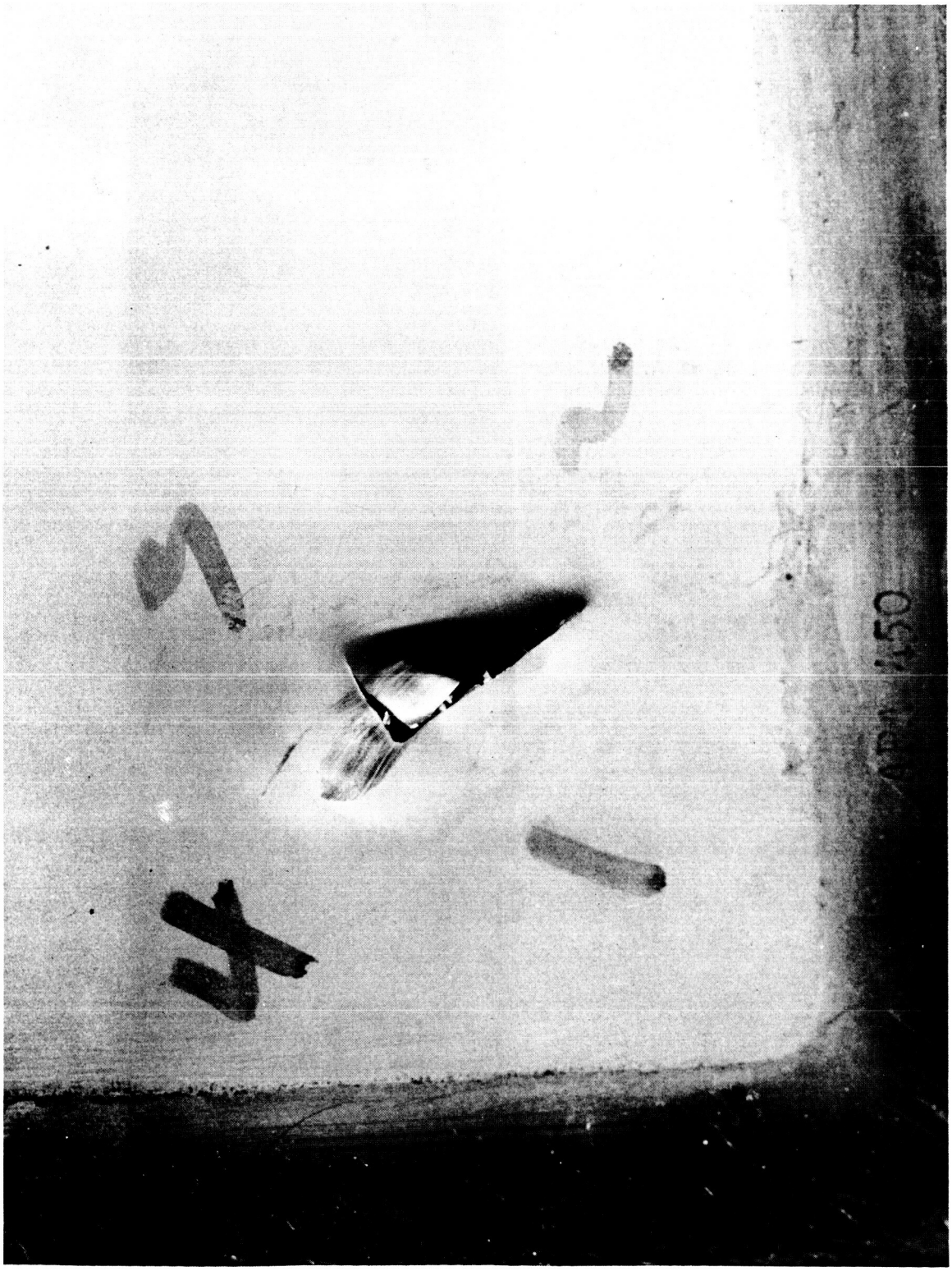

Figure 61 CREW COMPARTMENT DAMAGE DUE TO UNKNOWN CAUSE
12069

DISTRIBUTION

Addressee	No. of Copies
NAA/S&ID (+1 reproducible)	25
R.H. Hugghins (Avco Rep. at NAA)	1
F.B. Matthews (NAA Rep. at Avco)	1
Apollo Central File (+ 1 reproducible)	5
Central Files	1
Document Control	1
Research Library (+ 1 reproducible)	5
On-Site Avco Personnel	
C.F. Berninger	1
Y.G. Biry	1
F.W. Diedrich	1
G.C. Kipps	1
K. Goodman	1
A.J. Hanawalt	1
H. Hoercher	1
E. Hogan	1
M.E. Ihnat	1
F.J. Kaszynski	1
E.D. Kenna	1
R.S. Knower	1
J.A. Kyger	1
A.J. Lavigne	1
T.W. Mix	1
A. Ogman	1
A.A. Rothstein	1
Off-Site Avco Personnel	
P.T. Andrews	1
R.L. Bentley	1
E. Belason	1
F. Brown	1
R. Bussey	1
C. Cohen	1
J. Collins	1
F. DeGiacomo	1
R.E. Demming	1
M.G. Friedman	1
M. Guidi	1
L. Hammond	1
C.L. Huffine	1
H. Hurwicz	1
J.S. Johnson	1
E. Kaminsky	1

DISTRIBUTION (Concl'd)

Addressee	No. of Copies
J. Kossar	1
L. Levin	1
D. Moddie	1
D. Mosher	1
R. Mykytyn	1
E. Offenhartz	1
D. Pennington	1
J. Phaneuf	1
J.E. Richard	1
C.W. Spencer	1
D.E. Stafford	1
W. Winterling	1
A. Woodhull	1
W. Zeh	1

(NOT USED)